Photosynthetic Efficiency of Phototrophic Plankton and Bio-Optical Variability as Influenced by Mesoscale Processes In the Eastern Caribbean Basin

by

Ramón López-Rosado

A dissertation submitted in partial fulfillment of the requirements for the degree of

DOCTOR OF PHILOSOPHY

in

MARINE SCIENCES
(Biological Oceanography)

UNIVERSITY OF PUERTO RICO
MAYAGÜEZ CAMPUS
December 2008

Approved by:

_____	_____
Roy A. Armstrong, Ph.D. Member, Graduate Committee	Date
_____	_____
Jorge E. Corredor, Ph.D Member, Graduate Committee	Date
_____	_____
Fernando Gilbes, Ph.D. Member, Graduate Committee	Date
_____	_____
Julio Morell, M.S. Member, Graduate Committee	Date
_____	_____
José M. López, Ph.D. President, Graduate Committee	Date
_____	_____
Nilda E. Aponte, Ph.D. Chairperson of the Department	Date
_____	_____
Edgardo Lorenzo, Ph.D. Representative of Graduate Studies	Date

COPYRIGHT

ABSTRACT

This study comprises an analysis of photosynthetic potential of phototrophic plankton in eastern Caribbean Sea near-surface waters as influenced by the action of mesoscale processes. The massive freshwater plume from the Orinoco River and mesoscale cyclonic and anti-cyclonic eddies are two common types of features in the Eastern Caribbean Sea. The physiological state of phototrophic plankton was addressed by measuring its photosynthetic efficiency using a fast repetition rate fluorometer (FRRF) throughout the region. The *Fv/Fm* parameter measures the changes in phototrophic plankton physiology by a rapid, noninvasive assessment of in vivo fluorescence signatures. The FRRF provided fast and accurate quantification of changes in productivity in response to environmental forcing at the ecologically relevant scales of mesoscale processes. Enhanced biological activity has been associated with these features which stimulate the input of limiting nutrients into the euphotic zone. FRRF measurements showed that photosynthetic efficiency varied vertically in areas of upward pycnocline displacement of isohalines and thermal structures suggesting that nutrient upwelling is responsible for the higher photosynthetic efficiency observed at surface. The influence of the Orinoco River plume on the photosynthetic potential demonstrated increased *Fv/Fm* close to the surface, decreasing with depth, suggesting a relationship with river originated material. Independent measurements of photosynthetically mediated ^{14}C uptake produced a strong linear relationship (r = 0.91) with the FRRF-based primary productivity estimates for data collected throughout the region. These estimates covaried with satellite-based estimates of primary production through the environmental gradients created by the Orinoco River plume. Correlation analysis was used to describe the relationship between phototrophic plankton physiological state (Fv/Fm) and independent measurements of bio-optical variables.The beam attenuation to chlorophyll ratio (cp *) demonstrated inverse correlation with *Fv/Fm* as a result of the baroclinic instabilities created by eddies. The phytoplankton specific absorption coefficient (a_{ph}) showed reduced absorption in the region of 442 nm apparently in response to increased package effect for waters under the influence of the river plume. Variations in the a_{ph} slope were associated to a decrease in the quantum yield for carbon fixation in samples from oceanic waters far from the direct influence of the Orinoco River plume.

RESUMEN

Este estudio comprende un análisis del potencial fotosintético del plancton fototrófico en aguas superficiales del Mar Caribe oriental según son definidas por la acción de procesos a meso-escala. Remolinos a meso-escala ciclónicos y anti-ciclónicos y las plumas masivas de aguas dulce del Río Orinoco son fenómenos comunes en el Mar Caribe. El estado fisiológico del plancton fototrófico fue estudiado usando un fluorómetro de repetición rápida (FRR), para medir su eficiencia fotosintética (*Fv/Fm*) a través de la región. El parámetro *Fv/Fm* mide los cambios en la fisiología del plancton fototrófico con una evaluación rápida y no invasiva de las señales de fluorescencia en vivo. El FRR provee una cuantificación rápida y precisa de los cambios en productividad en respuesta a presiones ambientales a las escalas ecológicamente relevantes de procesos a meso-escala. El aumento en actividad biológica ha sido asociada a estos fenomenos, los cuales estimulan la incursión de nutrientes limitantes en la zona eufótica. Las medidas del FRR mostraron que la eficiencia fotosintética varió verticalmente en áreas de desplazamiento de la picnoclina hacia la superficie de estructuras isohalinas y estructuras termales sugiriendo que el afloramiento de nutrientes es responsable por la alta eficiencia fotosintética observada en superficie. La influencia del frente del Río Orinoco en el potencial fotosintético demostró incrementos en *Fv/Fm* cerca de superficie disminuyendo con profundidad, sugiriendo una relación con el material originado en el río. Los estimados de producción primaria basados en el FRR demostraron una relación lineal robusta (r = 0.91) con medidas independientes por estimados de ^{14}C obtenidos a través de la región. Estos estimados covariaron con estimados de productividad primaria realizados con datos de satélite, a través del gradiente ambiental creado por el Río Orinoco. Medidas bio-ópticas independientes también fueron consideradas en este estudio y asociadas al estado fisiológico del plancton fototrófico. La razón de atenuación del haz (cp *) con clorofila-a demostró una relación inversa con *Fv/Fm* como resultado de las inestabilidades baroclínicas creadas por los remolinos. El coeficiente de absorción específica de fitoplancton (a_{ph}) demostró una absorción reducida en la región de 442 nm aparentemente en respuesta al efecto de paquete en las aguas influenciadas por la pluma del rio. Variaciones en la pendiente de (a_{ph}) fueron asociados a una disminución en la

taza quántica de fijación de carbono en las muestras de aguas oceánicas lejos de la influencia directa de la pluma del Río Orinoco.

This work is dedicated to my parents,
Ramón and Rosa, and my brothers,
Javier and Joel,
for their love and unconditional support.

ACKNOWLEDGEMENTS

This journey was only possible because of the people it was share with, consequently I would like to express my most sincere gratitude to:

- My friends and laboratory mates Marla, Marcos, Milton, Alvaro, Suhey, Dihalia, Belitza, Jacquelyn, Ana, Helena, Miguel, Dieppa, Patrick, Vilmaliz and Ava, whom without their help, support and encouragement this research and manuscript would not have been possible. For believing in me, especially in the moments when the journey became harsh and the load unbearable.

- The bio-optical laboratory, Yazmin, Debby, Aurora, Maria and Sara whom were always there to provide help and support.

- My graduate committee, José M. López, Jorge Corredor, Julio Morell, Fernando Gilbes, Roy Armstrong and Jorge Capella for their support and guidance through this whole process.

- To the Crew of the R/V Chapman, R/V Sultana, R/V Pelican and R/V Ronald H. Brown for their assistance and help during the field operations.

This research was supported by the Office of Naval Research (ONR) (Grant number: N000140310904), Department of Energy (Grant number: DE-FG02-05ER64029 and DE-FG02-05ER64149), NASA-UPR Tropical Center for Earth and Space Studies (TCESS) and the NOAA-UPRM Cooperative Remote Sensing Science and Technology Center (NOAA-CREST) (Grant Number: NA17AE1625).

TABLE OF CONTENTS

LIST OF TABLES

LIST OF FIGURES

CHAPTER 1

1.1 General Introduction

Phototrophic plankton comprised by single-celled organisms , cyanobacteria and phytoplankton, inhabit three quarters of the earth's surface yet they account for less than one percent of the 600 billion metric tons of carbon contained within its photosynthetic biomass. Recent satellite-based estimates have demonstrated that phototrophic plankton incorporates approximately 45 billion to 52 billion metric tons of inorganic carbon into their cells each year (Falkowski, 2002), drawing as much CO_2 out of the atmosphere through photosynthesis as trees on land ecosystems. Consequently, it is of great interest to understand their role in Earth's carbon cycle as an integral part of the biological pump, which is the transport of organic carbon (and N and P) to deep sea by the settling of dead cells. It is estimated that the biological pump is responsible for seven to eight billion metric tons, or 15 percent, of the carbon that the phototrophic plankton assimilates every year (Falkowski, 2002). As the biological pump plays an important role in the Earth's carbon cycle, significant effort is spent quantifying its strength, especially into the understanding the biogeophysical dynamics affecting photosynthesis throughout our planet. This study focuses such efforts to increase understanding of the Eastern Caribbean Basin, a highly dynamic and complex region.

Caribbean water masses show seasonal cycles with temporal variations in their vertical structure. These seasonal cycles are influenced by mesoscale events such as freshwater inputs to the eastern Caribbean and mesoscale eddies that periodically move through the area. The fresh water impulses are a result of the Orinoco River and Amazon River plumes as they are transported by the eastern Caribbean inflow between South America and the Virgin Islands. Peak flow for the Orinoco River occurs between the months of August-September (Lewis and Saunders, 1989), while the Amazon River shows it's highest during May to June (Hedges et al., 1986). The influence of these fresh water inputs impact North Eastern Caribbean surface water structure throughout the year presenting a surface salinity below what is typically found at the Tropical Atlantic

Surface Water and elevated silicate content, unusual for the region (Corredor and Morell, 2001). The seasonality of these events on is influenced by the seasonal displacement of the Intertropical Convergence Zone (ITCZ) along a gradient from the Amazon River across the Orinoco River basin and into the central Caribbean. A dry season centered during the month of April is observed when the ITCZ is displaced south and strong easterly winds enhance surface flow through the Caribbean (Morrison Smith, 1990), inducing upwelling along the southern Caribbean (Corredor, 1979). During this period the Amazon river has a major effect on Caribbean waters even though part of its flow is retroflected eastward in the North Equatorial Countercurrent. The remaining flow is carried north by the North Equatorial Current and into the Caribbean current. The rainy season appears when the ITCZ is at its northernmost position over the Caribbean and the Orinoco River basin causing massive freshwater inputs to the Eastern Caribbean and to Caribbean surface current (Corredor and Morell, 2001).

The Caribbean current inflow , a major route by which riverine waters are transported through the Caribbean, has two sources; one north and one to the south of 15° N (Figure 1.1) . The northern inflow is primarily Gulf Stream water returning southwestward in the North Equatorial Current. These waters pass through the Leeward Islands of the Lesser Antilles, through the Windward Passage between Cuba and Hispaniola and through the Mona Passage between the Hispaniola and Puerto Rico (Johns et al., 2002). The southern inflow originates in the South Atlantic and crosses the equator through the North Brazil Current (NBC), which is part of the northward flowing western current. The NBC curls to the east and south near 6° N into what is known as a retroflection to feed the North Equatorial Countercurrent (NECC) (Figure 1.1). This retroflection is seasonal with episodes occurring from June through March. Otherwise this current continues and becomes part of the Guyana current along the coast of northern Brazil. During the retroflection period the NBC closes into itself forming eddies that dislodge continuing northwestward at around 15cm/sec (Johns et al., 2002). These mesoscale formations then collide with the Antilles and are advected through the passages along with the Guyana current and enter the Caribbean mostly through the Grenada, St. Vincent, and St. Lucia Passages in the southeast. This inflow that crosses the Caribbean westward transports about 28 Sv (1 Sv = 10^6 m^3/sec), 10 Sv of which enters

the Caribbean through the southern or Windward Islands passages, 8 Sv enters through the northern or Leeward Islands passages, and 10 Sv enters through the Greater Antilles Islands passages (Johns et al., 2002).

The inflow advection through the Antilles passages into the Caribbean region described above creates baroclinic instabilities, resulting in the formation of cyclonic and anticyclonic eddies. Murphy and Hurlburt (1999) suggest that most mesoscale eddies associated with the Caribbean current are primarily anticyclonic derived from the anticyclonic vorticity of the North Brazil Current rings and transit through a narrow corridor across the Caribbean basin along an axis at 14° to 15° N with average speeds of 0.15 m/s. Canals-Silander (2005) describes an anticyclonic eddy advected into the Caribbean area around 14° N and moved westward along the Jamaica Ridge. Using satellite-tracked surface drifters Richardson (2005) followed the trajectories of these drifters to analyze and describe the mean currents and eddies in the Caribbean Sea, he also describes anticyclones moving near the southeastern corner of the Caribbean westward up to the Jamaica Ridge near 80ºW. This eddy had a diameter of 167 km and moved westward at 11 cm/sec. The fastest swirl velocities measured in this area were around 70 cm/sec at a diameter of 200 km. Differently cyclonic eddies are suggested to be often formed by current flows through the Antilles passages, rather than being caused by instabilities of the North Brazil Current rings. Richardson (2005) established that some of these eddies can be formed from the cyclonic shear on the southern side of the main Caribbean Current where it flows along the boundary along the Venezuelan Basin. Canals-Silander (2005) describes one formed by entering through the Anegada Passage in the eastern Caribbean, in other occasion he describes a cyclone that as suggested by Cherubin and Richardson (2007) forms by cyclonic shear when an anticyclonic eddy develops while entering the Caribbean through the Lesser Antilles. Satellite imagery revealed that this eddy later advected the Orinoco River Plume (Corredor et. al., 2004) giving clues of the role played by these events in the biogeochemical structure of the Eastern Caribbean surface waters.

The intensification of the Caribbean current has been demonstrated to be associated to the Orinoco River Plume (Hernandez-Guerra and Joyce, 2000; Cherubin and Richardson, 2007). The arrival of freshwater coinciding with an increase of the sea

surface temperature (Ffield, 2005) and the combination of relative low salinity and warm temperatures contributes to a sharpening of the density front which intensifies the Caribbean current at 14° N. This intensification of the current is followed by an increase of the presence of anticyclones south of Puerto Rico and Hispaniola (Baums et al., 2006), as expected by the role of the current in the formation of this events.

Dust storms frequently affect the Caribbean region. Along with them arrive nitrogen, phosphorus and iron amongst other nutrients that perhaps act as a fertilizer to stimulate the production in the region affecting the structure of Caribbean plankton communities. Recent calculations suggest that the total deposition of aeolian iron to the global ocean ranges from 0.5 to 4 x 10^{12} g yr^{-1}, with the distribution varying strongly with season and from one ocean region to another (Gao et al., 2001). Latest models of aeolian iron transport suggest a direct positive relation between iron flux deposition and chlorophyll concentrations at the sea surface (Hernandez et al., 2001). These patterns show seasonal cycles with greatest iron deposition and chlorophyll maxima occurring from July to September in the eastern Caribbean and Atlantic Ocean. Zhu et al.(1997) noted during monitoring studies of mineral aerosols carried by trade winds in Barbados, that Fe constituted on average 3.4% of the mineral dust mass. The impact of aeolian Fe on the productivity of surface waters was observed in Mediterranean oligotrophic waters on the chlorophyll concentrations. Carbon fixation by a water column is proportional to its integrated Chl-a content, which varies approximately as the square root of surface Chl-a of surface waters. The presence of aeolian Fe lead to over estimates by a factor of two which in turns leads to an over estimate of 40% of carbon fixation (Claustre et al., 2002). In order for these algorithms to estimate water column chlorophyll concentration they consider the concentration to be proportional to its integrated content, which varies approximately as the square root of surface, therefore an increase in surface chlorophyll due to aeolian Fe over estimate the entire column estimate.

The events described above are important factors shaping the structure of Caribbean water masses. Therefore to better understand the biological, physical, and chemical structure of the Caribbean water masses, wider spatial and temporal measurements are needed. The study of structure of Eastern Caribbean water masses has relied mainly on studies done by taking discrete samples at several stations through the

area. None of these studies has addressed the possible relationship of the events described above and their impact on the biological spatial structure of these waters using data gathered continuously through transects. The use of towed profiling vehicles provides the means to effectively measure oceanic water mass properties at higher spatial scales. These vehicles and the growing use of active fluorescence techniques such as the fast repetition-rate fluorometer (FRRF) extend the range of the scales at which phototrophic plankton physiology can be observed *in situ* (Kolber et al., 1990; Behrenfeld et al., 1996; Suggettet al., 2001). This combination of a towed profiling vehicle and a FRRF proved to be successful during the IRONEX 2 cruise in the Equatorial Pacific south of the Galapagos Islands, where the first ever deployment of a fast repetition rate fluorimeter (FRRF) in an N*v*-shuttle (towed profiling vehicle) was featured (Martin et al., 1994), and Southern Ocean Iron Release Experiment (SOIRE) in the polar waters of the Australasian Pacific sector of the Southern Ocean (Boyd and Abraham, 2001). In both experiments this assemblage enabled measurements of photosynthetic parameters through the surface, iron-fertilized layer, down to the deep chlorophyll maximum at 70-80m, proving the potential that spatial distribution studies posses in quantifying rapid changes in productivity in response to environmental changes at the ecologically important scales of fronts and other mesoscale phenomena (Sharples et al.,2001).

In the Caribbean area, daily integrated variations of phototrophic plankton productivity have been made based on natural fluorescence and radiolabelled carbon uptake methods using discretely gathered samples at several stations (Alfonso-Sosa, 2000). These approaches are useful when determining the structure of water masses of local waters caused by the Orinoco River and Amazon River combined with specific astronomical conditions that facilitates the generation of internal tides (Alfonso et al., 2004). Recently basic models of primary productivity derived from fast repetition rate fluorometry have been used to estimate carbon fixation, suggesting in some cases a 1:1 relationship with ^{14}C studies (Kolber and Falkowski, 1993; Suggett et al., 2001)

The fast repetition rate fluorometer (FRRF) provides measurements of the progressive closure of photosystem II (PSII) reaction centers (Sakshaug et al., 1997) in response to flashes of excitation energy and is a technological development from the earlier pump and probe (PP) technique (e.g., Kolber et al., 1998). Both methods are based

on similar principles. However, the FRRF is a more flexible instrument which gives relatively instantaneous measurements of certain physiological parameters, thus shortening the overall protocol (Sakshaug et al., 1997). It provides measurements of the functional absorption cross section of PSII, which is a measure of the efficiency of energy transfer from the antennae pigments to the photosystem II reaction center, therefore the ability to promote a photochemical reaction (Falkowski and Raven, 1994). The normalized variable fluorescence measured with FRR fluorometry is used as a function of the functional reaction centers and it has been spatially correlated with nutrients distribution, indicating a close coupling between them and photosynthetic viability and growth rate of phytoplankton (Vaillancourt et al., 2003). In addition, the FRRF provides a better signal-to noise ratio and allows more robust measurements in low chlorophyll regions. The FRRF has the potential to provide more rapid and accurate measurements of productivity by allowing the coupling of phototrophic plankton productivity to physical forcing to be examined on the scales of transient phenomena such as mesoscale events.

Phototrophic plankton fluorescence is the emission by chlorophyll-*a* of the energy absorbed by the photosynthetic pigments that the plant failed to use in photosynthesis. When the reaction centers in the thylacoid membrane of the chloroplast are open, the photon energy can be trapped and passed to a quinone acceptor (Qa) that ultimately transfers this energy and is used to drive photochemistry providing the chemical energy (in the form of ATP and NADPH) for CO_2 fixation in the Calvin cycle. PSII extracts electrons from water releasing oxygen in the process. If Qa is already used by a previous excitation (considered to be closed) and cannot accept new electrons, the probability that the absorbed energy will be fluoresced increases. Because some energy is lost in this process the fluorescent light has a longer wavelength (it is redder). The intensity of the light emitted as fluorescence depends on how much energy was absorbed and how fast it can be passed through the photosynthetic system. The quantum efficiency of photosynthesis varies inversely to the quantum efficiency of fluorescence (Falkowski and Kolber, 1995). Therefore the primary use of fluorescence has been for the estimation of chlorophyll concentration and recent research has focused on the use of sun-stimulated fluorescence to estimate primary productivity (Morrison, 2003; Abbott et al., 1995), and

on actively induce methods such as pump and probe and fast repetition rate fluorescence fluorometry (Kolber et al., 1998; Vaillancourt et al., 2003). Based on this principle, remotely sensed acquired data of primary production has also been used recently to study large scale water masses and mesoscale events (Moore et al., 2002; Vaillancourt et al., 2003; Maritorena et al., 2000). Consequently, the use of airborne and satellite hyperspectral remote sensors such as NASA's Moderate Resolution Imaging Spectroradiometer (MODIS) capable of resolving fluorescence peaks, measurements of chlorophyll concentration and the derivation of primary productivity are possible (Dey and Singh, 2003; Beherenfeld and Falkowski, 1997).

The main purpose of this study is to investigate the spatial distribution of photosynthetic efficiency, and subsequently gross primary production as the phototrophic plankton communities are affected by mesoscale events that influence the three-dimensional structure of the water masses through the Eastern Caribbean region. It is hypothesized that the events described above deviate the eastern Caribbean surface waters from typically tropical oligotrophic waters to ones with phototrophic plankton communities rather more efficient in photosynthesis due to mesosocale forcing. In order to reach these goals the following objectives were proposed:

- Describe the spatial distribution and dynamics of phototrophic plankton photosynthetic efficiency through the northeastern Caribbean Sea.

- Determine the photosynthetic parameters derived from fast repetition rate fluorometry and its relationship traditional methods such as ^{14}C assimilation and derived production from natural fluorescence of phototrophic plankton.

And

- Compare remotely sensed derived primary production estimates to the modeled from data acquired in situ.

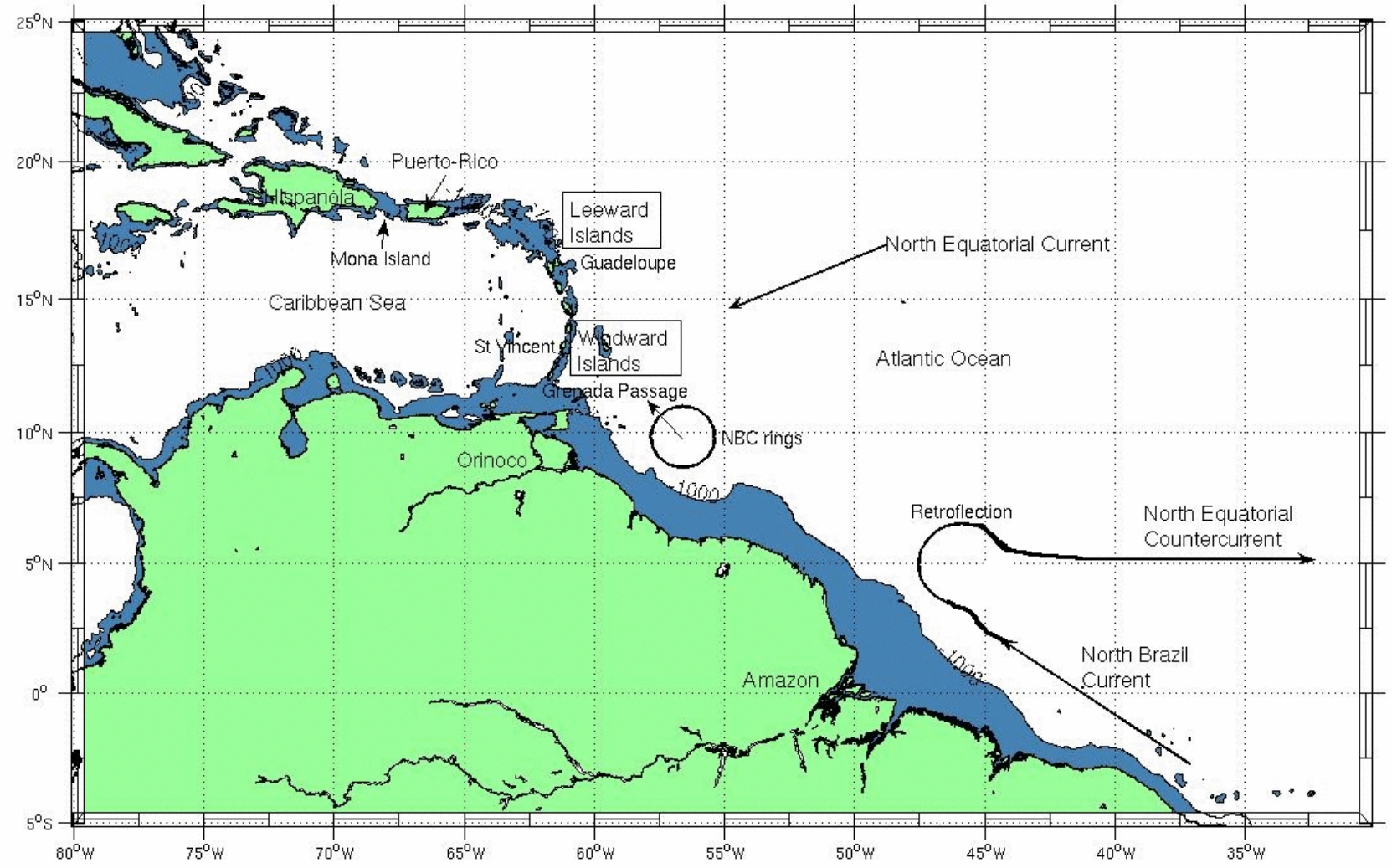

Figure 1.1 Map of the Caribbean Sea and of the nearby tropical Atlantic showing the Amazon and Orinoco Rivers (from Cherubin and Richardson, 2007)

CHAPTER 2

Fast Repetition Rate Fluorometry and optical indices of phototrophic plankton photosynthetic potential at Eastern Caribbean Mesoscale Processes

2.1 Abstract

The role of Caribbean mesoscale processes as agents enhancing the photosynthetic potential of phototrophic plankton populations was addressed in this study. Mesoscale (100-400 km) cyclonic and anti-cyclonic eddies and the massive freshwaters plumes from the Orinoco River are common features in the Caribbean Sea. These Caribbean eddies result from vorticity advected through passages into the Caribbean area as inferred from satellite Sea surface height Anomaly (SSHA). The Caribbean Vorticity Experiments (CaVortEx II and VI) undertaken from June 22-27, 2004 and August 28, 2006 to September 8, 2006 were intended to characterize the physical, biogeochemical, and optical structure of the eddies and to assess their influence on biological productivity of the Eastern Caribbean Region. The physiological state of phototrophic plankton was addressed using fast repetition rate fluorometry (FRRF) and the acquired photosynthetic efficiency (*Fv/Fm*) parameter. This parameter measures the changes in phototrophic plankton physiology by a rapid, noninvasive assessment of in vivo fluorescence signatures. FRRF measurements showed that photosynthetic efficiency varied vertically in areas of upward pycnocline displacement. This displacement suggests that nutrient upwelling is responsible for the higher photosynthetic efficiency observed between the surface to 90 meters. Another optical variable considered in the study and previously linked to phototrophic plankton physiological state is the beam attenuation to chlorophyll ratio (cp *). Enhanced Fv/Fm observed as a result of the baroclinic instabilities created by eddies denoted an inverse correlation with cp* at cyclonic regions, for other regions the parameters were directly correlated. This result suggests that the baroclinic instabilities promote influx of material from depth with a lower cp* ratio that enhance the photosynthetic potential of the cells possibly due to higher concentration of refractive materials.

The expeditions ORIPEX 7 and 8 cruises were carried out during November 19-24, 2005 and September 18-23, 2006, respectively, to analyze effects of the Orinoco River on the biogeochemical properties of the Eastern Caribbean Sea. The influence of the Orinoco River front on the photosynthetic potential of the eastern Caribbean phototrophic plankton populations demonstrated increased *Fv/Fm* close to surface decreasing with depth suggests a relation with river originated material. This increase in *Fv/Fm* coincided with a shift upward of the deep chlorophyll maxima.

2.2 Introduction

Fast repetition rate fluorometry provides rapid, noninvasive assessment of phototrophic plankton in vivo fluorescence signatures and increased sampling resolution of phototrophic plankton physiological state when undergoing environmental adaptations to dynamical biogeochemical processes influenced by physical forcing. (Moore et al., 2003; Vaillancourt et al., 2003; Falkowski et al., 1991) Fast repetition rate fluormetry provides the user with photosynthetic parameters including *Fv/Fm*, σ_{PSII}, τ_{Qa}, and p (Kolber et al., 1998). It is based on the principle that when dark-adapted phototrophic plankton cells are illuminated, all of the functional reaction centers are "open" and ready to receive an exciton, thus their fluorescence yield is low (*F*o) since maximal excitation energy can be efficiently used for photosynthesis. When a given reaction center has received an exciton, it is closed consequently associated fluorescence yield increases. When all the reaction centers are closed (or non-functional), the observed fluorescence is maximal (*F*m). For a phototrophic plankton cell in which all the reaction centers are functional, the maximum change in fluorescence yield is about 3-fold, while a cell with no functional reaction centers shows no change in florescence since its fluorescence yield is high from the beginning of the measurement. Variable fluorescence (Fv = *Fm - Fo)*, when normalized to *F*m, is thus an indicator of the proportion of photosystem II (PS2) reaction centers that are functional; *F*v/*Fm* has been empirically determined to be about 0.65 for cultures of phototrophic plankton growing under optimal conditions (e.g., Kolber et al., 1988).). The absorption cross section of PSII (σ_{PSII}) changes in response to cellular pigment concentrations and the efficiency of energy transfer from pigments to PSII reaction centers, thus making it subject to both nutrient and light availability (Kolber et al., 1988; Moore et al., 2006). σ_{PSII} is typically lower in nutrient replete cells relative to unhealthy cells (Kolber et al., 1988).

In recent years the FRRF technique has proven to be invaluable tool when the close to real time assessment of phototrophic plankton physiological state is needed. During experiments of iron as a limiting micronutrient the fast repetition rate fluorometer helped to address the changes in the photosynthetic potential of cells in hours after the

waters were enriched with Iron (Boyd and Abraham, 2001; Boyd, 2002). Iron limitation has been shown to cause structural changes in PS2 reaction centers, becoming non functional and slow in the photosynthetic electron transport rate (Falkowski et al., 1992, Falkowski and kolber, 1995). In these experiments, areas of the Pacific southern ocean, described as waters of high nutrient and low chlorophyll, the addition of iron increased the photosynthetic potential , ultimately increasing the biological production of the zone (Olson et al., 2000;Suggett et al., 2001; Sosik and Olson, 2002).

When an assessment in short time scales is needed the FRRF has been used successfully to monitor the enhancement of phototrophic plankton biomass or new production (the biological production associated with the rate at which new nutrients are incorporated into the euphotic zone) as it occur when the area under study is subject to a mesoscale event (fronts, eddies and river plumes). Events such as the new production may result from the addition of growth limiting nutrients to the euphotic zone when the passage of a mesoscale cyclonic eddy raises the isopycnals (Falkowski et al., 1991; Vaillancourt et al., 2003). Eddies influence biogeochemical processes by enhancing horizontal advection and lateral stirring of water masses, with the lifting of isopycnals surfaces that enables vertical transport by isoppycnal mixing, and the uplifting of nutrient-rich isopycnal surfaces into the euphotic zone. This zone is typically dominated by photosynthetic bacteria and micro algae, both of high surface to volume ratios, with increased efficiency of nutrient uptake and light harvesting (Andersen et al., 1996).

The uplifting of the isopycnals reveals a footprint at the ocean surface that can be perceived from satellite observations. Sea surface height observations provided by satellites are often used to detect the presence of these features (Siegel et al., 1999). In a cyclonic eddy the water column is denser than normal, which result in a lower than average sea level height or a negative sea level anomaly (SLA). Anticyclonic eddies high SLA will depress isopycnals out of the euphotic zone, transporting nutrient depleted waters downward. Satellite remotely sensed ocean color data also is a valuable tool when tracking these events, the input of colder water from depth into surface waters can be observed by using sea surface temperature (SST), obtained from (for instance) the Geostationary Operational Environmental Satellite (GOES) (Vaillancourt et al., 2003) and the Moderate Resolution Imaging Spectroradiometer (MODIS) (Benitez-Nelson et

al., 2007). Eddies create divergence and convergence zones when they collide with adjacent eddies that may cause upwelling and down-welling zones, promoting biological production that could also enhance biomass accumulation at depth in the down-welling portion (Lima et al., 2002).

Recent studies have addressed the relationship of inherent optical properties and biogeochemical variables on phototrophic plankton physiology , biomass, size distribution and refraction indices (Behrenfeld and Boss, 2003 and 206; Boss et. al., 2007,) . Some researchers specifically have addressed the relationship of beam attenuation and chlorophyll concentration as alternative optical indices of phototrophic plankton physiology and biomass. Beam attenuation at 660nm is a measure of light scattering by suspended particles and since attenuation by dissolved material is negligible at this wavelength, when the pure water contribution is subtracted, the remaining variability is then termed particulate beam attenuation coefficient (c_p). Because particles in the 0.5 and 20 μm size class dominate c_p in the open ocean type size distributions, this range includes the lower portion and the dominant component of the phototrophic plankton domain leading to a direct dependence of c_p on phototrophic plankton biomass (Boss et al, 2001;Beherenfeld and Boss, 2006). This is true in the absence of significant changes in inorganic, detrital and heterotrophic particles. Behrenfeld and Boss (2003) results suggest that c_p may provide a better estimate of algal carbon biomass than chlorophyll concentration in Case I waters and when c_p is normalized to chlorophyll concentration it highly correlates with independent measurements of phototrophic plankton physiology (E_k and P^b_{opt}), providing a proxy of spatiotemporal variability of cellular chlorophyll, incident light and growth rate. Consequently the study of the dynamics of eddies in the eastern Caribbean region (Figure 2.1) may provide an insight of these optical indices and phototrophic plankton photosynthetic efficiency as it varies with eddy pumping potential of materials to the ocean surface.

In this study the roll of Caribbean mesoscale processes as agents enhancing the photosynthetic potential of phototrophic plankton populations is addressed. To date few, if any, studies have attempted to comprehensively study the potential for Caribbean

eddies and the Orinoco River Plume to influence surface waters productivity at the spatial resolution provided by the FRRF and other optical sensors used during this study.

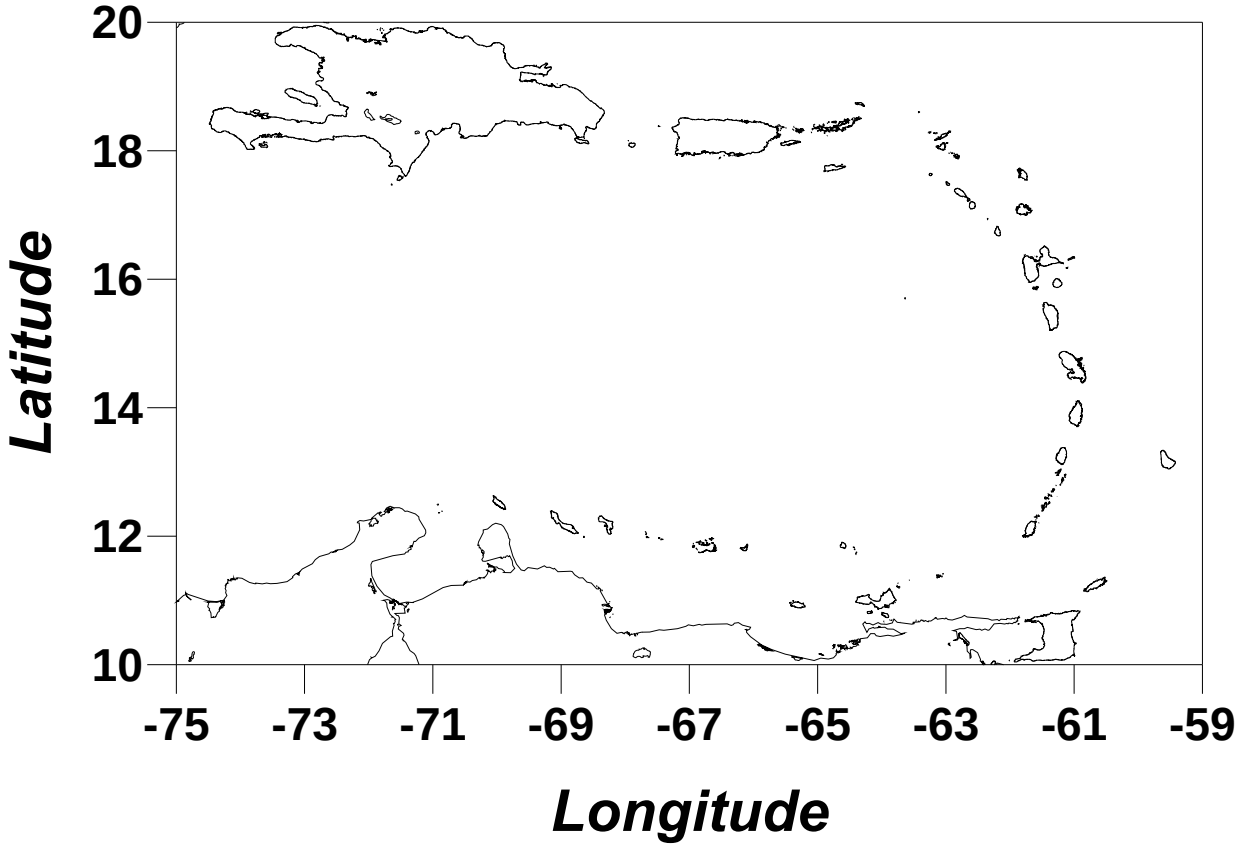

Figure 2.1. Map of the Eastern Caribbean Region sampled during ORIPEX and Cavortex expeditions..

2.2 Methodology

2.2.1 Field Work

Data was collected during four oceanographic cruises as part of the scientific expeditions of the Caribbean Vorticity Experiment (Cavortex) and the Orinoco river plume experiment (Oripex) on board the UPRM R/V Chapman and the LUMCON R/V Pelican. The Caribbean Vorticity Experiment (Cavortex II and VI) undertaken from June 22-27, 2004 and August 28, 2006 to September 8, 2006 respectively, were intended to characterize the physical, biogeochemical, and optical structure of the eddies and to assess their influence on biological productivity of the Eastern Caribbean Region. ORIPEX 7 and 8 cruises were carried out during November 19-24, 2005 and September 18-23, 2006, respectively, to analyze effects of the Orinoco River on the biogeochemical properties of the Eastern Caribbean Sea.

In order to identify, localize and to determine the trajectory of the eddies satellite acquired altimetry was used. JASON-1 Sea Surface Height Anomaly (J1SSHA) Product dataset, which is produced by Ssalto/*Duacs* and distributed by *Aviso*, with support from *CNES* were used. The use of ocean color products in the region was limited due to the high frequency of clouds, because the expeditions were performed during the period of influence of the Intertropical Convergence Zone (ITCZ).

In situ measurements were collected with a towed profiling vehicle (N*v*-Shuttle) manufactured by Chelsea Instruments Ltd, this maximized the spatial resolution and efficiency of the sampling. This vehicle is fitted with a Fast Repetition Rate Fluorimeter (FRRF) to measure the physiological state of phototrophic plankton, MINIpack (with a CTD-F and 24 channel integrated data logger capable of real time data acquisition), and a photosynthetically available radiation (PAR) irradiance meter. The N*v*-Shuttle was operated with continuous oscillations from surface to a maximum of 90 meters when possible. Diffuse attenuation coefficients were calculated over the depth of the euphotic zone according to $K_d = \ln[E(0^-)/E(Z_{1\%})] /Z$. The depth interval was chosen to extend from near the surface ($Z = 0^-$, i.e., ca 5 m) to the bottom of the euphotic zone ($Z=1\%E(0)$). The euphotic zone was defined as the depth at which irradiance is

diminished to 1% of the surface values, equivalent to an optical depth ($\xi = K_d Z$) of 4.6 (Kirk, 1994).

2.2.2 Variable Fluorescence

Variable fluorescence (Fv = *Fm – Fo*), photosynthetic efficiency (Fv/Fm, unit less), and functional absorption cross-section at photosystem II (σ_{PSII}, units $Å^2$ quantum $^{-1}$) were logged to an internal flash card in the FRRF and downloaded to a PC after each transect. The FRRF measures these parameters for seawater that is exposed to ambient irradiance, and also simultaneously on seawater passed through a 'dark chamber' placed in front of one of the photomultiplier tubes (PMT) window. Only the dark adapted data was analyzed, and most of the data presented in the analysis was gathered at night except when only day transects where possible. Data gathered during the day in the top 20 meters were considered unusable owing to saturation of the PMT from high surface irradiances and were removed. The instrument flash protocol was set for 100 saturation flashes per sequence with a saturating flash duration of 1.10 μs and an interflash delay of 51.6 μs. This was followed by 20 decay flashes each of 1.10 μs duration with an interflash delay of 51.6 μs. The raw data was processed using Chelsea's FRS processing software. Depth was provided by an internally logging, calibrated pressure sensor of the MINIpack throughout N*v*-Shuttle deployments. During some of the stations occupied the FRRF was mounted on a rossete sampler with an adjacent SeaBird SBE 19 SEACAT CTD profiler. CTD data was then processed, filtered, binned, and parameters derived using the SeaBird Data Processing software version 7.16a. Discrete depth water samples were also collected on all surveys using Niskin bottles mounted on the rosette sampler during upcasts. These water samples were processed for phototrophic plankton specific absorption data, chlorophyll-a, and nutrients. Concentration of chlorophyll-a was obtained from samples filtered through 0.7 μm glass fiber filters (Whatman GF/F) using the standard fluorometric method (Yentsch and Menzel, 1963) measured in a Turner AU-10 Fluorometer.

2.2.3 Bio-optical data

Chlorophyll-specific absorption coefficient of phototrophic plankton

Particulate absorption samples were collected on 0.7 μm GF/F filters and the absorption of the total particulate $a_p(\lambda)$ (relative to a blank filter saturated with distilled water) was measured with Perkin Elmer Lambda 18 UV/VIS Spectrometer fitted with an integrating sphere. Methanol extractable pigments were removed by slowly passing hot methanol through the filter pad (Roesler et al., 1989). The absorption spectrum of this pad was measured to determine the detritus absorption coefficient, $a_d(\lambda)$. Optical density measurements were divided by the geometrical path length (volume filtered divided by clearance area of the filter) and multiplied by a factor of 2.3 (conversion factor for transforming decimal logarithm to natural logarithm) to obtain the absorption coefficient. The value of the absorption coefficient at 750 nm was subtracted from the values at all other wavelengths, as a rudimentary correction for errors arising from cell scattering. The measurements were corrected for path-length amplification, β factor, using the method of Bricaud and Stramski (1990). The difference between the particulate and detritus spectra, before and after the methanol extraction, is considered the *in vivo* phototrophic plankton absorption, $a_{ph}(\lambda)$. The pigment specific absorption coefficient aph*(λ) was calculated by dividing absorption by the chlorophyll-a concentration obtained fluorometrically.

Bio-optical Rossette

The bio-optical rosette package deployed, include a ac-9 attenuation and absorption meter, Hydroscat-6 backscatter meter and a SeaBird SBE 19 SEACAT CTD. The ac-9 is designed to measure absorption, a, and beam attenuation, c, in 9 spectral bands (412, 440, 488, 510, 532, 555, 650, 676, and 715). Temperature and salinity along with scattering corrections were performed to the ac-9 data according to Pegau et al. (2001). Beam attenuation at 660 nanometers (nm) was measured by interpolation of ac-9 attenuation measurements at 650 nm and 676 nm. Hydroscat-6 measures volume scattering function at six spectral bands (442, 470, 510,589, 620, and 671) at a nominal

angle of 140 ° , β (140°) and backscatter b_b is estimated assuming a constant proportional between β (140°) and b_b [=2π (1.08) β (140°)] (Maffione and Dana, 1997).

The particle size distribution (PSD) slope was addressed for Cavortex 6 and 4 data by fitting a hyperbolic function to the particulate attenuation spectrum (Boss et al., 2001; Twardowski et al. 2001), this method provides an estimate of the spatial changes in the mean particle size. A factor of 3 was added to the slope, since, according to Boss et al. (2001) the attenuation spectral slope (γ) is related to the PSD slope (ξ) by $\xi = \gamma + 3$, in oceanic observations.

2.2.4 Flow cytometry during Cavortex 6

Flow cytometry analysis was performed on picoplankton samples gathered during the Cavortex 6 expedition. The samples were preserved and stored at -80 °C until analysis at the Flow Cytometry Facility , Department of Oceanography, Texas A&M University. *Prochlorococcus*, *Synechococcus* and pico-eucaryotic algal populations were then quantified using a Becton Dickinson FACSCalibur flow cytometer equipped with a 488 nm, 15 mW argon laser (Campbell, 2001).

2.4 Results

2.4.1 Variable Fluorescence during the Cavortex campaign

Variable fluorescence parameters (*Fv/Fm* and σ_{PSII}) across various mesoscale eddies was considered according to possible provinces (inside the cyclonic eddy, eddy edge, and anti-cyclonic eddy). Determined as areas within the observed satellite altimetry (Jason sea surface anomalies). For instance, the samples used for the analysis were consider to be in a cyclonic region when positioned at the lowest observed sea surface anomaly, and the opposite for the anticyclonic portion (e.g. Figure 2.2). Figure 2.2 shows the provinces determined during the Cavortex 6 analysis. During Cavortex 2 one transect was sampled extending from a cyclonic region to an anticyclonic region (Figure 2.3). For Cavortex 4 only data of the edge of the eddy was sampled with the FRRF therefore it is not analyzed in this section (Figure 2.4).

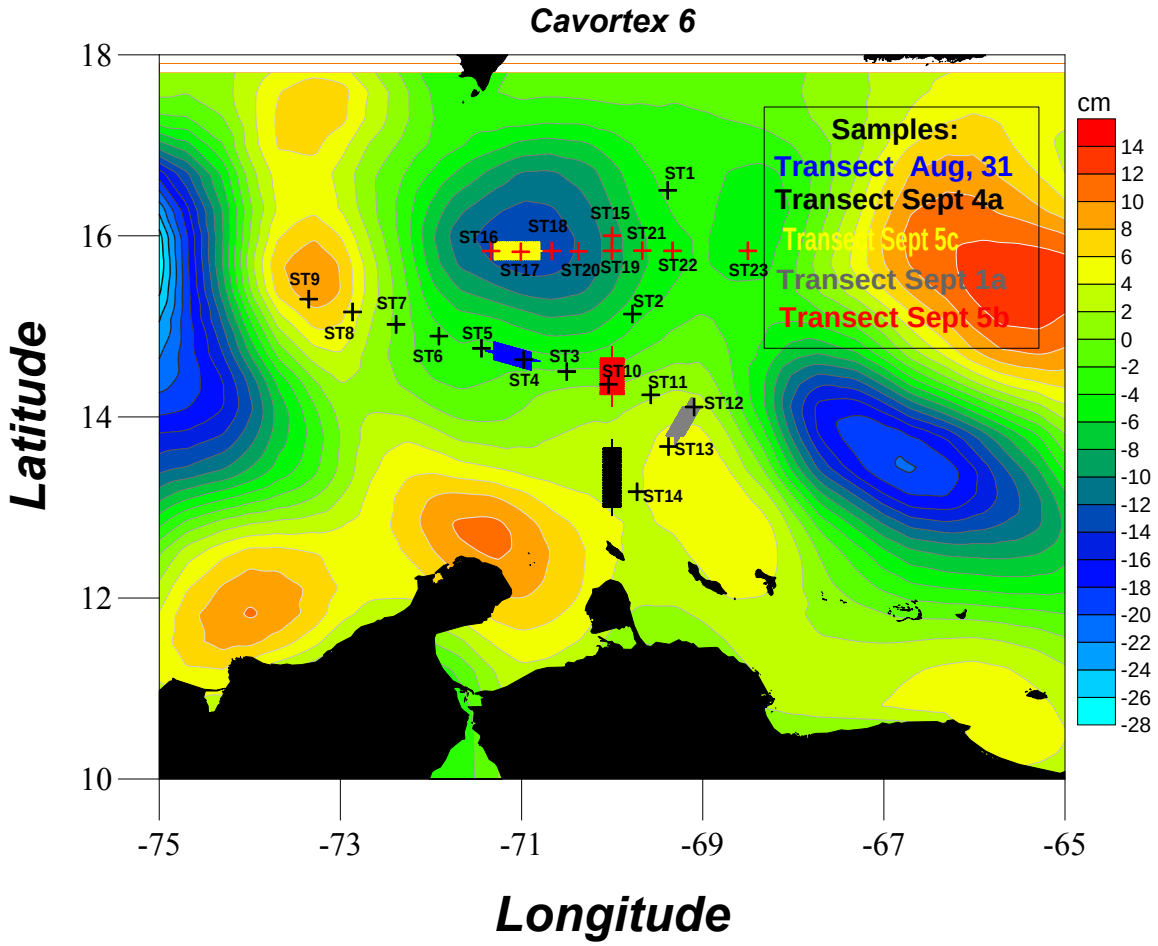

Figure 2.2 Sampled stations and transect during Cavortex 6 over Jason sea surface anomaly obtained from AVISO live access server (LAS). These altimeter products were produced by Ssalto/Duacs and distributed by *Aviso*, with support from *Cnes*.

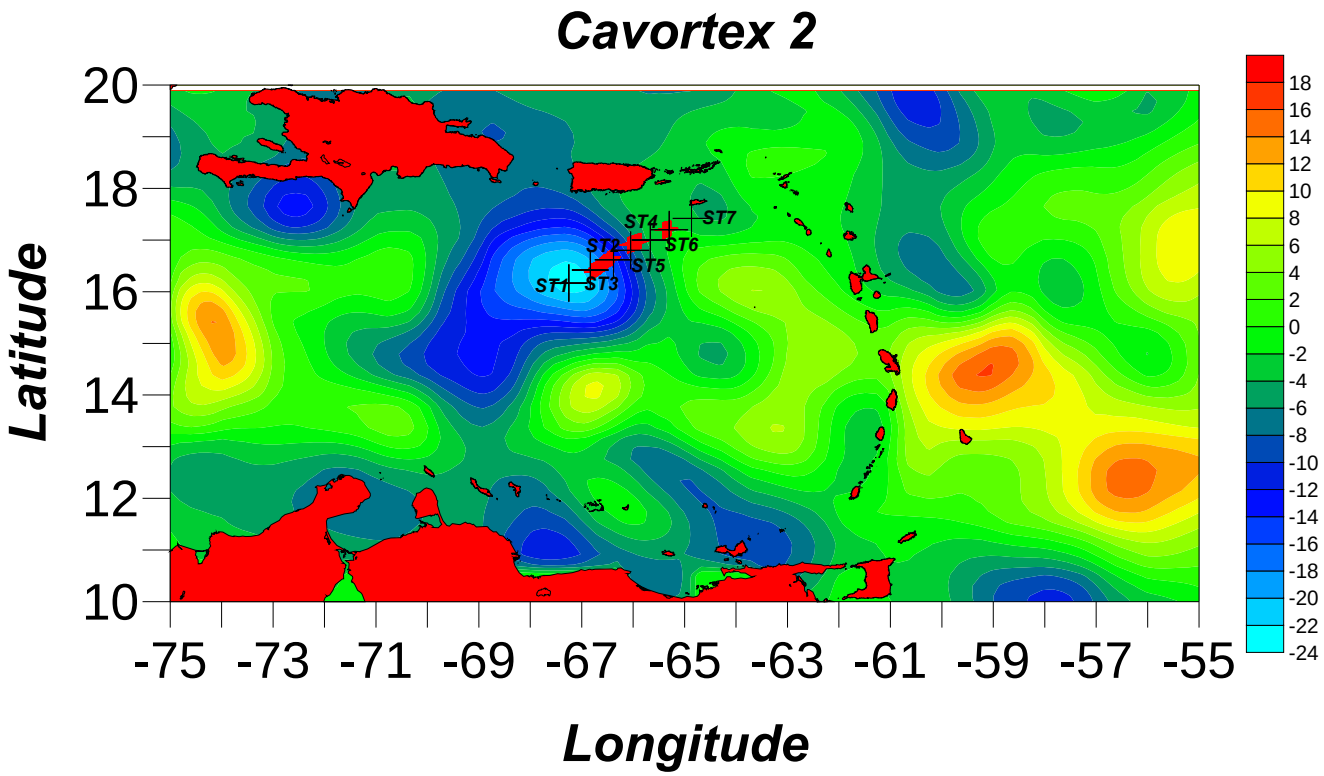

Figure 2.3. Sampled stations and transect during Cavortex 2 over Jason sea surface anomaly obtained from AVISO live access server (LAS). These altimeter products were produced by Ssalto/*Duacs* and distributed by *Aviso*, with support from *Cnes*.

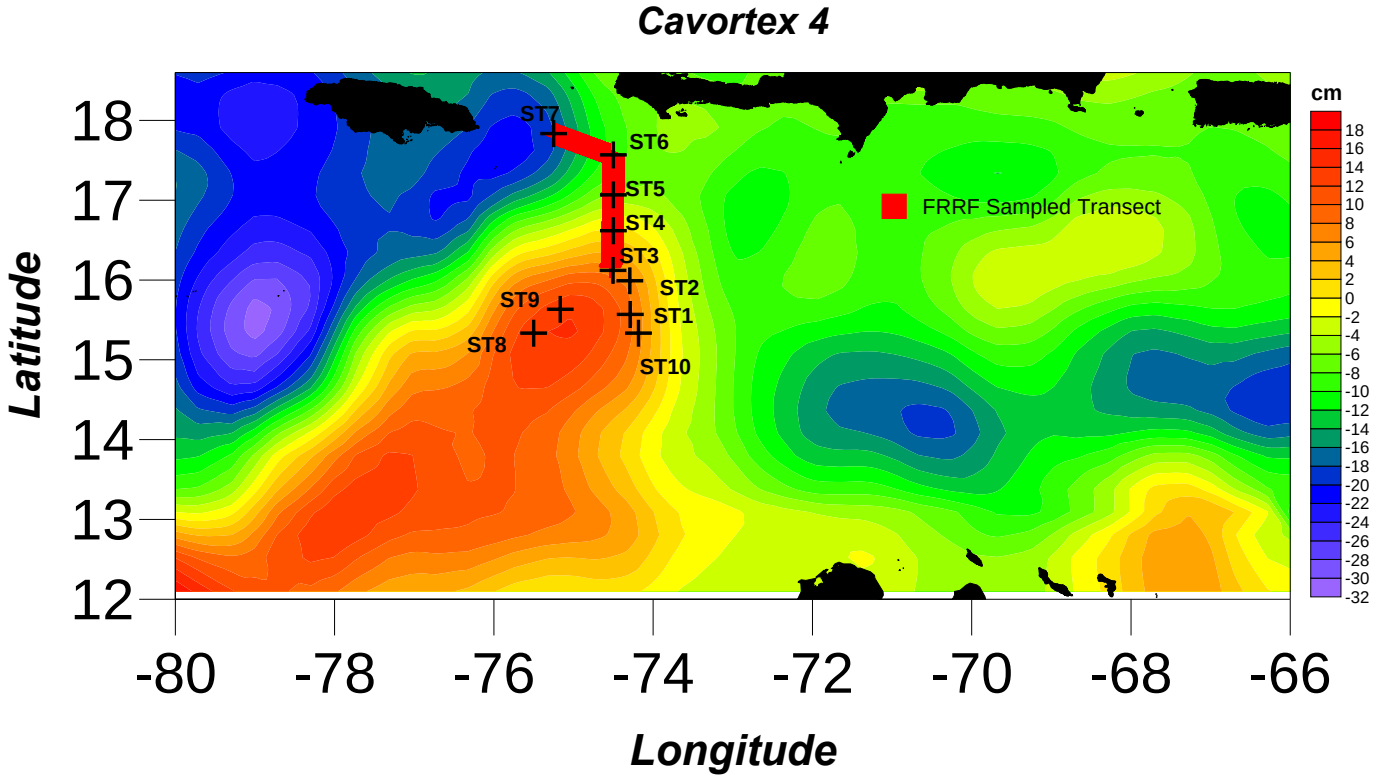

Figure 2.4. Sampled stations and transect during Cavortex 4 over Jason sea surface anomaly obtained from AVISO live access server (LAS). These altimeter products were produced by Ssalto/*Duacs* and distributed by *Aviso*, with support from *Cnes*.

Cavortex 6

The eddy edge of Cavortex 6 cyclonic eddy was sampled from east to west during the transect of August 31, and on September 5 (transect September 5b) from south to north (Figure 2. 2). During the transect of August 31, depressed *Fv/Fm* was apparent as a result from distinctive afternoon photo saturation of the photosystem II (photoinhibition) (Figure 2.5). According to Beherenfeld (et al., 1998) the diurnal pattern in variable fluorescence is a feedback interaction between changes in light intensity and PSII repair, specifically repair of photodamaged reaction centers through turnover of D1 proteins, inhibited when photosynthetic electron transport is saturated and stimulated when subsaturated (Gong and Ohad, 1991; Prasil et al., 1992). Nevertheless it can be observed that the effect was not enough to draw down the *Fv/Fm* to values below 0.30 (no units) as expected. The observed *Fv/Fm* during the afternoon ranged between to 0.30 and 0.37 (for the whole water column). Later into the night the *Fv/Fm* rose to values from 0.37 to 0.45 at surface, with increase in the value through the entire water column indicating a prevalence of higher photosynthetic potential through the water column. Evidence of a fast recovery of the photo-damaged centers is shown in Figure 2.5.

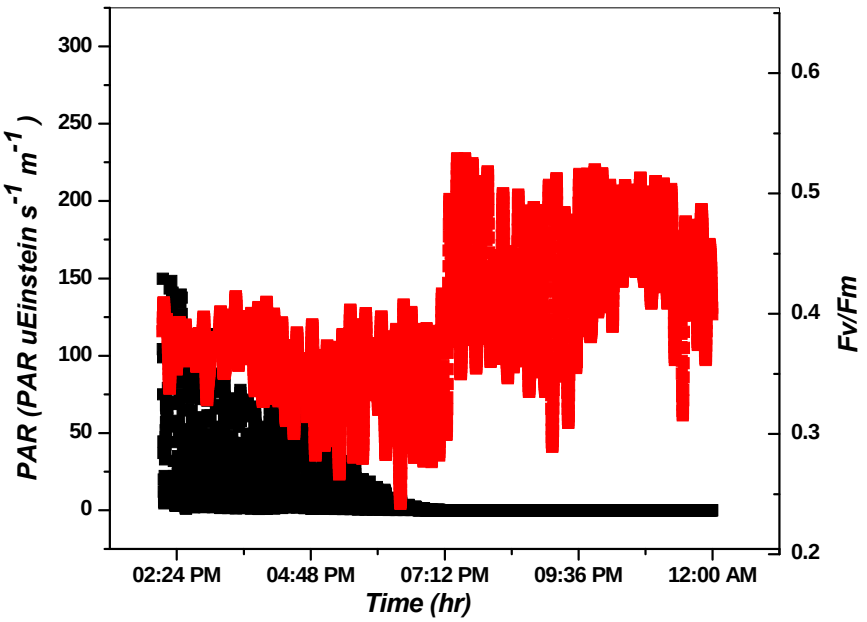

Figure 2.5 Photosaturation of photosystem II appeared depressed *Fv/Fm* values during late afternoon sampling but subsequent nighttime recovery denotes capacity for rapid photosytem repair during Cavortex 6 transect of august 31. Fv/Fm in red and PAR in black.

Considering the observed diurnal pattern on the *Fv/Fm,* only night sampled data was subsequently used for comparisons between provinces.

Surface *Fv/Fm* for this province ranged from 0.28 to 0.46 while in the deep portion *Fv/Fm* ranged from 0.31 to 0.53 (Table 2.1). The deep portion was considered to be from the 10 % of surface light around 60 to 90 meters, the greatest depth reached by the N*v*-Shuttle during the sampled transects. Surface was considered to be from 20 meters to the 10% of surface light.

Upwelling of cold water towards the surface appears to be the result of eddy edge shear against an anticyclone neighbor figure 2.6. When the samples were analyzed against transect isotherms, the coldest water temperature range was observed from 25.4 to 26.4 ° C (Table 2.2 and Figure 2.7) and showed an *Fv/Fm* that ranged from 0.29 to 0.53. The intermediate temperature range was considered to be from 26.8 to 28.2 ° C and *Fv/Fm* ranged from 0.34 to 0.53. Surface isotherms from 28.2 and up showed values from 0.30 to 0.52, suggesting the flow of material to surface as a result of the eddy-eddy interaction.

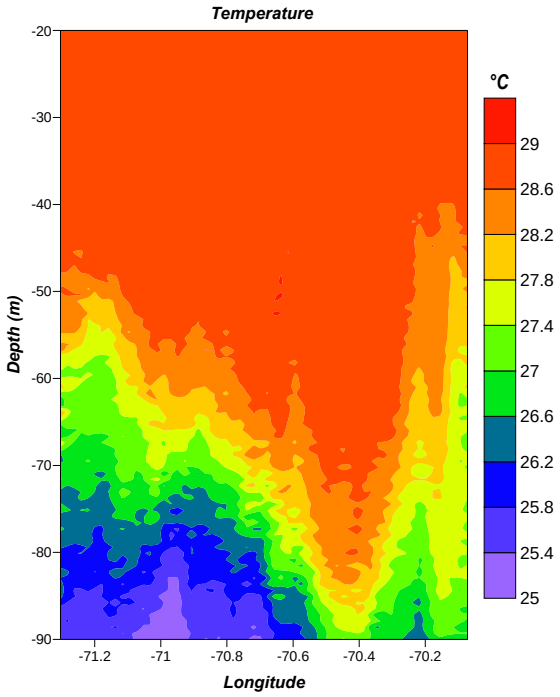

Figure 2.6. Temperature isotherms at cyclonic eddy edge during transect of August 31 during Cavortex 6 .

The center of the cyclonic eddy was sampled during the transect of September 5 through 8, 2006. The transect of September 5c started during the afternoon in a zonal

transect across the eddy. Temperature and salinity contour maps of the cyclonic eddy zone illustrate the upwelling of saltier colder water (Figure 2.8).

During the afternoon sampling the observed *Fv/Fm* showed depressed values (ranged from 0.28 to 0.40) due to light saturation of photosystem II, through the whole water column to the maximum sampled depth of 90 meters. These portions were analyzed against isotherm and *Fv/Fm* ranged from 0.40 to 0.51 at the coldest observed water mass 25.4 to 26.4 ° C. The intermediate temperatures ranges (26.8 to 28.2 ° C) showed *Fv/Fm* that ranged from 0.34 to 0.51, and at surface (above 28.2 ° C) ranged from 0.22 to 0.47.

The incursion of cold water from depth reached up to 65 meters in some portions of the eddy center (Figure 2.6) a negative relationship was observed when *Fv/Fm* against temperature was analyzed (Figure 2.9), denoting increase in *Fv/Fm* with colder

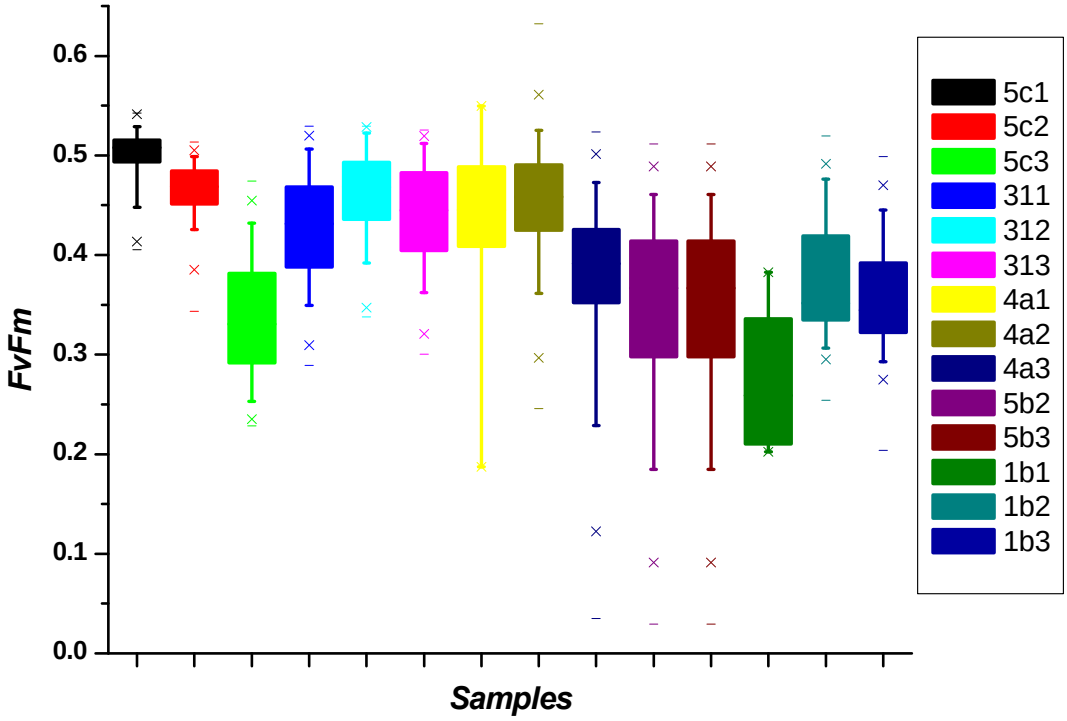

Figure 2.7. Phototrophic plankton photosynthetic efficiency per temperature ranges (Temperature Ranges 1 (*25.4 – 26.4 ˚C*) 2 (*26.8 – 28.2 ˚C*) 3 (*28.2 – 29˚C*)) through the sampled areas during Cavortex 6. (Example 5c1 corresponds to sample September 5c at temperature range 1).

Table 2.1. Phototrophic plankton Photosynthetic efficiency through the Cavortex 6 sampled regions analyzed at surface and depth

Sampled Transect	Mean	Standard Deviation	Standard Error	Lower Confidence Interval of the Mean	Upper Confidence Interval of the Mean	Median	Variance	Number of Points
Sept5c-Deep	0.45	0.067	0.001	0.45	0.46	0.47	0.004	2071
Sept5c-Surf	0.32	0.105	0.004	0.32	0.34	0.35	0.011	592
AUG31-Deep	0.43	0.047	0.001	0.44	0.44	0.44	0.002	1599
AUG31-Surf	0.38	0.037	0.002	0.38	0.38	0.38	0.001	350
Sept5b-Deep	0.40	0.069	0.001	0.39	0.40	0.40	0.005	2825
Sept5b-Surf	0.31	0.083	0.003	0.31	0.32	0.32	0.007	669
sept1-Surf	0.34	0.017	0.002	0.34	0.34	0.34	0.000	108
sept1-Deep	0.39	0.023	0.002	0.39	0.40	0.39	0.001	159
Sept4a-Surf	0.29	0.045	0.001	0.29	0.30	0.28	0.002	950
sept4a-Deep	0.36	0.036	0.001	0.36	0.36	0.37	0.001	1143

* surface was consider to be from 20 meters to the 10% of surface light and deep portion was considered to be from the 10 % of surface light around 60 m to 90 meters the deepest the N*v*-Shuttle dived during the sampled transects.

Table 2.2. Phototrophic plankton Photosynthetic efficiency through the Cavortex 6 sampled regions analyzed against isothermal temperature ranges

Sampled Transect	Mean	Standard Deviation	Standard Error	Lower Confidence Interval of the Mean	Upper Confidence Interval of the Mean	Minimum Value	Maximum Value	Median	Variance	Variation Coefficient	N
Sept 5c_1*	0.50	0.02	0.001	0.50	0.50	0.41	0.54	0.51	0.001	4.00	278
Sept 5c_2	0.46	0.02	0.001	0.46	0.47	0.34	0.51	0.47	0.001	4.35	394
Sept 5c_3	0.33	0.05	0.001	0.33	0.34	0.23	0.47	0.33	0.003	15.15	1276
Aug 31_1	0.42	0.05	0.001	0.43	0.43	0.29	0.53	0.43	0.003	11.90	1952
Aug 31_2	0.46	0.03	0.003	0.46	0.47	0.34	0.53	0.47	0.002	6.52	139
Aug 31_3	0.44	0.04	0.001	0.44	0.45	0.30	0.53	0.44	0.002	9.09	699
Sept 4a_1	0.43	0.08	0.023	0.39	0.49	0.19	0.55	0.45	0.008	18.60	14
Sept 4a_2	0.45	0.05	0.003	0.45	0.46	0.25	0.63	0.46	0.003	11.11	288
Sept 4a_3	0.37	0.07	0.004	0.37	0.39	0.04	0.52	0.39	0.005	18.92	335
Sept 5b_2	0.34	0.08	0.002	0.34	0.35	0.03	0.51	0.37	0.007	23.53	1155
Sept 5b_3	0.34	0.08	0.002	0.34	0.35	0.03	0.51	0.37	0.007	23.53	1155
Sept 7_1	0.50	0.01	0.002	0.50	0.51	0.46	0.53	0.50	0.000	2.00	74
Sept 7_2	0.46	0.02	0.002	0.46	0.47	0.41	0.51	0.47	0.001	4.35	69
Sept 7_3	0.42	0.02	0.002	0.42	0.43	0.34	0.49	0.43	0.001	4.76	120
Sept 1b_1	0.27	0.06	0.014	0.24	0.30	0.20	0.38	0.26	0.004	22.22	19
Sept 1b_2	0.37	0.05	0.002	0.37	0.38	0.25	0.52	0.35	0.003	13.51	416
Sept 1b_3	0.35	0.04	0.002	0.35	0.36	0.20	0.50	0.34	0.002	11.43	501

Legend: *Temperature Ranges 1 *25.4 – 26.4* **2** *26.8 – 28.2* **3** *28.2 - 29*

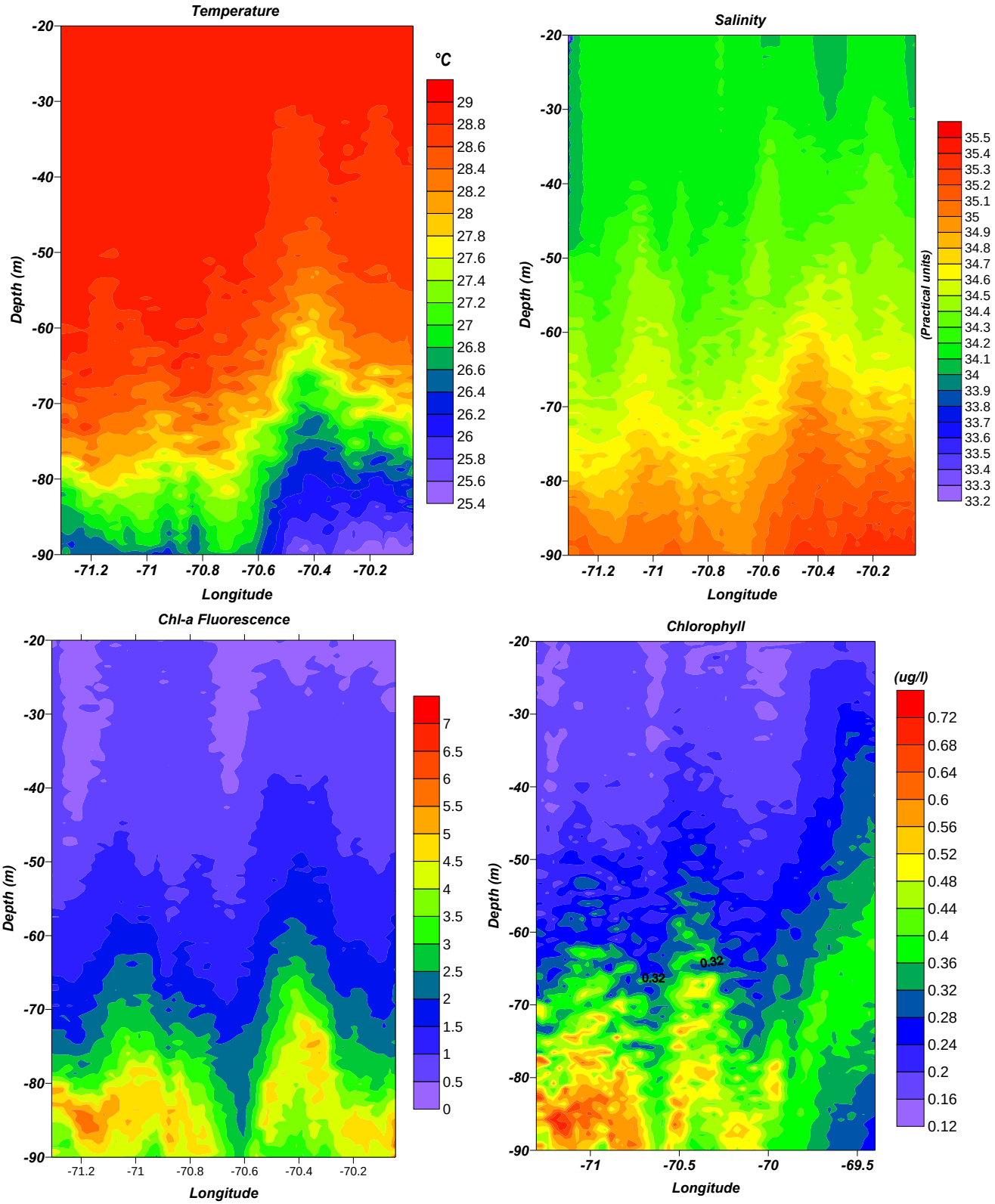

Figure 2.8 Sampled parameters at cyclonic eddy center during transect of September 5 during Cavortex 6.

water (at eddy center, between 60 and 90 meters) which suggest input of materials to the euphotic zone of the cyclonic eddy. The contour plot in figure 2.10 demonstrates this relationship between *Fv/Fm* and temperature. *Fv/Fm* was analyzed against Sigma -t at stations 18 and 20 (Figure 2.11) and showed a high positive correlation between the parameters (r= 0.97 and 0.86 respectively), indicating also higher photosynthetic potential possibly due to advection of nutrients into the euphotic zone.

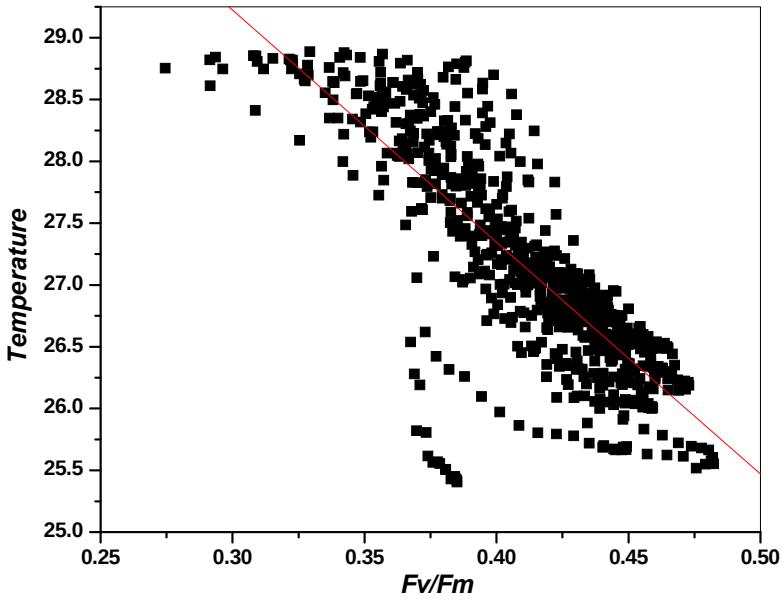

Figure 2.9. Temperature and photosynthetic efficiency relationship at eddy center (between 60 and 90 meters) during Cavortex 6. The correlation coefficient r was -0.80, n=764.

The σ_{PSII} varied inversely with *Fv/Fm* with higher correlation at the surface temperature range (above 28.2 ° C) R = 0.8 (Figure 2.12); at the lowest temperature range no apparent relationship was observed. The coldest temperature range showed σ_{PSII} values that ranged between 319 to 614 (A^2 / quanta) the intermediate range from 361 to 691 (A^2 / quanta), and near-surface 165 to 947 (A^2 / quanta) (Table 2.3).

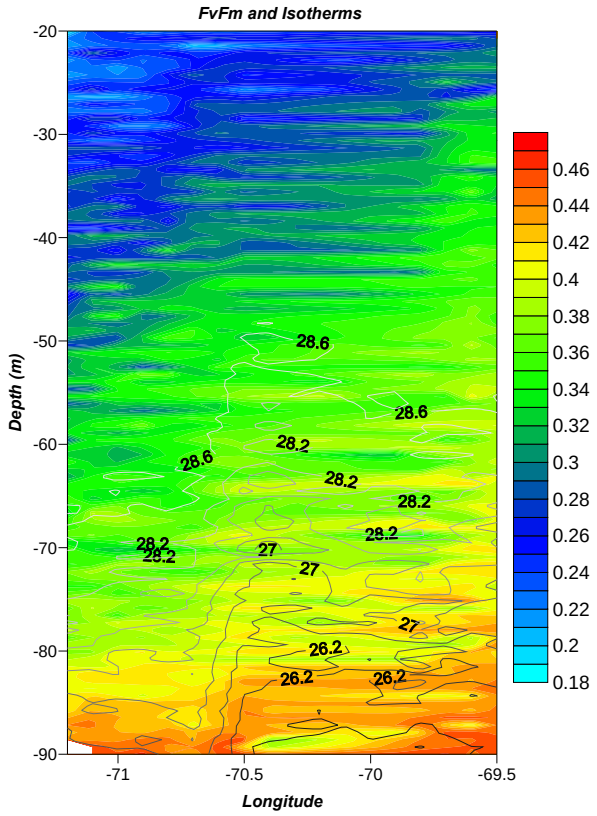

Figure 2.10. Photosynthetic Efficiency and temperature isotherms at cyclonic eddy during Cavortex 6 .

A single factor ANOVA province-specific analysis (including cyclonic, anticyclonic eddy edge and waters outside the eddy influence) showed significant differences between provinces ($a= 0.05$ $P < 0.001$) with a marked increase in the photosynthetic potential for waters inside the cyclonic zone.

The September 1, 2006 transect over an anti cyclonic zone showed a decrease on the *Fv/Fm* from values around 0.49 to 0.31. When the water temperature ranges were examined for this area (Table 2.2) the deepest colder water regime demonstrated an *Fv/Fm* that varied from 0.20 to 0.38 with a mean value of 0.27. The surface and intermediate water temperature ranges showed values that ranged from 0.25 to 0.49. The relationship of *Fv/Fm* and Sigma T in this area was also addressed for stations 11. This relationship for station 11 and a portion of transect of September 1b showed lower correlation ($r= 0.52$ and 0.75 respectively) (Figure 2.13). The σ_{PSII} at the coldest temperature range showed values that ranged between 352 to 948(A^2 / quanta), the

intermediate range was 388 to 882 (A^2 / quanta) and near-surface 790 to 1240 (A^2 / quanta) (Table 2.3).

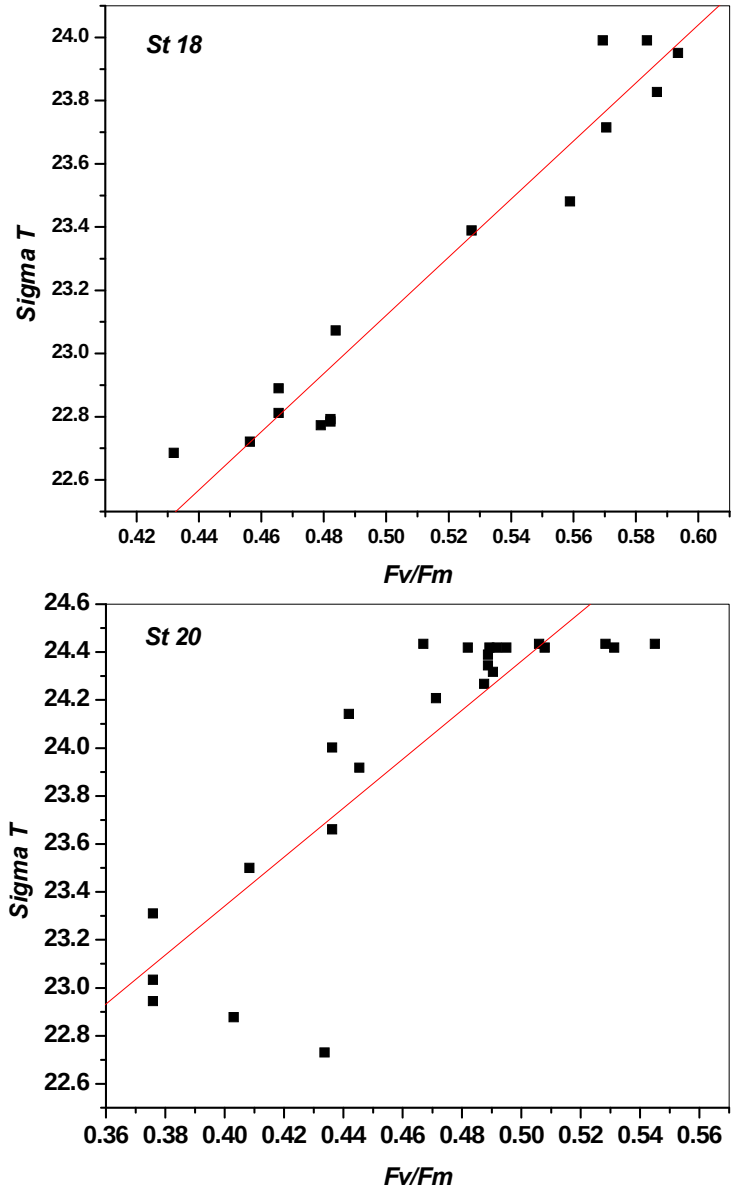

Figure 2.11. Phototrophic plankton photosynthetic efficiency against Sigma-t at cyclonic eddy center from 40 to 90 meters. The observed correlation coefficients for the station 18 and 20 was of 0.97 and 0.86 respectively.

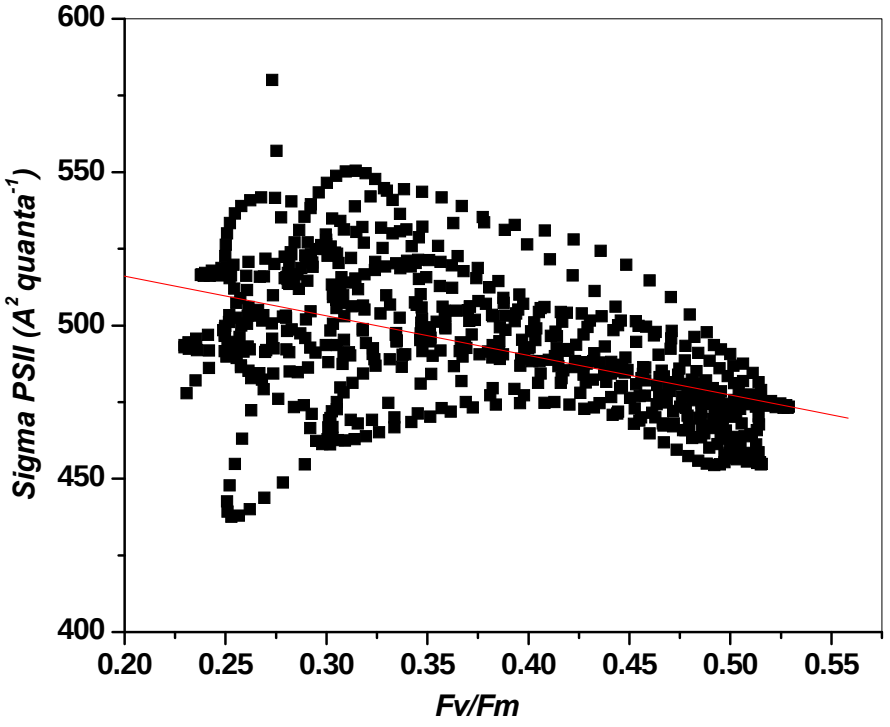

Figure 2.12. Functional absorption cross-section correlation with photosynthetic efficiency at cyclonic eddy center during Cavortex 6. The observed correlation coefficient was r = -0.5.

On September 4, 2006 a portion of the transect was analyzed in an area that by satellite altimetry showed no sea surface anomaly (Figure 2.2). For this portion of the expedition mean surface *Fv/Fm* were around 0.38 at surface, and the deepest coldest water range (25.4-26.4) showed a mean value of 0.44 (Table 2.2 and Figure 2.7). The σ_{PSII} at the coldest temperature range showed values that ranged between 425 to 700 (A^2 / quanta), the intermediate range was 370 to 700 (A^2 / quanta) and at surface 1240 to 790 (A^2 / quanta) (Table 2.3).

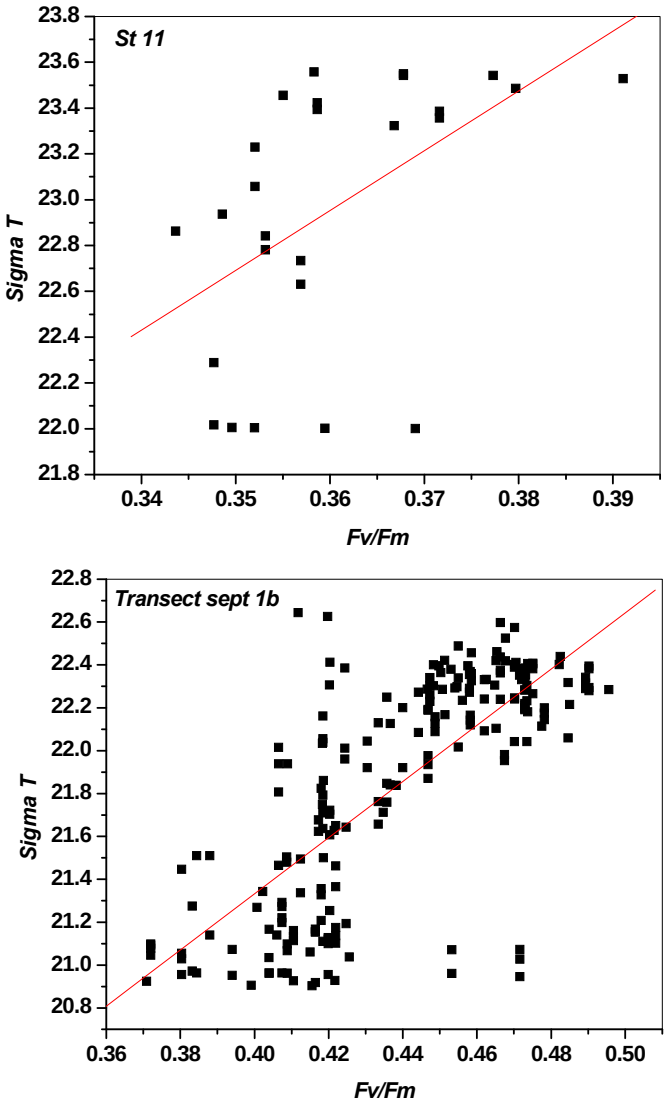

Figure 2.13. Phototrophic plankton photosynthetic efficiency against sigma-t at anti-cyclonic area from 40 to 90 meters. The observed correlation coefficients for the station 11 and transect Sept 1b was of 0.51 and 0.75 respectively.

Table 2.3. Phototrophic plankton photosynthetic functional absorption cross-section through the Cavortex 6 sampled regions analyzed against isothermal temperature ranges

Sampled Transect	Mean	Standard Deviation	Standard Error	Lower Confidence Interval of the Mean	Upper Confidence Interval of the Mean	Minimum Value	Maximum Value	Median	Variance	Variation coefficient	N
Sept 5c_1*	481.47	50.77	4.42	472.72	490.21	319.21	614.29	472.84	2577.97	10.54	132
Sept 5c_2	465.16	41.13	2.07	461.08	469.23	361.43	691.12	462.06	1691.55	8.84	393
Sept 5c_3	483.80	100.76	2.30	479.29	488.32	165.01	947.76	475.04	10152.47	20.83	1916
Aug 31_1	501.54	66.44	5.64	490.39	512.68	234.94	700	491.66	4414.24	13.25	139
Aug 31_2	509.90	63.77	2.41	505.16	514.64	296.73	813.36	501.13	4067.00	12.51	699
Aug 31_3	515.97	72.56	2.39	511.27	520.66	329	911.57	507.26	5265.24	14.06	920
Sept 4a_1	563.39	73.94	13.28	536.26	590.51	424.99	700	568.16	5467.15	13.12	31
Sept 4a_2	526.44	57.33	3.72	519.11	533.78	369.84	700	523.16	3286.98	10.89	237
Sept 4a_3	524.14	88.75	4.65	515.00	533.28	213.9	784.12	525.85	7877.03	16.93	365
Sept 7_1	480.52	51.70	4.48	471.65	489.39	324	700	478.37	2672.90	10.76	133
Sept 7_2	492.21	46.89	6.00	480.20	504.22	389.52	636.67	492.05	2199.12	9.53	61
Sept 7_3	514.40	78.63	5.05	504.44	524.36	313.1	886.81	506.06	6183.15	15.29	242
Sept 1b_1	580.17	143.68	33.87	508.72	651.62	351.77	948.06	559.45	20644.65	24.77	18
Sept 1b_2	599.33	81.61	3.75	591.97	606.70	387.78	882.26	591.34	6660.12	13.62	474
Sept 1b_3	545.21	96.87	3.61	538.13	552.28	239.75	790.44	548.90	9383.65	17.77	722
Sept 5b_2	513.94	55.81	2.10	509.82	518.07	331.84	701.53	510.88	3114.36	10.86	706
Sept 5b_3	507.74	91.41	2.65	502.54	512.95	226.13	959.67	507.65	8356.52	18.00	1189

Legend: *Temperature Ranges 1 *25.4 – 26.4* **2** *26.8 – 28.2* **3** *28.2 - 29*

Cavortex 2

During Cavortex 2 the interaction of a cyclonic eddy with and anti cyclonic eddy was sampled. Increased photosynthetic potential was observed through the sampled transect in correspondence with the input of colder water from depth at the cyclonic portion. This is an observation consistent with dynamics of this parameter during Cavortex 6 (Figure 2.14). *Fv/Fm* at the coldest sampled temperature range was around 0.53. The shallower depth where this temperature regime was sampled was 55 meters. The cyclonic and the anti cyclonic portions at depths from 40 to 70 meters showed elevated *Fv/Fm* (0.51 and 0.49 respectively). A single factor ANOVA ($a= 0.05$ $P< 0.001$) demonstrated that are significantly different photophysiological capacity in two these areas. The statistical analysis summary of the area is presented in table 2.4 and figure 2.15. The σ_{PSII} varied inversely with *Fv/Fm* along the transect, the coldest temperature range showed the strongest inverse relationship ($r = 0.83$). The anti cyclonic eddy portion showed a minor relationship between the parameters at the same temperature range ($r = 0.2$).

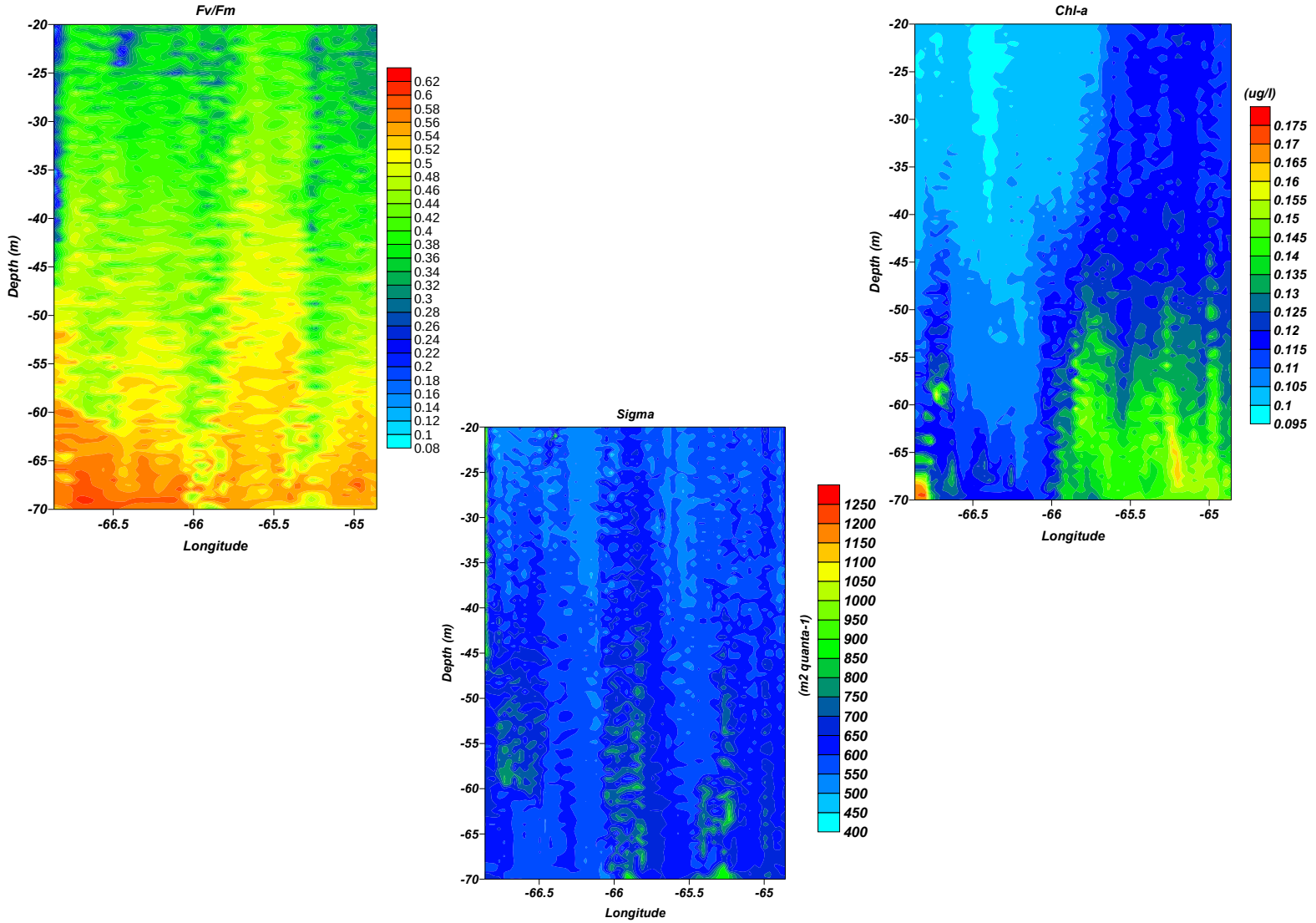

Figure 2.14. Phototrophic plankton photosynthetic efficiency, chlorophyll concentration and photosystem II photo absorbance cross-section during Cavortex 2.

Table 2.4. Phototrophic plankton Photosynthetic Efficiency (FvFm) and functional absorption cross-section of photosystem II (σ_{PSII}) statistical analysis against isothermal temperature ranges for the eddy pair sampled during Cavortex 2.

Region	Mean	Standard Deviation	Standard Error	Lower Confidence Interval of the Mean	Upper Confidence Interval of the Mean	Minimum Value	Maximum Value	Median	Variance	Variation Coefficient	N
FvFm											
Cyclon 1*	0.53	0.05	0.002	0.52	0.53	0.39	0.62	0.55	0.002	9.43	551
Cyclon 2	0.48	0.05	0.002	0.47	0.48	0.26	0.59	0.47	0.003	10.42	723
Cyclon 3	0.35	0.09	0.002	0.34	0.35	0.07	0.54	0.35	0.008	25.71	1806
Ant 1	0.55	0.02	0.002	0.54	0.55	0.48	0.59	0.54	0.000	3.64	118
Ant 2	0.49	0.04	0.001	0.49	0.49	0.26	0.57	0.49	0.002	8.16	1189
Ant 3	0.38	0.06	0.001	0.385	0.39	0.18	0.55	0.38	0.003	15.79	2166
σ_{PSII}											
Cyclon 1	642.16	79.25	3.37	635.53	648.80	543.49	818.29	606.45	6280.59	12.34	551
Cyclon 2	637.55	69.92	2.60	632.44	642.65	477.11	977.23	619.08	4889.05	10.97	723
Cyclon 3	620.76	183.48	4.31	612.29	629.23	368.44	1676.19	571.49	33665.1	29.56	1806
Ant 1	669.69	32.49	2.99	663.76	675.61	605.19	752.05	669.68	1055.95	4.85	118
Ant 2	678.89	86.12	2.49	673.99	683.79	530.20	895.30	649.28	7417.58	12.69	1189
Ant 3	587.81	45.89	0.98	585.87	589.74	483.46	777.44	586.03	2106.46	7.81	2166

Cyclon = Cyclonic Eddy Ant = Anti Cyclonic Eddy

***Temperature Ranges 1** *25.4 – 26.4* **2** *26.8 – 27.6* **3** *27.6 - 29*

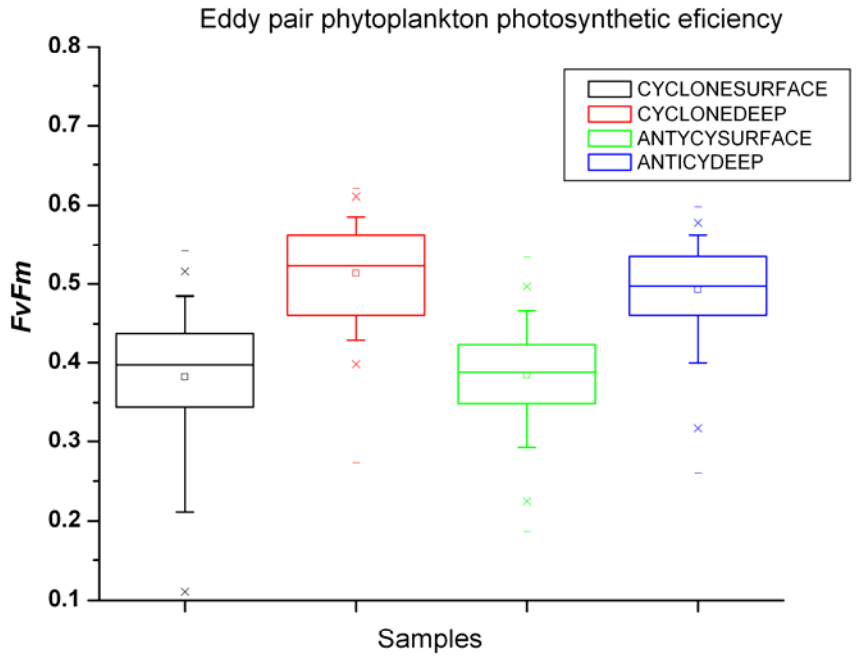

Figure 2.15. Phototrophic plankton photosynthetic efficiency at eddy pair during Cavortex 2.

2.4.2 Bio-Optical data

Chlorophyll-specific absorption coefficient of phototrophic plankton

During Cavortex 6 the specific absorption coefficient of phototrophic plankton showed consistent peaks (Figure 2.16) between the zones (surface and Deep chlorophyll maximum) for the majority of the samples. Surface absorption curves denoted uniformity in the spectra, indicating the prevalence of similar pigments comprising the total spectra. The shape and magnitude of the absorption spectra for phototrophic plankton are reflections of the pigment composition and concentration. Each group has its own pigment signature, and the combination of the pigments that compose this signature determines the shape of the absorption spectra (Lohrenz et al., 2003). The magnitude of the absorption was observed to be higher for stations 4, 15, and 17. The last two were sample within the center of the cyclonic area and station 4 at the edge of this area. The

magnitude of the absorption is influenced by pigment composition and packaging. Pigment packaging is a function of two properties of the cell: its size and its intracellular pigment concentration (Platt and Jasby, 1976). An increase in cell size or intracellular pigment concentration will result in a corresponding decrease in pigment absorption efficiency (Platt and Jasby, 1976; Sathyendranath et al., 1987). This decrease in the *in vivo* specific absorption of aggregated pigments, compared with that of the same quantity of pigment evenly dispersed in solution, is referred to as the packaging or flattening effect (Kirk, 1994). Deep chlorophyll maximum (DCM) samples demonstrated a similarly distributed spectrum. All the sampled spectra denote a typical accessory shoulder in the area between 470-480 nm, this region of the spectra is one where the accessory chlorophylls and carotenoids have their maximum absorptions. These shoulders have been related to marked increases in the concentration of divinyl chlorophyll-b within and below the DCM (Bouman et al., 2000) and are characteristic of samples taken in deeper layers of blue subtropical waters (Bricaud and Stramski, 1990; Sathyendranath, 1992; Hoepffner and Sathyendranath, 1992; Lee- Borges, 2003). This shoulder is notably in the samples of the DCM where the peak of absorption of chlorophyll–a at 442 nm has a lower magnitude, that is comparable with the accessory shoulder creating a flattening of the spectra between 440 to 550 nm. Phototrophic plankton cells at the DCM may show and increase in the packaging within the cell due to increase in the amount of pigments as an adaptation to a lower light regime; therefore a decrease in the magnitude of the absorption is expected. In summary, there are two main sources of variation in the magnitude and shape of the absorption coefficient: changes in pigment composition and changes in pigment packaging (Bricaud et al., 1988; Lee-Borges, 2003).

For these samples no apparent differences are observed in the spectra apart from differences in the magnitude of the absorption. The spectra for all stations also showed similar magnitudes within the areas indicating consistency in the pigments and in the populations sampled through this region of the eastern Caribbean. Surface samples presented higher absorption coefficients specially at stations, 15, and 17 (Figure 2.16), that coincidently were associated to the cyclonic event. Smaller cells have lower pigment

packaging than larger cells of the same intracellular pigment concentration, leading to a higher absorptive efficiency per unit pigment (Platt and Jassby, 1976).

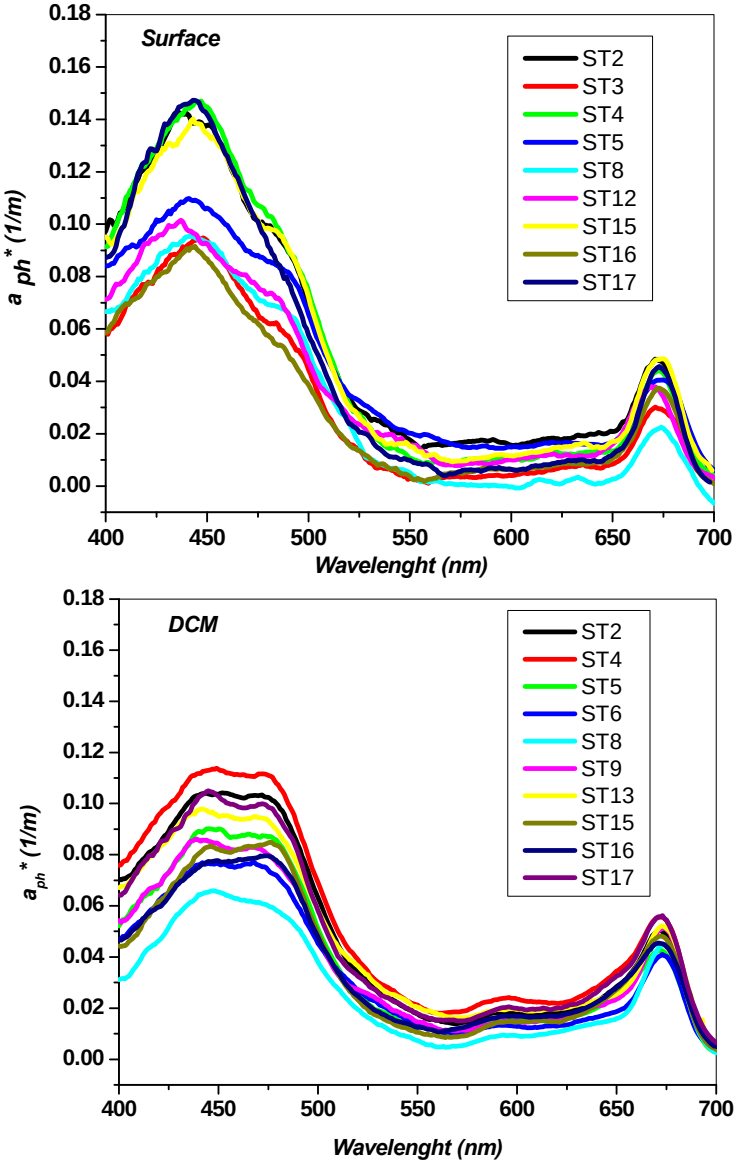

Figure 2.16. Chlorophyll-specific absorption coefficient of phototrophic plankton at stations during Cavortex 6.

A summary of discrete samples for surface and DCM is presented in table 2.5, in it a significant positive relationship between the phototrophic plankton specific absorption ratios 674/442 and 676/490 and *Fv/FM* was found (r = 0.53 and r = 0.48

respectively at $P < 0.05$). The study of Aiken et al.(2004) in the western English Channel demonstrated that the optical ratio a674/a443 and Chla/Tpig significantly correlated with *Fv/Fm* through changes in an annual cycle indicating optical signatures for these parameters. In this study chlorophyll concentration (sampled along with the absorption samples) also showed a significant relationship with *Fv/Fm* ($r = 0.76$ $P < 0.05$). Data from the iron enrichment experiments, IronEx II (Behrenfeld et al., 1996) and SOIREE (Boyd et al., 2000; Boyd & Abraham, 2001) showed significant linear correlations between Chla/Tpig and *Fv/Fm* (at night). Aiken et al.(2004) established that the relationship of *Fv/Fm*, Chla/Tpig and the optical ratio a674/a443 is greater when plants are actively growing. During periods of nutrient sufficiency all of these parameters are linear functions of mean total photon flux.

Table 2.5 Summary of phototrophic plankton chlorophyll-specific absorption coefficients and photosynthetic efficiency for discrete samples during Cavortex 6.

Station	Mean aph *	a674/442	a674/490	Chl-a (mg/l)	Fv/Fm	σ (A^2/quanta)	aph * 442	aph * 676
2 DCM	0.09	0.54	0.70	0.10	0.344	605	0.029	0.112
3 DCM	N/A	0.28	0.48	0.18	0.507	520	0.016	0.023
4 DCM	0.05	0.49	0.59	0.21	0.528	586	0.023	0.053
5 DCM	0.04	0.48	0.61	0.19	0.541	509	0.017	0.040
6 DCM	0.03	0.54	0.71	0.19	0.445	566	0.015	0.039
7 DCM	N/A	0.15	0.39	0.28	0.433	609	0.030	0.011
8 DCM	0.03	0.71	0.89	0.32	0.530	597	0.020	0.044
15 DCM	0.04	0.60	0.72	0.21	0.478	637	0.018	0.046
16 DCM	0.04	0.59	0.68	0.28	0.613	453	0.021	0.043
17 DCM	0.05	0.54	0.68	0.27	0.587	467	0.027	0.053
21 DCM	0.06	0.36	0.65	0.25	0.541	510	0.039	0.052
2 s	0.06	0.36	0.55	0.09	0.340	671	0.012	0.046
3 S	0.03	0.34	0.60	0.07	0.422	280	0.007	0.029
4 S	0.05	0.29	0.48	0.09	0.317	497	0.013	0.042
5 S	0.05	0.37	0.55	0.14	0.338	562	0.014	0.040
7 S	0.04	0.17	0.33	0.14	0.331	573	0.021	0.025
8 S	0.03	0.26	0.37	0.12	0.297	607	0.011	0.021
15 S	0.05	0.34	0.55	0.09	0.463	556	0.012	0.048
16 S	0.03	0.45	0.74	0.11	0.381	528	0.010	0.036
17 S	0.05	0.32	0.56	0.15	0.410	443	0.023	0.043

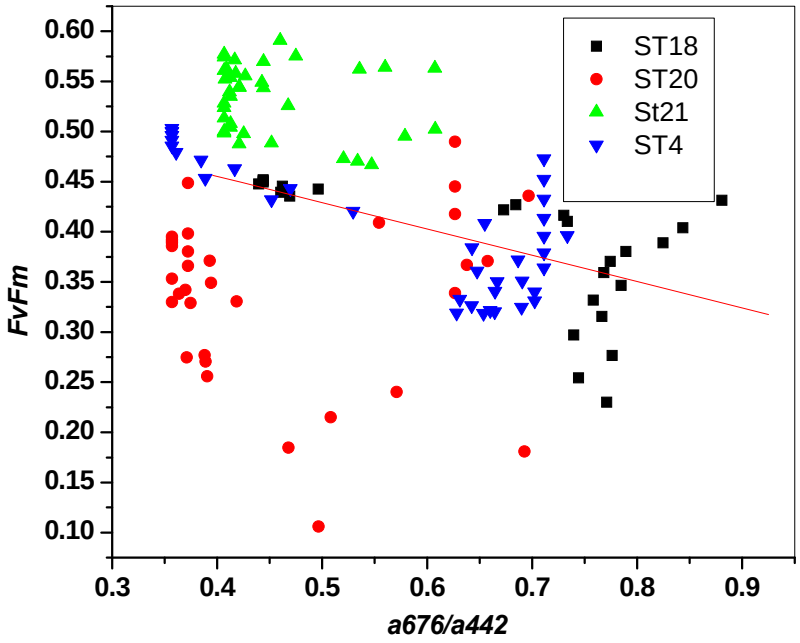

Figure 2.17. Phototrophic plankton photosynthetic efficiency and absorption ratio 676/442 relationship for stations at cyclonic eddy center and edge during Cavortex 6. The observed correlation coefficient was r = -0.60.

For Cavortex 6, the ac-9 cast profiles (from 40 to 90 meters) of the a676/a442 ratio analyzed against *Fv/Fm* showed a significant negative relationship ($R = -0.60$ $P < 0.001$), for the stations at the eddy center and edge (Figure 2.17). The stations at the anti-cyclonic region showed a significant positive relationship ($R = 0.71$ $P < 0.001$) (Figure 2.18). This apparent discrepancy in the regions probably is related to differences in the physiological state of the cells between the provinces; as previously stated the samples at the eddy center and edge are exposed to new environmental conditions as water from depth surface, which promotes higher *Fv/Fm*. This increase in *Fv/Fm* occurs in a matter of hours as observed by the observations in iron enrichment experiments in the Southern Ocean (Boyd & Abraham, 2001), possibly leading to an increase in chlorophyll absorption at a different time scales. The samples of the anti-cyclonic portion are in a stratified and stable environment where the variations in *Fv/Fm* are not related to the availability of new nutrients but to recycling of materials. In the steady nutrient conditions *Fv/Fm* may remain high even while phototrophic plankton growth remains low (Parkhill et al., 2001). During Cavortex 2 stations 3 and 6 showed the same

negative correlation, (R = -0.76 P< 0.001) (Figure 2.19); station 3 was sampled close to the center of the cyclonic eddy and station 6 at the edge with an anti-cyclonic area.

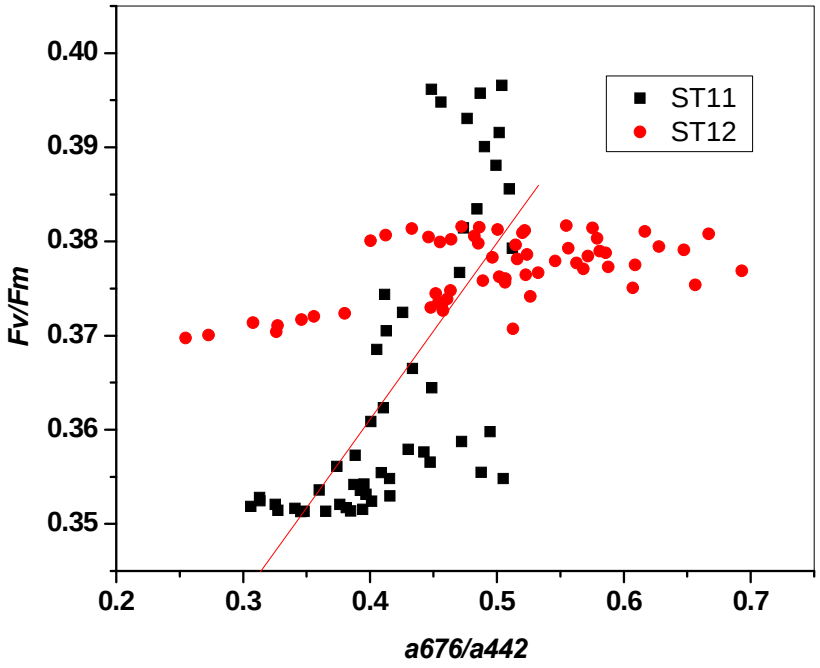

Figure 2.18. Phototrophic plankton photosynthetic efficiency and absorption ratio 676/442 relationship for stations at anti-cyclonic eddy during Cavortex 6. The observed correlation coefficient was r = 0.71.

The beam attenuation at 660 nm showed a positive relationship with chlorophyll concentration through all the samples implying that changes in chlorophyll were related to changes in phototrophic plankton abundance through the sample areas, and not to intracellular changes in chlorophyll concentration which is indicative of photoacclimation. It is important to note that the samples used in the analysis are from 40 to 90 meters, therefore their degree in photoacclimation should be similar.

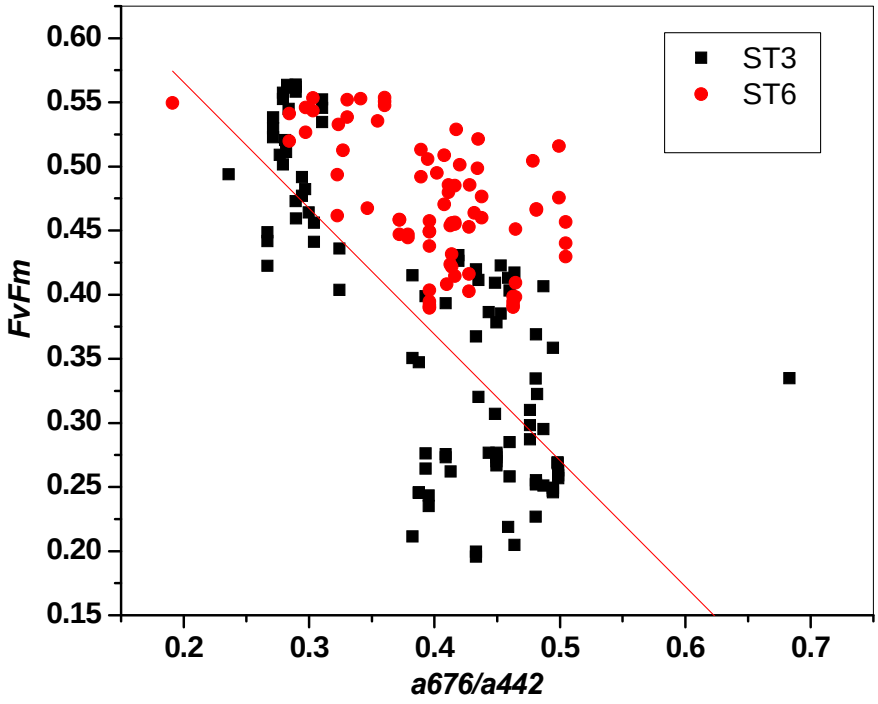

Figure 2.19. Phototrophic plankton photosynthetic efficiency and absorption ratio 676/442 relationship for stations at cyclonic eddy center and edge during Cavortex 2. The observed correlation coefficient was r = -0.76.

The beam attenuation (c_p) cast profiles (Figure 2.20) for the stations during Cavortex 6 showed higher beam attenuation near surface declining at around 80 meters. The chlorophyll normalized beam attenuation at 660 nm (c_p*) was observed to vary accordingly to eddy features during Cavortex 2 and 6 (Figure 2.21 and 2.22). Cavortex 6 stations inside the cyclonic eddy showed lower attenuation than stations outside (st 11 and 12) or at the edge (st 3 and 4) (Figure 2.20). Cyclonic eddies are characterized by the uplifting of isopycnals and the creation of a concave depression at surface as water is moved out of the center, consequently this lower attenuation may be attributed to fewer particles as this waters emerge from depths below the euphotic zone.

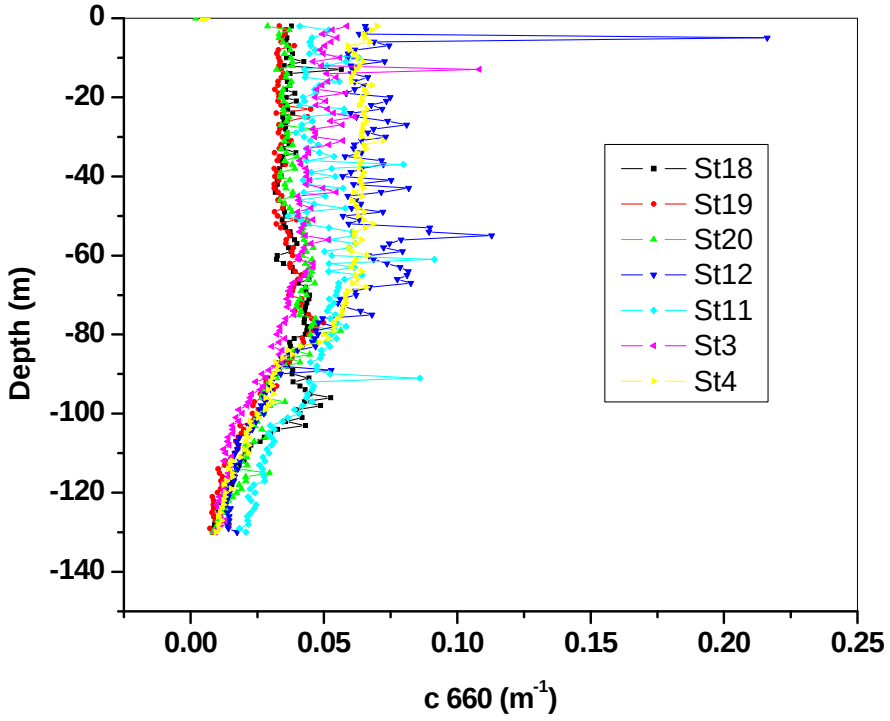

Figure 2.20. Beam attenuation coefficient at 660 (nm) with depth through the sampled regions during Cavortex 6. Higher beam attenuation is observed at stations outside of the cyclonic eddy. Stations 18,19,20 were sampled inside the cyclonic eddy, stations 3 and 4 were sampled at the eddy edge, and stations 11 and 12 at a portion with anti-cyclonic altimetry.

When the c_p* was related to *Fv/Fm* an inverse relationship (Figure 23) (R = -0.94, P= 0.0001) was observed at stations in the cyclonic eddy center and edge during Cavortex 6. The stations at the anti-cyclonic portion showed a direct relationship, stations 11 and 12 (R= 0.81 and 0.54 respectively P= 0.0001) (Figure 2.24). During Cavortex 2 a significant negative relationship was observed for stations at the center and edge of the cyclonic eddy (Figure 2.25) (R= 0.70, P= 0.0001). For Cavortex 4 a station (station seven) in the cyclonic area also showed a negative relationship (Figure 2.26) (R= -0.86 P= 0.0001) and a positive relationship for stations 4and 6 (R= 0.66 and 0.51 P 0.001). Behrenfeld and Boss (2003) using field data from five oceanographic studies found consistency between spatio-temporal changes in c_p* an two indices of photoacclimation (P^b_{opt} and E_k), stating that these parameters were not casually linked but that they simply covary under certain environmental conditions. In our case the

relationship is observed between c_p* and *Fv/Fm* an index of physiological state of the cell which reflects changes in the photosynthetic machinery to environmental conditions.

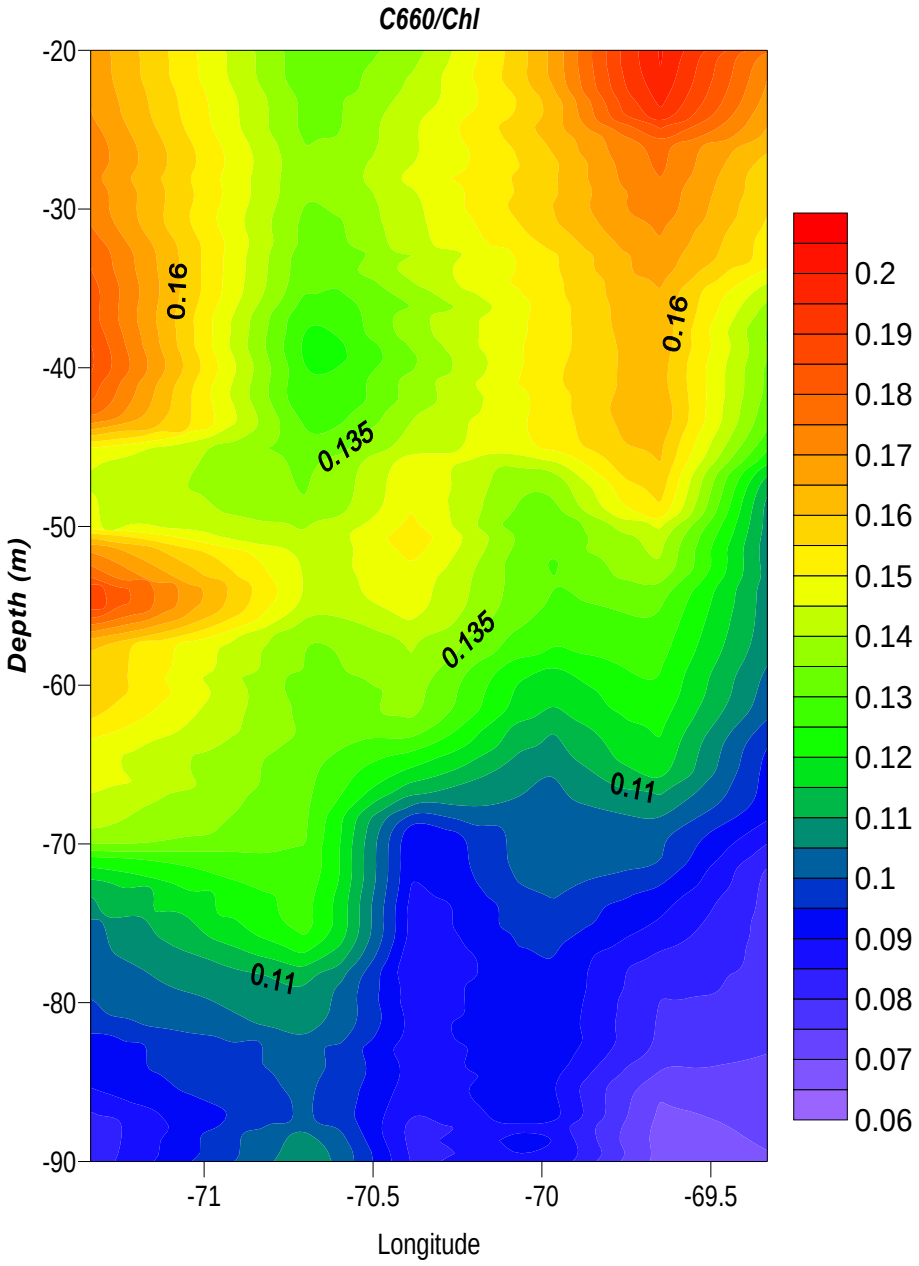

Figure 2.21. Chlorophyll normalized beam attenuation (660 nm) at cyclonic eddy center during Cavortex 6. The ratio varies accordingly with eddy influenced changes in environmental conditions.

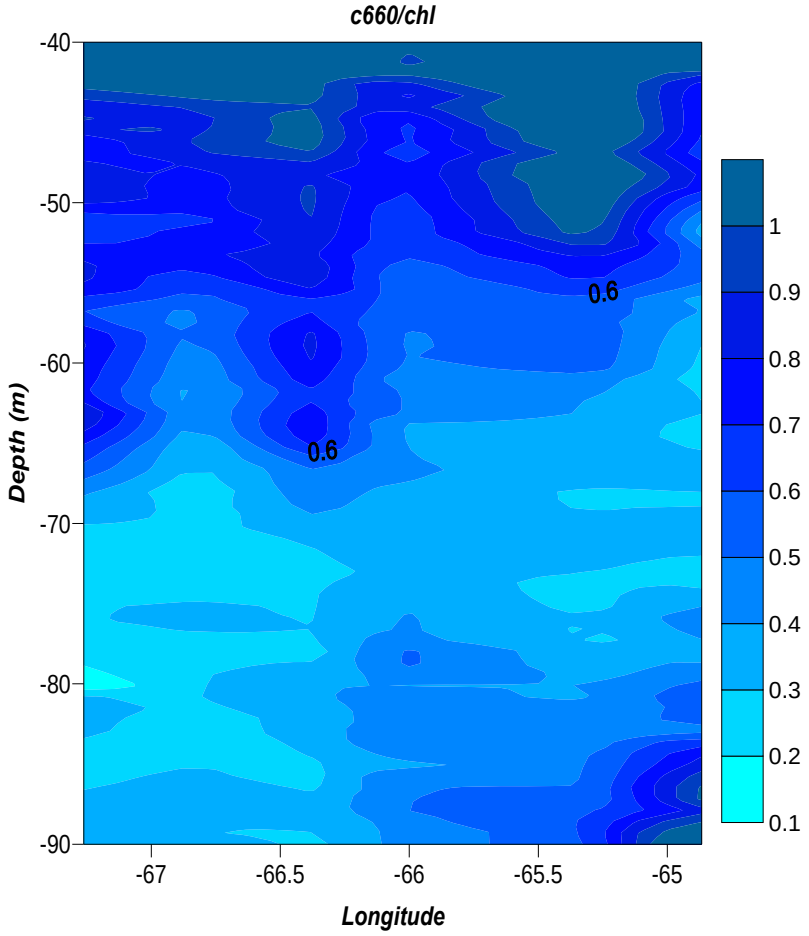

Figure 2.22. Chlorophyll normalized beam attenuation (660 nm) at cyclonic eddy center during Cavortex 2. The ratio varies accordingly with eddy influenced changes in environmental conditions.

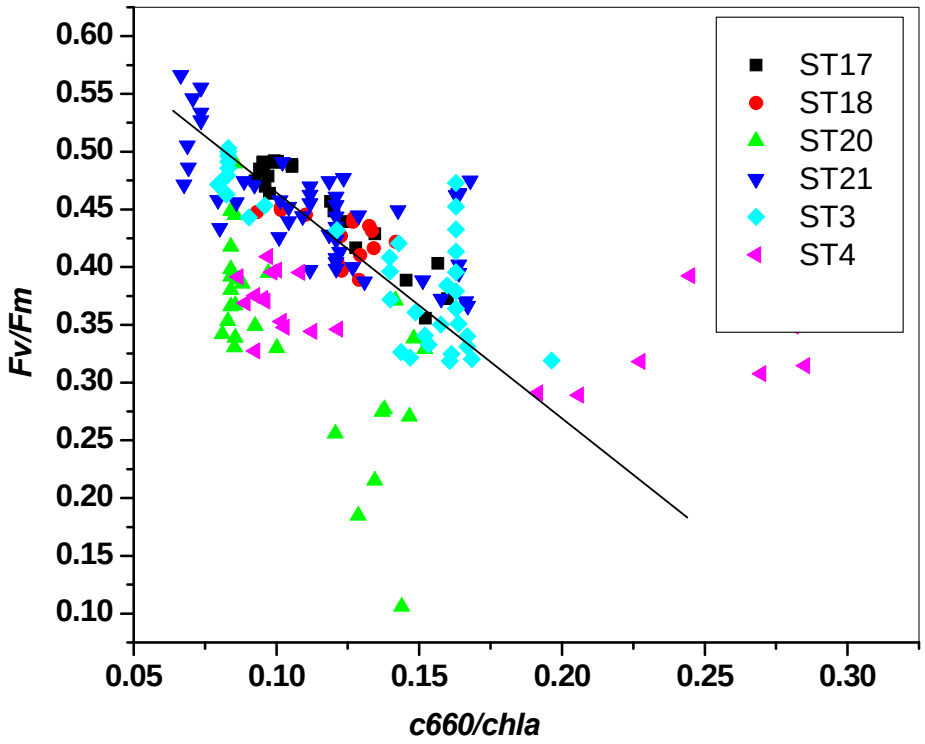

Figure 2.23. Phototrophic plankton photosynthetic efficiency and beam attenuation normalized to chlorophyll relationship for stations at cyclonic eddy center and edge during Cavortex 6. The observed correlation coefficient (r) was – 0.94.

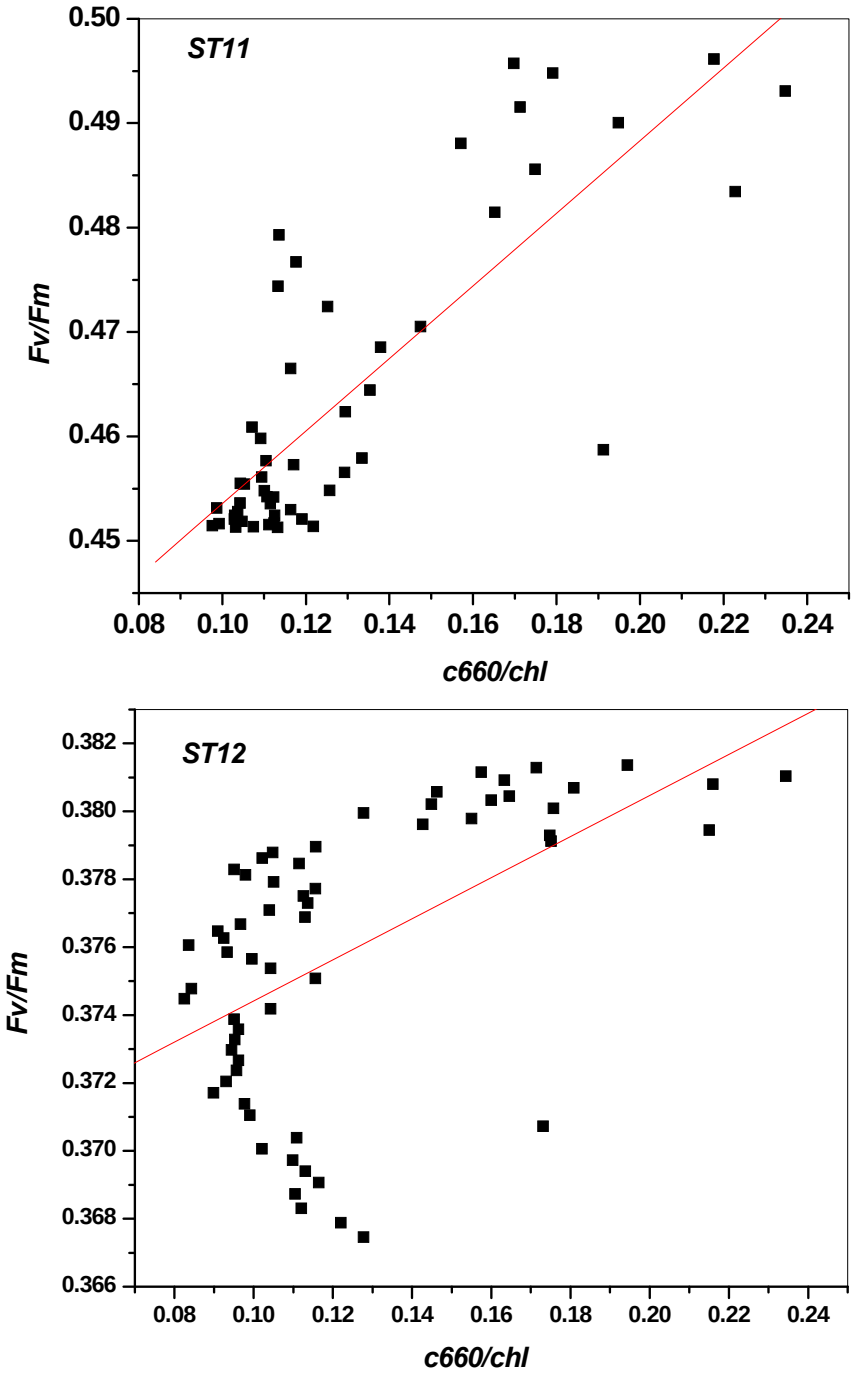

Figure 2.24. Phototrophic plankton photosynthetic efficiency and beam attenuation normalized to chlorophyll relationship for stations at anti-cyclonic eddy during Cavortex 6. The observed correlation coefficient (r) was 0.81 (st11) and 0.54 (st 12).

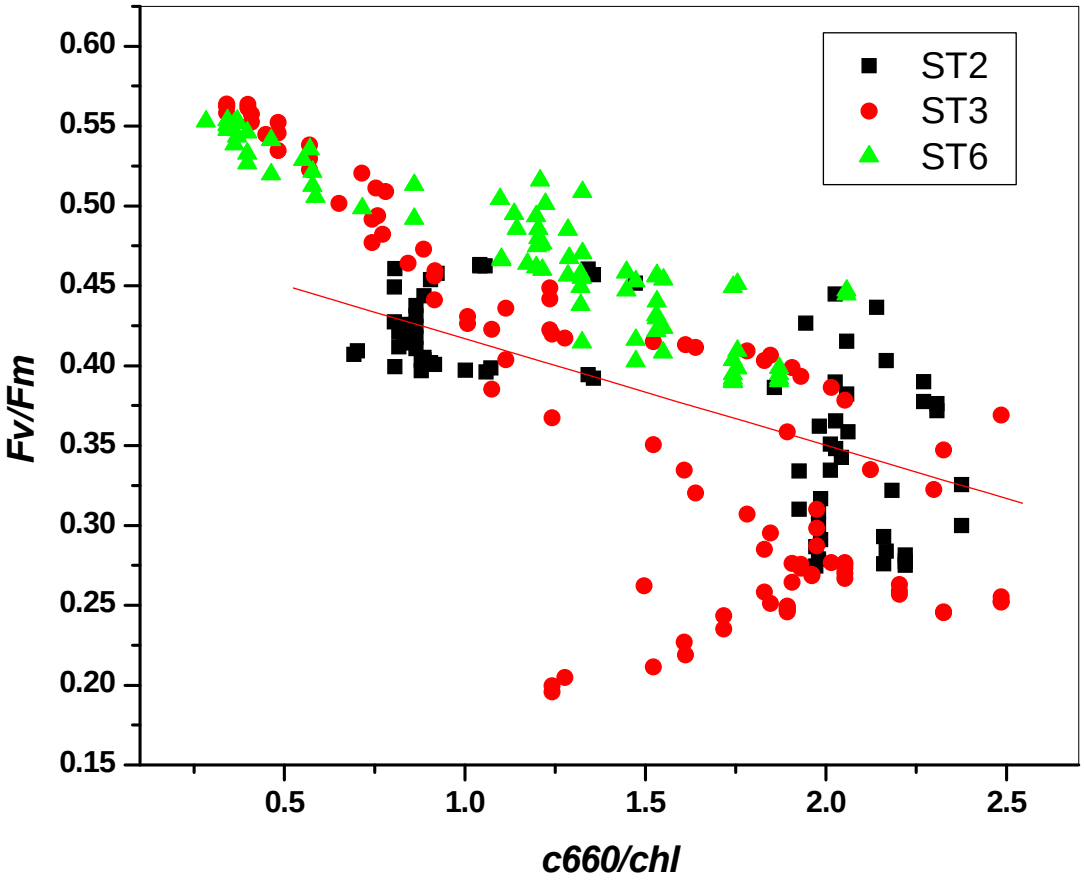

Figure 2.25. Phototrophic plankton photosynthesis efficiency and beam attenuation normalized to chlorophyll relationship during Cavortex 2. The correlation coefficient (r) was -0.69.

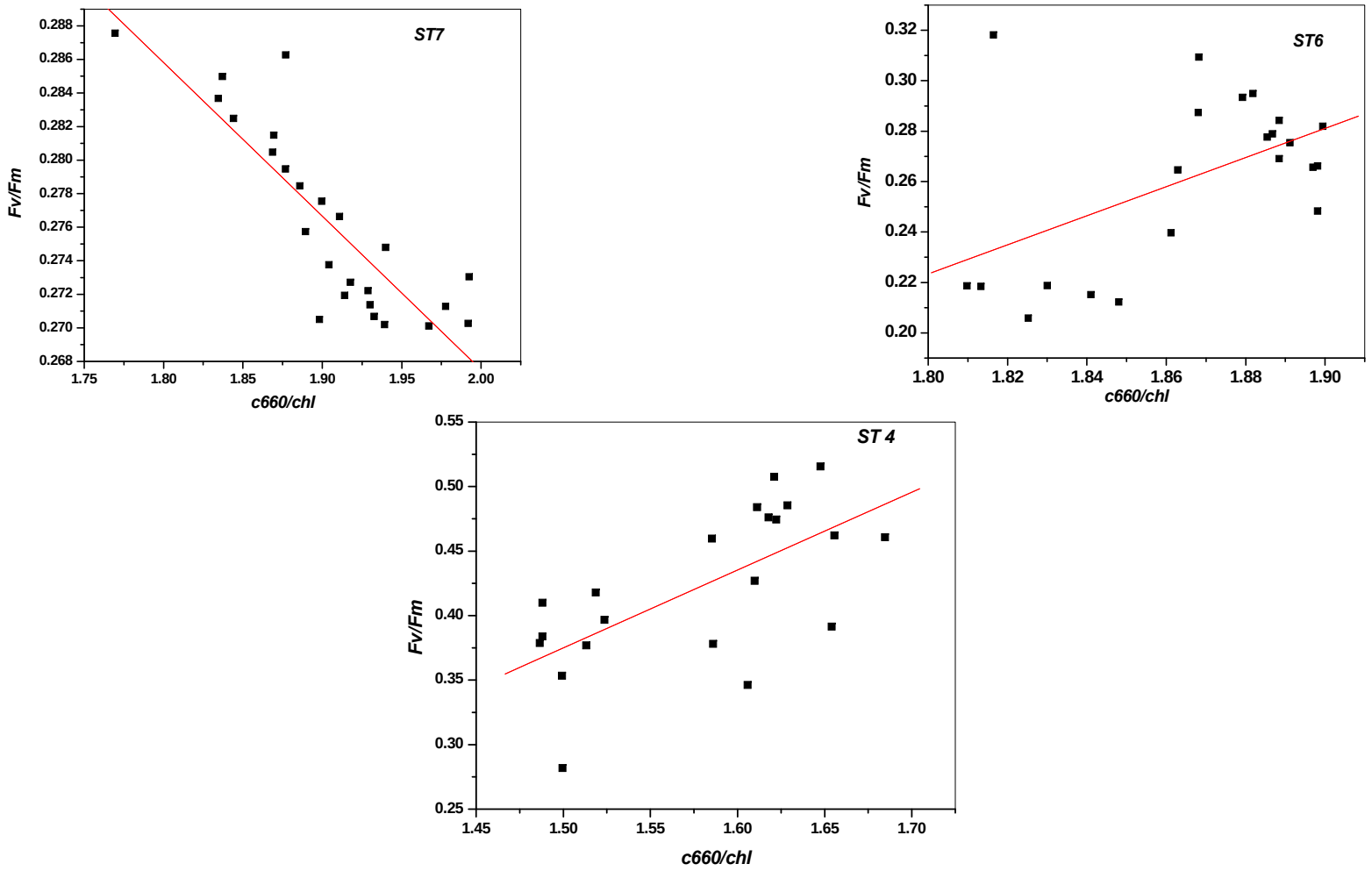

Figure 2.26. Phototrophic plankton photosynthesis efficiency and beam attenuation normalized to chlorophyll relationship during Cavortex 4. The observed correlation coefficient (r) was -0.87 (st7), 0.62 (st6) and 0.86 (st4)

The particle size distribution (PSD) slope was addressed against the backscatter ratio at 510 nm b_{bp}/b_p (the ratio of particulate backscatter to particulate scattering) (Twardowski et al. 2001) for Cavortex 6 and Cavortex 4 data (Figure 2.27 and 2.28). The PSD slope varied for all the data around 4 to 5.4, a range within the observed by previous works (Boss and Collier, 2007; Boss et al., 2004). The observed b_{bp}/b_p (510nm) for all the samples during Cavortex 6 ranged around 0.005 typical values for phototrophic plankton and organic materials (Boss et al., 2004), for Cavortex 4 the values were below and around 0.001.

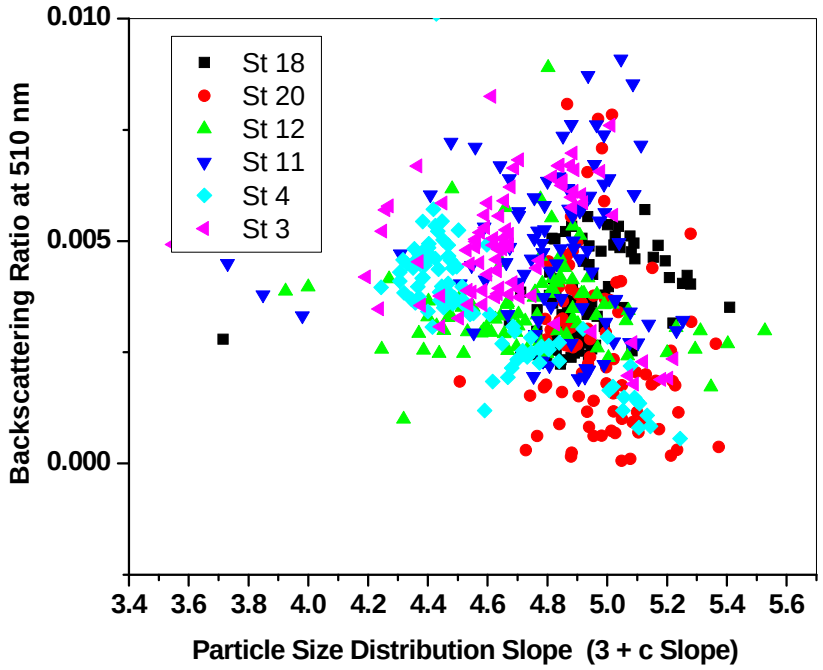

Figure 2.27. Particle Size distribution slope versus backscatter ratio at 510 nm during sampled stations of Cavortex 6. The particle distribution slope shows lower values at stations in the anti-cyclonic region (ST 3 and 4) and centered values at the cyclonic eddy center (ST 18and 20).

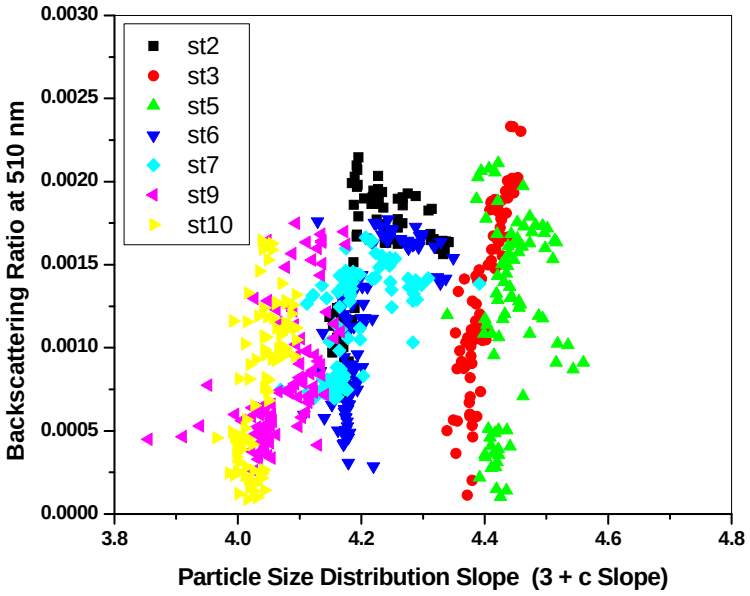

Figure 2.28. Particle Size distribution slope versus backscatter ratio at 510 nm during sampled stations of Cavortex 4.

2.4.3 Flow cytometry during Cavortex 6

The flow cytometry data demonstrated that the samples for Cavortex 6 were dominated by picoplankton (Prochlorococcus spp and Synechococcus spp), at surface no apparent differences were observed except for station 23 that showed a lower count (Figure 2.29). Prochlorococcus dominates Synechococcus in all samples by one order of magnitude, ranging from 700 to 25,000 and 34 to 1700 cells per milliliter respectively. Picoeukaryotes were minimum reaching a maximum cell count per milliliter, around 84 cells/ml.

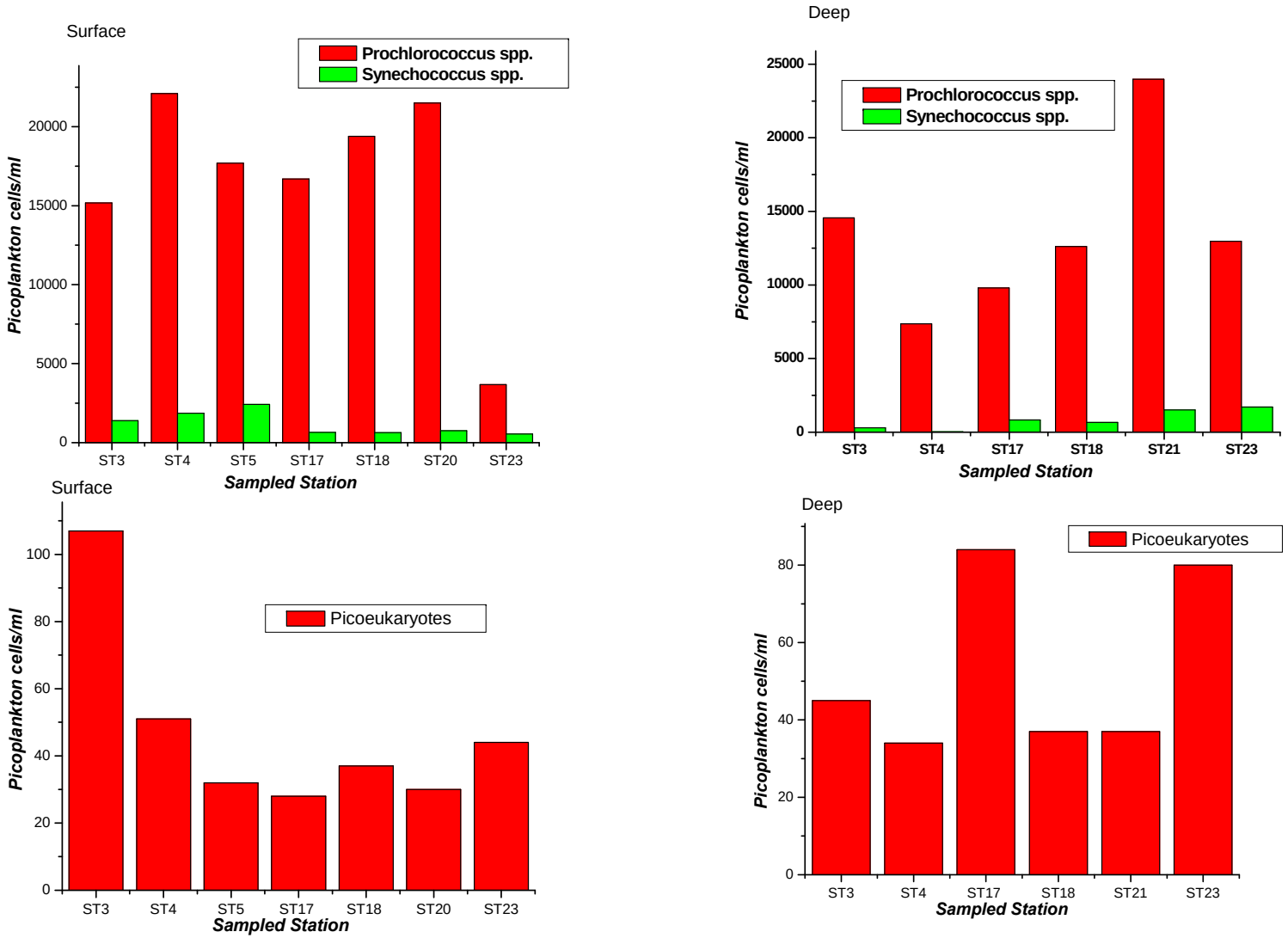

Figure 2.29. Flow cytometry data for discrete samples during Cavortex 6

2.4.4 Variable Fluorescence during the Oripex campaign

The effect of the Orinoco River plume on the photosynthetic efficiency was addressed during Oripex 7 and 8. Higher *Fv/Fm* was observed throughout the river-influenced zone. The Orinoco river plume during Oripex 7 was observed to have its direct influence in Eastern Caribbean waters as far north to latitude 13 and during Oripex 8 the influence of the front reached latitude 16 (Figure 2.30). The statistic summary of the sampled regions during Oripex 8 is presented in Table 6. *Fv/Fm* in the zones directly impacted by the river plume showed median values above 0.40 for most of the water column (Table 2.6) (Figure 2.31 and 2.32). The areas sampled include an area west of Saint Lucia and Martinique visited on the transect of September 20, 2008. *Fv/Fm* for the zone presented higher than expected values, with maxima around 0.67. These values persisted both at surface and depth, denoting a generalized effect through the water column. Surface salinity around 31 practical units, suggested waters influenced by the river plume (Figure 2.31). The area visited on September 22, 2006 east of the island of Grenada, appeared to be out of the direct effect of the river plume as interpreted by the observed surface salinity (Figure 2.32). Only a small portion of the transect showed a decrease in the surface salinity around longitude 61.2. Oceanic waters south of Puerto Rico sampled during the same campaigns denoted typical *Fv/Fm* distributions through the water column (Figure 2.33). Median values for the zone were around 0.31, and the observed maximum reached .043. Surface salinity remained within the expected range for oceanic waters.

Maximum fluorescence depth profiles of selected portions within the Oripex 8 transects are presented in Figure 2.34. The deep chlorophyll maxima (DCM) for stations south of Puerto Rico show appears at depths around 80 to 90 meters for station CaTS, typical for oceanic waters. The same was observed for stations southeast of Grenada during transect Sept 22. The DCM is observed close to surface for samples of transect sept 18(around 55 m), and for the region visited on transect Sept 20 the maxima appears around 30 m. *Fv/Fm* increased with depth for all the samples; sample Sept 20 was the more conservative, with almost constant values (Figure 2.34).

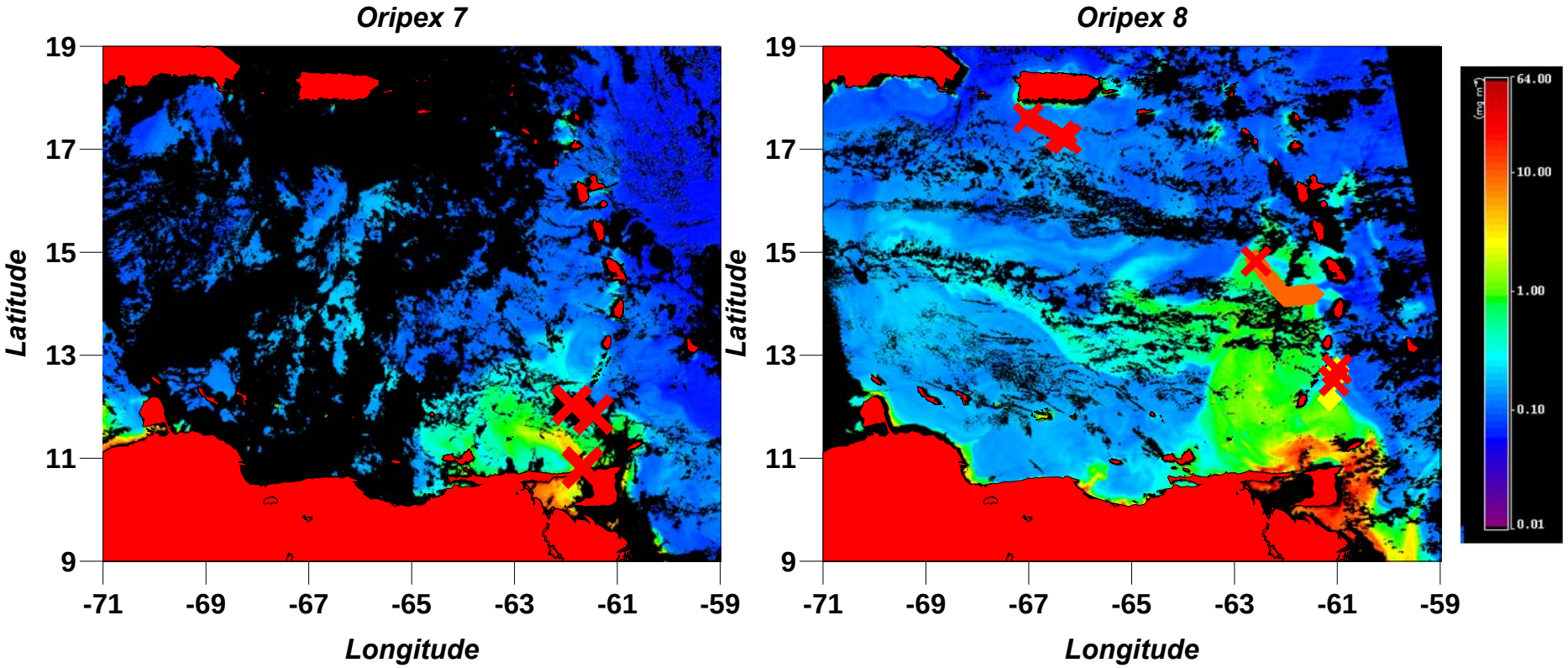

Figure 2.30. MODIS Aqua chlorophyll-a images during the Oripex expeditions. The images were capture November 24, 2005 for Oripex 7, and September 20, 2006 for Oripex 8. Red crosses mark the stations analyzed. During Oripex 8 the sampled transects appear in red (transect south of Puerto Rico), orange (transect west of Saint Lucia) and yellow (transect east of Granada).

Table 2.6. Fv/Fm statistics of sampled transects during Oripex 8. Partial data presented as surface (< 40 m) and depth (> 40 m).

Sample	N total	Mean	Standard Deviation	Sum	Minimum	Median	Maximum	Variation Coefficient
Surface Sept 18	545	0.31	0.040	169.14	0.18	0.31	0.41	12.90
Depth Sept 18	863	0.34	0.03	301.88	0.23	0.35	0.43	8.82
Surface Sept 22	561	0.31	0.08	177.36	0.11	0.32	0.55	25.81
Depth Sept 22	1174	0.42	0.07	503.57	0.11	0.43	0.60	16.67
Surface sept 20	1494	0.44	0.07	664.83	0.20	0.46	0.61	15.91
Depth sept 20	605	0.51	0.04	310.22	0.26	0.51	0.67	7.84
All Sept 18	1408	0.33	0.04	471.02	0.18	0.33	0.43	12.12
All Sept 22	1735	0.39	0.09	680.93	0.11	0.40	0.60	23.08
All sept 20	1495	0.48	0.05	732.07	0.22	0.49	0.67	10.42

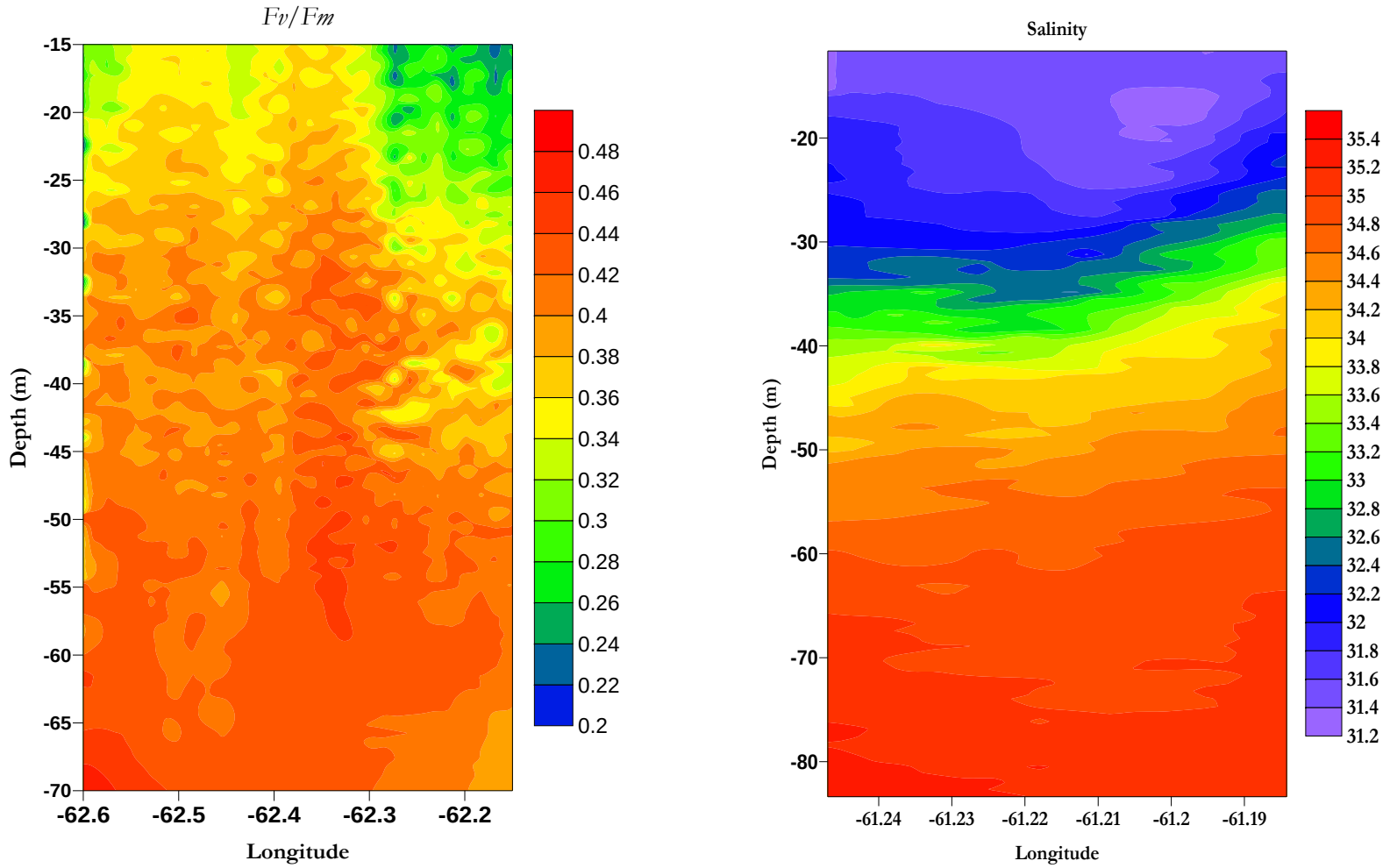

Figure 2.31. Fv/Fm and salinity countor maps during Oripex 8 for transect sampled during September 20, 2006. The sampled transect denotes the inclusion of low salinity waters over the zone from the Orinoco River front. . The transect was mostly sampled over river influenced west of St Lucia.

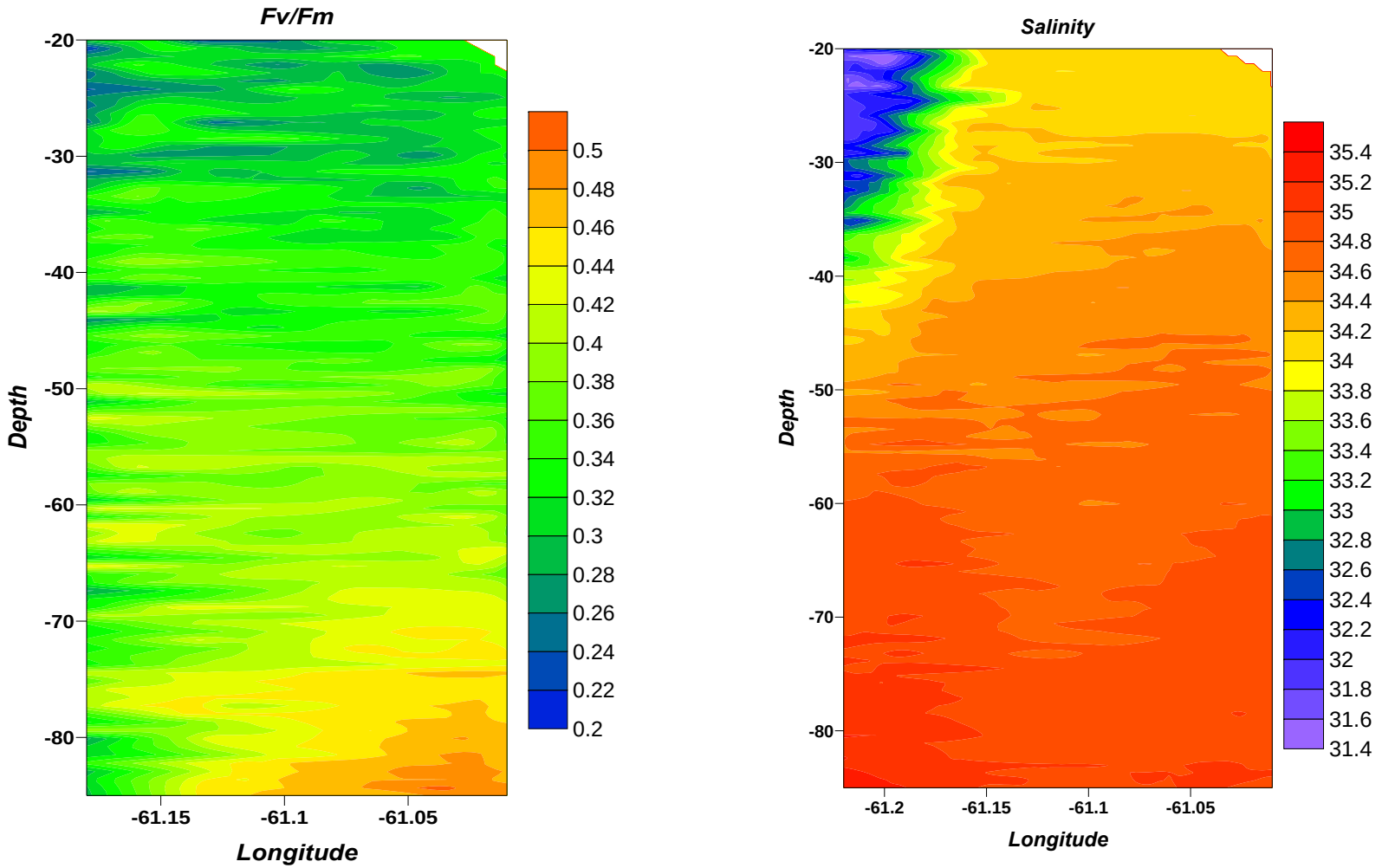

Figure 2.32. Fv/Fm and salinity contour maps during Oripex 8 for transect sampled during September 22, 2006. The sampled transect denotes some of the inclusion of low salinity waters over the zone from the Orinoco River front. The transect was mostly sampled over blue waters east of the coast of Granada.

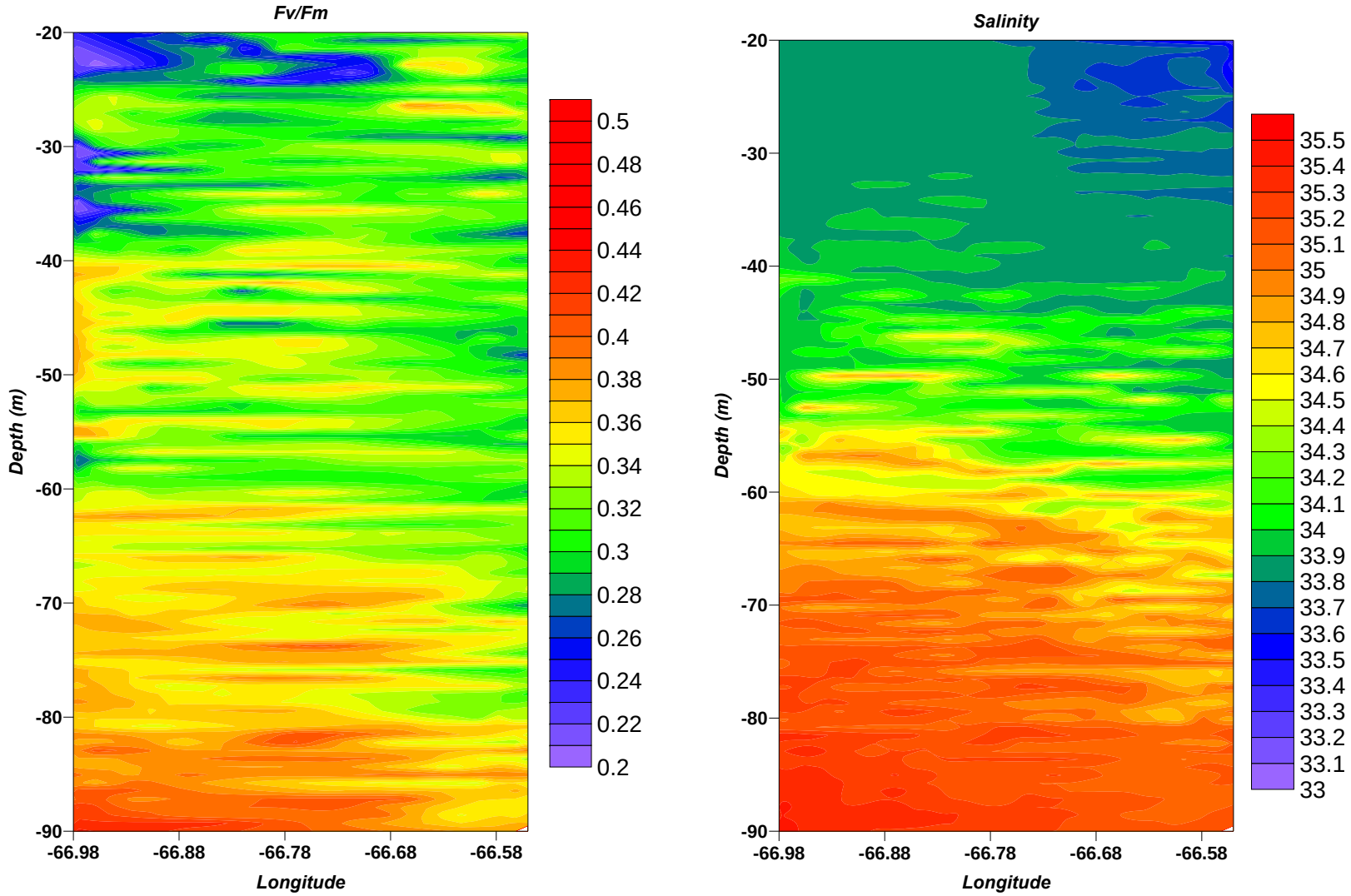

Figure 2.33. Fv/Fm and salinity contour maps during Oripex 8 for transect sampled during September 18, 2006. The transect was sampled over blue waters south of the island of Puerto Rico.

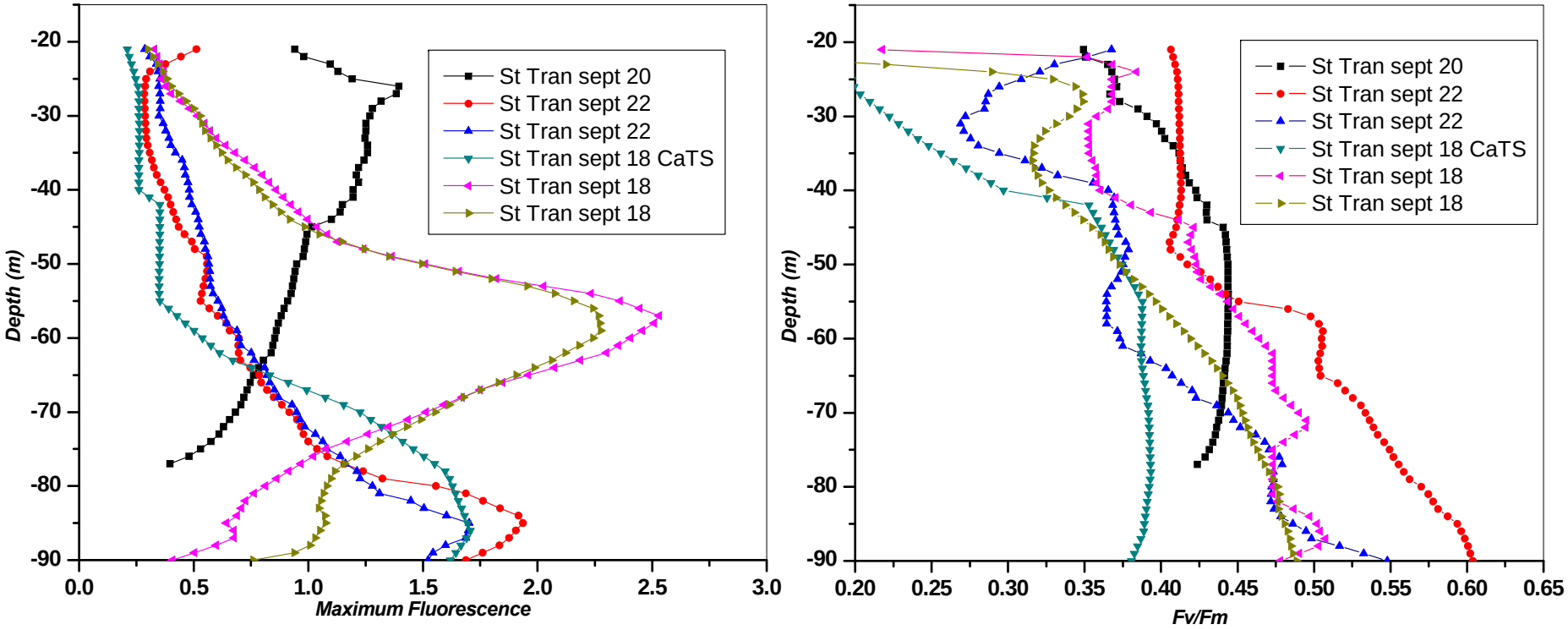

Figure. 2.34. ***Fv/Fm*** **and maximum fluorescence profile casts for sampled stations during Oripex 8. The sampled stations were localized at the sampled transects west of Saint Lucia (St Tran Sept 20) influenced by the river front; South East Granada (St Tran Sept 22) in waters close to the river plume and south of Puerto Rico (St Tran Sept 18) in oceanic waters.**

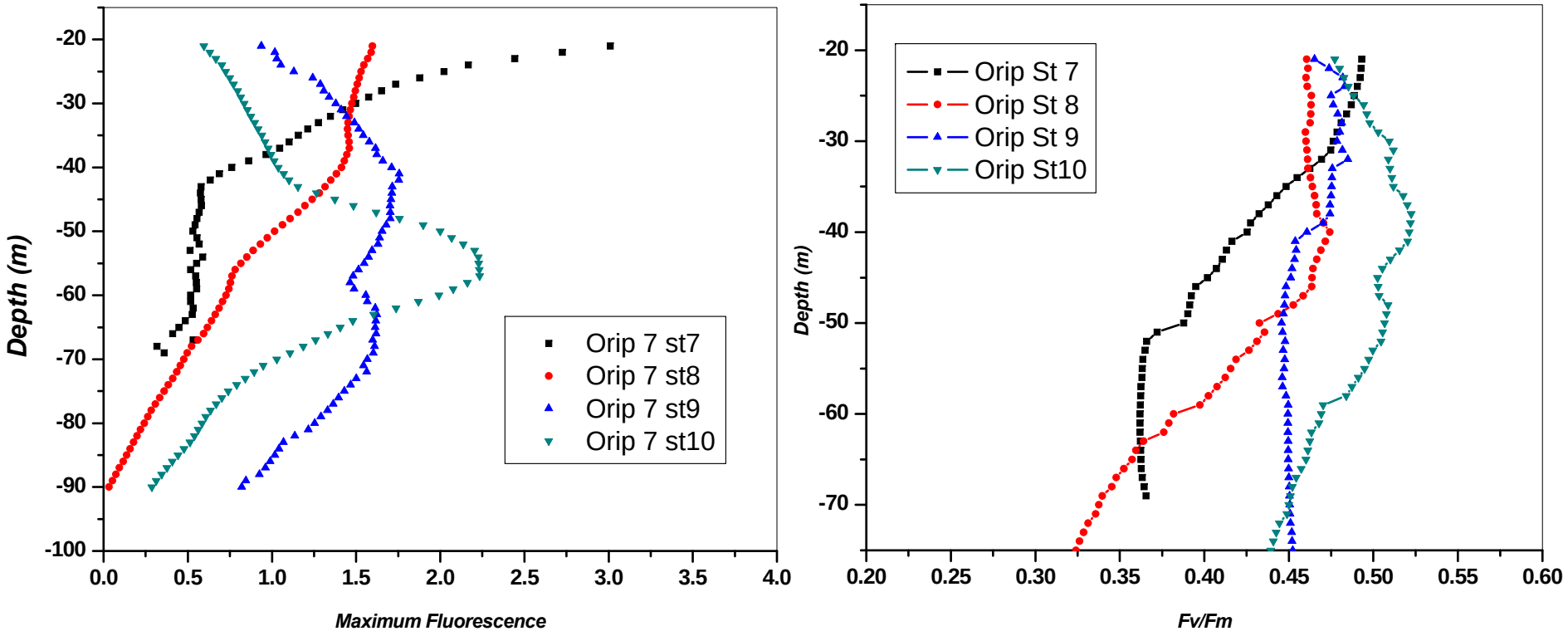

Figure 2.35. ***Fv/Fm*** **and maximum fluorescence profile casts for sampled stations during Oripex 7 The sampled stations were localized from the Dragon's Mouth (St 7 and St 8) toward waters West of Granada (St 9) and South East Granada (St 10).**

Maximum fluorescence profiles during Oripex 7 are presented in Figure 2.35. These samples were collected close to the river origin between the islands of Trinidad and Grenada. Stations 7 and 8 were collected at the Dragon's Mouth between Trinidad and Venezuela. These stations denoted chlorophyll maxima close to surface. Station 10 east of Grenada presented a maximum around 55 m. *Fv/Fm* for all stations decreased with depth, apparently responding to river-originated materials close to the surface. For station 7 the observed surface salinity was 25, for station 8 the surface salinity was 28. At both stations the salinity increased to normal values around 3 m. Stations 9 and 10 exhibited a normal range of surface salinity values.

2.5 Discussion

Photosynthetic efficiency at Caribbean mesoscale eddies

Our investigations of mesoscale processes shed some light into the processes occurring through the basin while these perturbations move across the Caribbean. The perturbation caused by the passage of cyclonic eddies uplifted materials towards the surface while exposing the phototrophic plankton to nutrient rich waters. Photosynthetic efficiency (*Fv/Fm*) exhibited vertical and horizontal variations that are consistent with control by recent light history and nutrient status. Decreased daytime *Fv/Fm* denoted the photoinhibitory processes occurring through the zone. Photosynthetic efficiency of dark acclimated populations is substantially reduced under nutrient limitations or at high surface irradiances owing to the inactivation or damage to PSII reaction centers pigment-protein complexes (Falkowski and Kolber, 1995). Photoinhibition has been shown to be exacerbated by nutrient limitation if sufficient nutrient resources are not available to provide the substrate to repair damaged photosynthetic reaction centers (Falkowski and Raven, 1994). Suppression of photosynthetic efficiency was evident during the daytime transects with the N*v*-Shuttle, but this suppression although registered in samples up to 90 meters did not lower *Fv/Fm* below the normal expected values for oligotrophic waters (around 0.3). Consequently we consider that the passage of the cyclonic eddy supplied the entire area the materials needed to rebuild the affected photosynthetic centers. The observed fast recovery of the phototrophic plankton from daytime *Fv/Fm* suppression evidently suggests that the cells were suffering some degree of non-photochemical quenching that did not involved structural damage to the PSII photosynthetic centers. Non photochemical quenching in the pigments of PSII relaxes on the time scale of 5- 60 minutes (Olaizola and Yamamoto, 1994). Coincidently, our sampled transect showed recovery at this time range. However the available data provides only a snap-shot of this process and no experiment was specifically performed to address this issue.

The nutrient data was limited to depths below the 80 m due to the delectability of the method at the concentrations found in our samples. But there is well documented

positive co-variation between the maximum carbon based photosynthetic quantum yield, *Fv/Fm* and nitrate concentration in a wide range of ocean waters (Babin et al., 1996; Kolber et al., 1990). Falkowski et al. (1991) measured nitrate concentrations and variable fluorescence in a cyclonic eddy near Hawaii showing high values of *Fv/Fm* (around 0.56); close to those observed at the coldest temperature ranges registered here. The maximal theoretical value for this parameter is 0.65. The observed negative relationship of *Fv/Fm* with temperature and a positive one with density at the eddy center during Cavortex 6 strongly support the hypothesis of nutrient uplifting by eddy pumping potential.

Despite the fact that higher *Fv/Fm* was observed in the cyclonic eddy compared to the other provinces sampled, the inverse relationship observed with σ_{PSII} (at depths 60 to 90 m) suggests that the cells were recently relieved from nutrient stress. As stated before, when phototrophic plankton growth is slowed due to inadequate supply of nitrogen or iron, the efficiency of photochemistry at PSII is submaximal due non-functional pigment-protein complexes, iron-containing cytochromes, and enzymes in PSII reaction centers (Falkowski, 1992). On the other hand, the PSII absorption cross section (σ_{PSII}) will increase under nitrogen or iron limitation owing to preferential synthesis under nitrate stress of nuclear-encoded antennae pigment protein complexes over the chloroplast genome–encoded pigment-protein complexes of the photosynthetic reaction centers (Kolber et al., 1988; Falkowski et al., 1989) . Compared to nutrient replete cell, there are relatively fewer reaction centers serving a given-sized antenna under nutrient depletion, and therefore electron flow and charge separation at PSII is increased relative to light absorption (Vaillancourt et al., 2003b). In other words, the fewer functional PSII reaction centers per cell are served by a large complement of antennae pigments assuring efficient transfer of photochemical energy to PSII and higher values of σ_{PSII} .

The inverse relationship of *Fv/Fm* and the specific absorption ratios suggest an apparent increase in the chlorophyll absorption that is not synchronized with an increase in photosynthetic efficiency. The increase in chlorophyll-a (Chl-a) absorption is probably due to an increase in Chl-a relative to other pigments. Preferential Chl-a synthesis is observed for healthy algae and vice versa when nutrient-starved, consistent with the high energetic requirements of Chl-a (Heath et al., 1990). The increase in *Fv/Fm* could be

considered to occur at shorter timescales than Chl-a synthesis. Therefore as phototrophic plankton cells become exposed to the new nutrients and limiting micronutrients like iron, the rate of transfer of electrons increases but with not enough time to reconstruct the damaged chloroplast structures to increase the Chl-a concentration accordingly to *Fv/Fm* increments. In iron fertilization experiments the phototrophic plankton bloom was apparent days after the addition of iron even though the changes in *Fv/Fm* were observed within hours (Boyd & Abraham, 2001). Consequently, the resulting inverse relationship of *Fv/Fm* and absorption ratios becomes apparent at the eddy's center and edge, in contrast, the anti-cyclonic portion has a positive relationship due to stable stratification as would be expected.

Chlorophyll normalized particle beam attenuation in Caribbean mesoscale eddies

Chlorophyll normalized particle beam attenuation (c_p*) at 660 nm has previously suggested as another optical estimate of phototrophic plankton physiology. Behrenfeld and Boss [2003] suggested that c_p should likewise be well correlated with phototrophic plankton carbon biomass, particularly since the particle size domain dominating c_p more closely matches that of phototrophic plankton than particulate organic carbon. Consequently, they proposed the c_p* ratio as an index of phototrophic plankton C:Chla and subsequently demonstrated a first-order correspondence between c_p* ratio and independent ^{14}C-tracer measures of physiological condition (Behrenfeld and Boss, 2003). Our observations also suggest such relationships with *Fv/Fm*, and, as previously observed for the absorption ratios, it varied inversely with the c_p* ratio at stations influenced by the cyclonic eddy. High c_p* ratio is indicative of high concentration of phototrophic plankton and is consistent with low refractive material (relatively low contribution from inorganic particles) a low c_p* ratio is indicative of relative low concentration of phototrophic plankton and is consistent with high refractive material (large contribution from inorganic particles). The dynamics of the cyclonic eddy appears to increase the amount of refractive material through the water column which supports higher *Fv/Fm* through this zone. The anti-cyclonic portion relies on the recycling of phototrophic plankton originated materials and the changes of the c_p* ratio are related to

changes in phototrophic plankton abundance (as was observed by the strong relationship of c_p and Chl-a through all the samples). Its relationship to *Fv/Fm* indicates higher photosynthetic efficiency related to particles of phototrophic planktonic origin, thus the increased *Fv/Fm* responds to recycling of phototrophic plankton materials not to new inorganic particles, as observed in cyclonic regions.

The nature of c_p as a robust index of particle variability is determined by particles in the ~ 0.5 and 20 μm range for the typical open ocean (Boss et al., 2001) Therefore, in the open ocean only a fraction (but often dominant) of c_p can be attributed to phototrophic plankton (Fennel and Boss, 2003); and its variability is more influenced by the fractions of ultraplankton and nanoplankton and less by the picoplankton (Durand and Olson, 1996). Thus, notice that the c_p* ratio showed sensitivity to particle distribution at the eddy center even in a region dominated by the picoplankton *Prochlorococcus* and *Synechococcus* spp. In fact, generally all the Cavortex 6 regions were dominated by similar phototrophic planktonic communities widely homogenous as suggested by the correspondence in the chlorophyll specific absorption coefficient spectra within regions. Further support of these observations is the relatively low backscattering ratio (centered on 0.005) and a similar particle size distribution slope.

In summary, the passage of these mesoscale events across the eastern Caribbean region appears to have an impact on the photosynthetic potential of the phototrophic planktonic communities. Increased *Fv/Fm* potential could be associate to the effect of cyclonic eddies and, although further evidence is needed, it seems that their impact did not originate the expected changes in the phototrophic planktonic community structure observed by Vaillancourt et al. (2003) in the Hawaiian cyclonic eddies. They observed an increase in abundance of the pico eukaryote community while our flow cytometry observations do not suggest a change in taxonomic composition through the sampled regions. The abundance of these cells appears to remain constant through the samples, but due to the limited information no conclusion could be derived.

Additionally, the correlations of *Fv/Fm* with independent optical indices of phototrophic plankton physiological condition provides further evidence for the potential of c_p* ratio as an independent probe of phototrophic plankton responses to changing

environmental conditions. *Fv/Fm* together with c_p* is suggested here to some degree shed some information on the factors influencing photosynthetic potential and its origins.

Photosynthetic efficiency in the Orinoco River Plume

The influence of the Orinoco River plume on the photosynthetic potential of eastern Caribbean phototrophic plankton populations is demonstrated by the previous analysis. Increased *Fv/Fm* close to the surface decreasing with depth suggests a relation with river originated material. Samples during Oripex 7 close to the river origin denote this phenomenon. The observed chlorophyll maxima close to surface probably originated in relation to the river water haline interface, the effect of fresh water was observed to reach depths of 3 meters. Del Castillo et al. (1999) documented the observed vertical displacement of Chl-a along the latitudinal gradient, where the maxima was closer to surface at lower latitudes and gradually displaced to greater depths towards the north, reaching depths of 50 to 100 m close to the south of Puerto Rico. In this region of the water column a density gradient occurs apparently leading to accumulation and microbial degradation, and the consequent increase of *Fv/Fm*. However the observed increase in *Fv/Fm* through the water column was higher at stations farther from the Gulf of Paria (Oripex 7 St10 Figure 2.35). It has been suggested that dissolved inorganic nitrogen in the plume is depleted before it exits the Gulf of Paria (Bonilla et al., 1993). Then the enhanced photosynthetic potential is probably results of riverine material degradation, that could be the result of both microbial remineralization and dissolved organic nitrogen photomineralization as suggested by Morell and Corredor (2001). The areas sampled during Oripex 8 farther from the river origin registered also the increase in the *Fv/Fm* through the water column suggesting a similar influence by the river plume .

The entrainment of the river plume by a cyclonic eddy (Corredor et al., 2004) evidentiated the complex dynamics of the eastern Caribbean waters. The observed eddy potential for increasing available materials in surface waters and the experimental evidence of photomineralization of dissolved organic matter (Morell and Corredor, 2001) denotes the variety of fertilization mechanisms occurring in the region. The role of these factors in shaping the photosynthetic potential of Caribbean surface waters was evidentiated with the correlated variability of *Fv/Fm* through the areas sampled. The

resolution of the FRRF-acquired data with the use of a towed vehicle during these oceanographic expeditions provided high assurance of the validity of the evidence presented here. The use of the N*v*-Shuttle permitted the acquisition of data at 5 second resolution over shuttle oscillations of about a kilometer. This was advantageous and facilitated the interpretation of the changing biogeochemical features from the surface down to 90 meters while the zones were impacted by the mesosocale phenomena.

Conclusion

In conclusion phototrophic planktonic communities in eastern Caribbean waters are constantly changing as a result of these mesoscale processes. This as consequence results in higher photosynthetic potential for the region determined by the gradient created by the Orinoco River plume part of the year and the disruption in the surface waters by mesoscale eddies. We should then expect higher potential decreasing with increasing latitude from the Orinoco River origin to waters north deep in to the Caribbean. This potential should then correlate with the increasing degradation of the dissolve organic matter through the zone, as it liberates the phototrophic planktonic communities from nutrient starvation. Thus at least in some period of the year these waters then deviate from the expected oligotrophic state to a mesotrophic one with higher potential for primary production.

CHAPTER 3
Carbon fixation estimates and bio-optical characteristics of phototrophic plankton in eastern Caribbean waters

3.1 Abstract

The structure of Eastern Caribbean surface waters is defined by the action of several mesoscale processes including the continental forcing created by the Orinoco river as it deliver the effluents into this waters. This river creates a seasonal front that covers part of the eastern Caribbean, having direct effects as far as the islands of Puerto Rico. Consequently the occurrence of this seasonal surface front imparts distinctive bio-optical properties to these waters, creating unique light and nutrient regimes to the phototrophic plankton cells across the region. These environmental changes then impart these phototrophic plankton ic cells photo-physiological characteristics that remain as record of phototrophic plankton recent life history. Ultimately these adaptations are then reflected into the phototrophic plankton efficiency for primary production.

The Caribbean Vorticity experiment (Cavortex 2 and 6) from June 22-27, 2004 and August 28, 2006 to September 8, 2006, and the Orinoco River plume experiment (ORIPEX 7 and 8) November 19-24, 2005 and September 18-23, 2006, were intended to characterize the physical, biogeochemical, and optical structure of the Eastern Caribbean Region as mesoscale processes (eddies and the Orinoco River plume) influence the biological productivity of the Easter Caribbean.

The FRRF-based productivity estimates produced a strong linear relationship (r=0.91) with independent measurements of ^{14}C for data collected throughout the Eastern Caribbean Sea. The chlorophyll specific absorption coefficient ($\boldsymbol{a_{ph}}$) showed reduced absorption in the region of 442 nm apparently in response to increased package effect for waters under the influence of the river plume. This observed packaging suggest lesser action by chlorophyll and probably an increase in photoprotective carotenoids as interpreted by the variations of the a_{ph} slope around the region of 488 to 532 nm. These variations in the a_{ph} slope were then correlated to a decrease in the quantum yield for carbon fixation at samples in oceanic far from the direct influence of the Orinoco River

plume. Satellite based estimates of primary production varied accordingly with *in-situ* measurements and the gradients created by the river plume.

3.2 Introduction

The structure of Eastern Caribbean surface waters is defined by the action of several mesoscale processes including the continental forcing created by Amazon and Orinoco rivers as they deliver their effluents into these waters. These rivers create seasonal plumes that cover part of the eastern Caribbean having direct effects as far as the islands of Puerto Rico. The impact of these fresh water inputs on the coast of Puerto Rico are marked by a shift upward of the deep chlorophyll maxima (DCM) and apparent seasonal increase in the chlorophyll through the region as interpreted from remote sensed data (Corredor and Morell, 2001). This increase in the chlorophyll at surface waters is consequence of the residence of these waters above the pycnocline and the nutrient recycling within the buoyant river plume (Corredor et al., 2003). Consequently the occurrence of this seasonal surface front should impart distinctive bio-optical properties to these waters, creating unique light and nutrient regimes to the phototrophic plankton cells across the region. These environmental changes then impart to these cells photo-physiological characteristics that remain as record of recent life history. Ultimately these adaptations then should be reflected in the efficiency for primary production.

One property related and relevant to analysis of water column primary production is the absorption coefficient of phototrophic plankton. Absorption by photosynthetic pigments and accessory pigments serves to assess the physiological condition of phototrophic plankton, species identities, and biomass in marine environments (Falkowski and Raven, 1997). The absorbed energy by phototrophic plankton once absorbed follows three possible pathways: (1) is used in photosynthesis, (2) is liberated as fluorescence or (3) is converted to heat energy. Accessory pigments are subdivided into photosynthetic carotenoids involved in the transfer of energy in the reaction centers during photosynthesis, and photoprotective carotenoids involved in the protection of the chloroplast from excess irradiances. Variations in the composition of photoprotective and photosynthetic pigments as well as pigment packaging reveal changes in the total absorption spectra of phototrophic plankton. These changes in consequence affect the productivity by decreasing efficiency of energy transfer. When the proportion of photoprotective carotenoids increases, the rate of electron transfer for photosynthesis diminishes (Prieto et al., 2008). Owing to the fact that their purpose is to help prevent

damage to chloroplast from excess light by reducing the efficiency of energy transfer among photosynthetically active pigments through the modification of chlorophyll-chlorophyll interactions (Frank et al., 2001), consequently photoprotective carotenoids have the lowest transfer efficiencies with minimum values of 20 % (Rabinowitch and Govindjee, 1969). The slope of the absorption spectra from 488 to 533 nm (normalized to 676 nm) has been found to be steeper in high-light compared to low-light adapted cultures (Johnson et al. 1994 cited in Eisner et al., 2003). Such spectral variations are due to physiological changes in cellular pigment ratios and pigment packaging, under high light, increases in photoprotective carotenoids, decreases in photosynthetic carotenoids, and a reduction in pigment packaging may cause the absorption spectral slopes to become steeper, while the reverse is true for low-light conditions.

The efficiency in energy conversion by phototrophic plankton is measured through estimates of variable fluorescence which provide the means to study their physiology as it respond to nutrient limitation (Sosik and Olson, 2002), algal photoinhibition and photoprotection due to excessive visible and UV radiation (Beherenfeld et al., 1998), and changing nutrient and light fields (Babin et al., 1996). Variable fluorescence(Fv = Fo - Fm) is measured by analyzing the difference between the initial fluorescence (Fo), obtained from the original fluorometer flash sequence when all the reaction centers are open , and the maximal fluorescence (Fm), obtained once all the reactions centers are transporting electrons and temporally closed to further excitation. When variable fluorescence is normalized to the maximal fluorescence the photochemical conversion efficiency of photosystem II (*Fv/Fm*) is obtained.

Estimates of primary production from variable fluorescence measurements have been available in recent years through the use of active fluorescence techniques, such as pump and probe fluorescence (PPF), Pulse amplitude modulation (PAM) and fast repetition rate fluorometry (FRRF). FRRF fluorometry has become the dominant methodology in recent years; it is a technology that provides measurements of phototrophic plankton physiology using a progressive closure of photosystem II (PSII) reaction centers in responses to flashes of excitation energy. This methodology makes possible estimates of primary productivity with a resolution of seconds (Kolber and Falkowski, 1993; Sugget et al., 2001; Smyth et al., 2004 Cermeño et al., 2005), and

without the need for time consuming incubations providing an advantage over other traditional approaches, the oxygen evolution method (Strickland and Parsons, 1972) and the radioactive ^{14}C tracer for carbon assimilation method (Steeman-Nielsen 1952).

Kolber and Falkowski (1993) developed a model of primary production based on the relationship between PSII fluorescence and electron transport using *Fv/Fm*. Since PSII is the site where oxygen evolution occurs, there is a relationship between variable fluorescence and oxygen production and although carbon fixation occurs at later stages of the process during photosynthesis dark reactions, a fraction of the electrons passed from PSII to PSI are used for this purpose. Consequently carbon fixation has some degree of relation with to PSII fluorescence by the photosynthetic quotient, the ratio of moles of oxygen released to moles of carbon fixed. Kolber and Falkowski (1993) applied the model using the PPF technique and compared them to estimates of ^{14}C uptake. This productivity estimates indicted a 1:1 relationship with a slope of 1.06 ($r^2 = 0.86$). Sugget et al., (2003) applied a variation of this model using the FRRF technique and obtained a slope 2.116 with a lower r^2 (0.56) . Recently, Melrose et al. (2006) found better results with a regression slope that ranged between 0.23 and 1.04 and their r^2 was usually high above 0.9. They also suggested that due to the variability between the FRRF productivity and ^{14}C estimates, FRRF field measurements should be calibrated against other productivity measurements techniques.

The advent of ocean color measurements from satellites has recently facilitated the effort to measure net primary production (NPP) on global scales. These estimates has traditionally primarily based their NPP approximations on the biomass estimated through chlorophyll concentration, incident light and a scaling parameter that accounts for variations in plant physiology (Behrenfeld and Falkowski, 1997a). These estimates perform poorly when compared to *in-situ* estimates due to their inefficiency in tracking physiological changes that are not displayed on chlorophyll concentrations alone. Most changes in chlorophyll concentration reflects intracellular changes in response to photoacclimation and not necessarily phototrophic plankton growth (Behrenfeld et al., 2005). Based on these observations Behrenfeld et al. (2005) developed estimates of NPP based on the information of particle backscatter (b_{bp}) of the ocean color reflectance. This information was then directly related to phototrophic plankton biomass, the Chl:C ratio

reflects photoacclimation and nutrient stress and has been shown to track phototrophic plankton physiology both in the laboratory and in the field (Behrenfeld and Boss, 2003; Behrenfeld et al., 2005). Based on this parameter the community growth rate can be estimated more precisely resulting in the ability to calculate fully resolved vertical profiles of phototrophic plankton NPP (Westberry et al, 2008).

Our goals in this work are first to determine the extent to which the variable conditions of surface eastern Caribbean waters affect the spatial variations in surface water production estimates by fluorometry. This is addressed by examining the photosynthetic efficiencies and related quantum yield of carbon fixation as they vary with light adaptations, interpreted by the spectral slope of normalized absorptions curves. Second to evaluate the satellite estimates of NPP and their relationships with the *in-situ* acquired data. The presence of river originated materials across the region should impart unique adaptations to the phototrophic plankton through a gradient from those waters closed to origin of the plume to waters deep into the center of the eastern Caribbean.

3.3 Methodology

3.3.1 Field Work

The data used in this analysis was collected during oceanographic cruises part of the Caribbean Vorticity experiment (Cavortex 2 and 6), and the Orinoco River plume experiment (ORIPEX 7 and 8); aboard the UPRM R/V Chapman and the LUMCOM R/V Pelican (Figure 3.1). The Caribbean Vorticity Experiment (Cavortex II and VI) undertaken from June 22-27, 2004 and August 28, 2006 to September 8, 2006 were intended to characterize the physical, biogeochemical, and optical structure of the eddies and to assess their influence on biological productivity of the Eastern Caribbean Region. ORIPEX 7 and 8 cruises were carried out during November 19-24, 2005 and September 18-23, 2006 to analyze effects of the Orinoco River on the biogeochemical properties of the Eastern Caribbean.

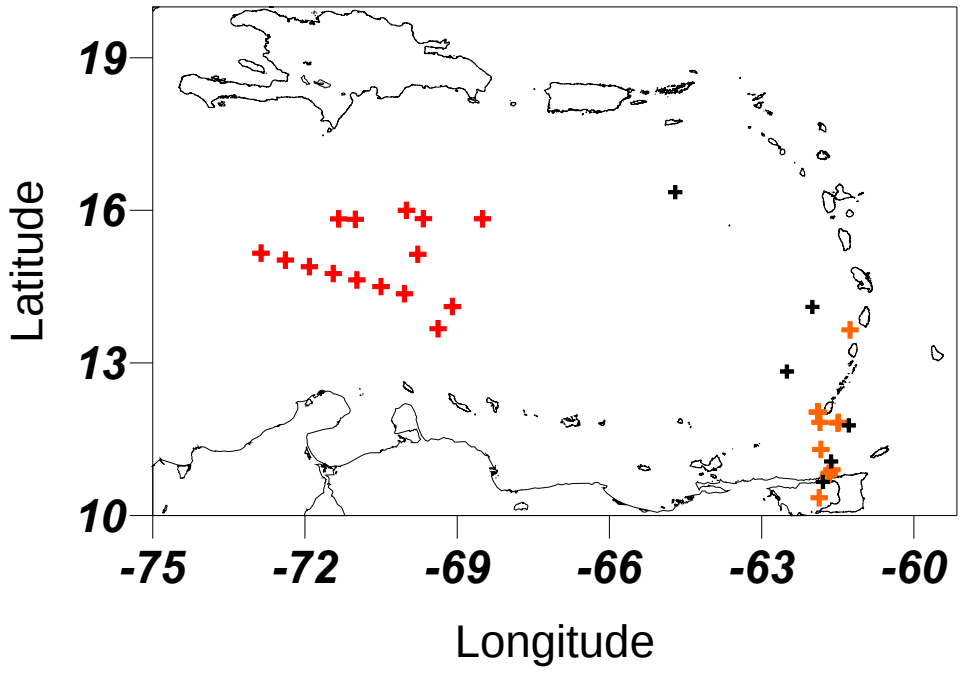

Figure 3.1. Stations sampled for phototrophic plankton bio-optical characteristics during Cavortex 6 (Red) and Oripex 7 (black) and 8 (orange).

In situ measurements were collected with a towed profiling vehicle (N*v*-Shuttle) manufactured by Chelsea Instruments Ltd, which maximized the spatial resolution and efficiency of the sampling. This vehicle is fitted with a Fast Repetition Rate Fluorometer (FRRF) to measure the physiological state of the phototrophic plankton, MINIpack (with a CTD-F and 24 channel data logger integrated capable of real time data acquisition), and a photosynthetically available radiation (PAR) irradiance meter. The N*v*-Shuttle was operated with continuous oscillations from surface to a maximum of 90 meters when possible. Diffuse attenuation coefficients were calculated over the depth of the euphotic zone according to $K_d = \ln[E(0^-)/E(Z_{1\%})] /Z$. The depth interval was chosen to extend from near the surface ($Z = 0^-$, i.e., ca 5 m) to the bottom of the euphotic zone ($Z=1\%E(0)$). The euphotic zone was define as the depth at which irradiance is diminished to 1% of the surface values, equivalent to an optical depth ($\xi = K_d Z$) of 4.6 (kirk 1994).

In addition the FRRF was deployed on oceanographic rosette cast at some of the sampled stations during the experiments. The rosette was fitted with 24 Niskin bottles which were used to obtained discrete water samples for phototrophic plankton specific absorption data, phototrophic plankton chlorophyll-a, nutrients and ^{14}C assimilation experiments. A SeaBird SBE 19 SEACAT CTD profiler was also fitted in the rosette and its data was processed, filter, binned, and parameters derived using the SeaBird Data Processing software version 7.16a. The concentration of phototrophic plankton chlorophyll-a was obtained from samples filtered through 0.7 μm glass fiber filters (Whatman GF/F) using the standard fluorometric method (Yentsch and Menzel, 1963) measured in a Turner AU-10 Fluorometer.

3.3.2 Variable Fluorescence

Variable fluorescence (*Fv/Fm*, unit less) and functional absorption cross-section at photosystem 2 (σ_{PSII}, units $Å^2$ quanta $^{-1}$) were logged on an internal flash card and downloaded to a PC after each transect. The FRRF measures these parameters for seawater that is exposed to ambient irradiance, and also simultaneously on seawater passed through a 'dark chamber' placed in front of one of the photomultiplier tube (PMT) window. Only the dark adapted data was analyzed, and most of the data presented in the analysis was gathered at night except when only day transects were possible. Data gathered during the day in the first 20 meters were consider unusable owing to saturation of the PMT from high surfaces irradiances and was removed. The instrument flash protocol was set for 100 saturation flashes per sequence with a saturating flash duration of 1.10 μs and an interflash delay of 51.6 μs. This was followed by 20 decay flashes each of 1.10 μs duration with an interflash delay of 51.6 μs. The raw data was processed using Chelsea's FRS processing software. Depth was provided by an internal logging calibrated sensor of the MINIpack throughout N*v*-Shuttle deployments.

The variable fluorescence is determined when dark-adapted cells are illuminated, all of the functional reaction centers are "open" and ready to receive an exciton, thus their fluorescence yield is low (*F*o) (since maximal excitation energy can be efficiently used for photosynthesis). When a given reaction center has received an exciton it is closed, consequently associated fluorescence yield increases. When all the reaction centers are closed (or non-functional), the observed fluorescence is maximal (*F*m). Variable fluorescence (Fv = *Fm - Fo)*is then obtained when normalized to *F*m, and it is an indicator of the proportion of photosystem II (PS2) reaction centers that are functional; *F*v/*Fm* has been empirically determined to be about 0.65 for cultures of phototrophic plankton growing under optimal conditions (e.g., Kolber et al., 1988).). The absorption cross section of PSII (σ_{PSII}) changes in response to cellular pigment concentrations and the efficiency of energy transfer from pigments to PSII reaction centers, thus making it subject to both nutrient and light availability (Kolber et al., 1988; Moore et al., 2006). σ_{PSII} is typically lower in nutrient replete cells relative to unhealthy cells (Kolber et al., 1988).

Blanks were collected from waters samples gathered at depths from 250 to 300 meters. Sea water from these depths then was placed and dark adapted for 30 minutes and then measured

in the FRRF dark chamber. In some of the cruises water above the 200m was collected and filtered through a 0.2μm filter and used as a blank. The resulting fluorescence transients from these samples were then used as blanks. This methodology represents a practical solution correcting low *in-situ* fluorescence signals as demonstrated by Cullen and Davis (2003). The FRRF maximum fluorescence signal of every cast or transect acquired was also compared with the SeaBird fluorometer mounted on the rosette in the cast profiles and with the Chelsea MiniPack CTD-F mounted on the N*v*-Shuttle to monitor the fluorometer sensitivity to changes in chlorophyll concentration.

The FRRF parameters were filtered for noise using the low pass signal filter function Butterworth in the Matlab signal processing tool box.

3.3.3 Maximum quantum yield of carbon fixation

The maximum quantum yield of carbon fixation was calculated from FRRF parameters and it is related to PSII characteristics according to the following relationship (Kolber and Falkowski, 1993):

$$\varphi_{max} = \eta PSII\ \sigma PSII\ \varphi_e\ f\ (a^*_{ph}\ R)^{-1} \qquad (1)$$

where $\sigma PSII$ is the effective absorption cross section of PSII ($10^{-20} m^2$ quanta^{-1}); φ_e is the maximum quantum yield of electron transport for O_2 evolution in PSII (mol O_2 (mol electron)$^{-1}$); R is the photosynthetic quotient (mol O_2 (mol C)$^{-1}$); ηPSII is the total number of PSII per unit of chlorophyll (mol electron (mg Chl-a)-1); a^*_{ph} is the phototrophic plankton absorption coefficient normalized to Chl-a (m^2 (mg Chl-a)$^{-1}$); f is the proportion of functional PSII reaction centers, calculated as (Fv/Fm)/ 0.65. Equation 1 represent the different stages occurring during photosynthesis light capture by the photosynthetic apparatus: the total number of photosynthetic units and its absorption cross section, charge separation at the reaction center represented by the proportion of active reaction centers and finally CO_2 reduction by the electrons reduced during light reactions represented by the maximum quantum yield of electron transport for O_2 evolution and the photosynthetic quotient. The φ_c is considered to be 0.25 O_2 (electron)$^{-1}$ for data at

irradiances lower than Ek (*u*mol quanta m-2 s-1) (Kolber and Falkowski, 1993). R varies depending to irradiances and on the type of nitrogen assimilated, being close to 1.4 in eutrophic environments were nitrate is the principal nitrogen source, and close to 1 where ammonia is N source. In this study most of the waters are consider to be based on N from ammonia as by the evidence observed by Morell and Corredor (2001) on the photomineralization of dissolved organic matter originated from the river plume.

3.3.4 FRRF based Primary Production

FRRF measurements of quantum yield were calculated according to the following equation using the model developed by Kolber & Falkowski (1993) and adjusted by Melrose et al. (2006):

$$P\mathrm{c}^{\mathrm{B}} = I\ \sigma\mathrm{PSII}\ q\mathrm{p}\ \varphi\mathrm{e}\ f\ \eta\mathrm{PSII} / \mathrm{PQ} \qquad (2)$$

$P\mathrm{c}^{\mathrm{B}}$ is the rate of carbon fixation normalized to chlorophyll *a* (Chl *a)* at irradiance *I* (μmol quanta $\mathrm{m}^{-2}\ \mathrm{s}^{-1}$). PQ is the photosynthetic quotient, and a typical value of 1.2 mol oxygen mol^{-1} carbon was assumed. The functional absorption cross section of PSII is σPSII (Å2 quanta^{-1}). A conversion factor of 0.291409 was applied to the results of Eq. (2) to give the final productivity results (in mg C mg^{-1} Chl-*a* h^{-1}). This factor includes conversions for micromoles quanta to moles quanta, moles Chl *a* to milligrams Chl *a*, quanta to moles quanta, square ångströms to square meters, seconds to hours, and moles C to milligrams C. The ηPSII term in Eq. (2) is the ratio of PSII reaction centers to Chl *a* (mol electrons mol^{-1} Chl *a*). This term cannot be measured by the FRRF (Kolber et al., 1998, Suggett et al., 2001), nor can it easily be determined by other means. This limitation also applied to the PPF technique used by Kolber & Falkowski (1993). Their solution was to estimate the value of ηPSII by assuming a typical value for the western North Atlantic of 0.002 mol electrons mol^{-1} Chl *a* (Kolber and Falkowski, 1993). The use of a constant value for ηPSII introduces a potential source of error to the calculations of productivity. Kolber and Falkowski (1993) suggest this value may vary by a factor of 3 in the oceans.

The *q*p term in Eq. (1) describes photochemical quenching, and can be expanded to:

$$\boldsymbol{q}\mathbf{p} = (\boldsymbol{F}\mathbf{m}' - \boldsymbol{F}') / (\boldsymbol{F}\mathbf{m} - \boldsymbol{F}\mathbf{o}) \qquad (3)$$

*F*o' and *F*m' are measure in the FRRF 'light chamber' exposed to ambient light and *F*o and *F*m are measured at the 'dark chamber' were the samples have been subjected to a period of dark adaptation.

The theoretical maximum photosynthetic energy conversion efficiency, f, is given by Eq. (4) such that:

$$f = (1/0.65)\ [(Fm - Fo)/Fm] \quad (4)$$

In-situ irradiance profiles were used to determine the diffuse attenuation coefficients (Kd) for the sampled areas. This parameter was later used to model the irradiance at solar noon of each cast or transect using the latitude and solar declination, according to the procedure described by Alfonso-Sosa (2001). This procedure ensures equality in the distribution of the light field through the estimates, independent of changes in the light field due to the environmental factors such as clouds or aerosols.

The FRRF instantaneous estimates were then extrapolated to day length to estimate daily primary production. These estimates were then integrated to a depth of 100 meters to determine the daily integrated production estimate of the zone.

3.3.5 Monte Carlo model to calculate uncertainties in the primary production estimates derived from FRRF.

The Monte Carlo approach is based on repeat calculations of production using randomly generated numbers. Random numbers based on the observed in situ distributions, of normal distribution and within the expected limits, were generated for the phototrophic plankton photosynthetic efficiency (*Fv/Fm*) and absorption cross section of PSII ($\sigma PSII$) using Matlab in built function Random. A total of 1000 interactions per sample were performed and the result of every pair of random combination of the parameters was introduced into equation 2 to estimate production. To estimate the distribution of each 1000 interactions the confidence intervals at 95% were calculated along with the mean and standard deviation values.

3.3.6 Natural Fluorescence based Primary Production

Optical data were acquired by a PRR-600 profiler spectroradiometer (Biospherical Instruments Inc., San Diego) which can collect data at a maximum rate of 3 Hz. The instrument can measure downwelling irradiance, $E_d(\lambda,z)$, and upwelling radiance, $L_u(\lambda,z)$, at six bands: 412, 443, 490, 510, 555, and 665 nm. In addition, it measures the downwelling photosynthetically available radiation, $E_d(PAR,z)$ and the upwelling radiance at 683 nm, $L_u(683,z)$. The instrument was equipped with temperature, pressure and tilt-roll sensors. A similar radiometer with identical irradiance bands, the PRR-610, was located above sea surface at the highest point at the vessels, to avoid shadows. The downwelling irradiance measurements were normalized to the surface irradiance measurements on deck taken by a PRR-610 radiometer. This reduces the effect of cloud interference during a cast. The data were binned to 1m intervals. From these data we obtain the PAR diffuse attenuation coefficient profile, $K_d(PAR,z)$.

The upwelling radiance measurements centered at 683 nm (10 nm bandwidth), $L_u(683,z)$, were used to estimate the natural fluorescence flux, $Ff(z)$. The PAR downwelling irradiance was converted to scalar irradiance multiplying it by a factor g = 1.3 (Morel, 1991). The $L_u(683,z)$ readings above the 6 m depth level were discarded due to a contribution by direct light and elastic backscattering light. The equation used to estimate the natural fluorescence profile, $Ff(z)$, from the nadir radiance at 683 nm, $L_u(683,z)$ and PAR comes from (Kiefer and Chamberlin, 1989)

$$Ff(z) = 4\pi\, 27 Lu(683, z) \times [k(PAR, z) + a(683, z)] \qquad (5)$$

where a(683,z) is the 683 nm absorption coefficient profile and K_d (PAR,z) is the attenuation coefficient profile of the scalar irradiance, $E_0(PAR,z)$. The absorption coefficient for clear water is 0.47 m^{-1} (Pope and Fry, 1997). The factor 27 in equation 5 comes from the fact that the total fluorescence in the far red is 27 times higher than the emitted at the band centered at 683 nm.

To obtain the photosynthetic rate from natural fluorescence we use the equation developed by Chamberlin et al. (1990),

$$F_c = F_f \frac{k_{cf}\, \varphi_{rmax}}{k_{cf}\, E_o\,(PAR)} \qquad (6)$$

where k_{cf} and $\varphi_{rmax\_}$ are empirical constant and are the maximum value of the ratio of the quantum yields of photosynthesis to fluorescence and irradiance at which this ratio is one–half the maximum. A value of 4.0 carbon atoms per photon has been assigned to $\varphi_{rmax\_}$ and for k_{cf} a value of 133 ($mEm^{-2}sec^{-1}$).

3.3.7 ^{14}C assimilation experiments

Measurements of photosynthetic parameters (P^B max and α^B) from the ^{14}C method were made during the cruise Oripex 7 in the *P*/*E* parameters were determined on water samples collected from the surface mixed layer and deep chlorophyll maximum at dawn and incubated with $H^{14}CO3$ for 1 to 2 h in a light gradient cooled incubator. Carbon fixation rates were normalized to chlorophyll concentration and *P*/*E* curves were fitted to the equations of Platt et al. (1980)

3.3.8 Satellite Based Net Primary Production Estimates

3.2.8.1 *Eppley*-VGPM Net Primary Production (NPP) calculations

MODIS remotely acquired chlorophyll and temperature data were used to calculate the Vertically Generalized Production Model (VGPM) (Behrenfeld and Falkowski, 1997a). The VGPM is a "chlorophyll-based" model that estimates net primary production from chlorophyll using a temperature-dependent description of chlorophyll-specific photosynthetic efficiency. The *Eppley*-VGPM is a hybrid model that employs the basic model structure and parameterization of the standard VGPM but replaces the polynomial description of Pb_opt with the exponential relationship described by Morel (1991) and based on the curvature of the temperature-dependent growth function described by Eppley (1972). The foundation of the *Eppley*-VGPM is that NPP varies in a predictable manner with chlorophyll concentration (Chl a):

$$\mathbf{NPP = Chl\text{-}a\ P^{b}_{opt}\ day\ length\ [0.66125 * par / (\ par + 4.1\ )]\ *\ z_{eu}} \qquad (7)$$

where P^{b}_{opt} is the Maximum C fixation rate within a water column, mgC (mg Chl)$^{-1}$ h^{-1}; Chl-a is the satellite estimated chlorophyll concentration; day length is the number of hours of day light at the location of interest; [0.66125 * par / (par + 4.1)] is the light dependent term determined empirically using thousands of field productivity measurements; and z_{eu} is the euphotic depth and is calculated using the Morel and Berthon (1989) Case I model. This model estimates z_{eu} from surface chlorophyll concentrations and is based on empirical equations to fit field data. P^{b}_{opt} reflects a correlation between sea surface temperature (SST) and photoacclimation; warmer waters generally have shallower physiological surface mixing depths and higher incident PAR. These conditions favor high-light acclimated phototrophic plankton, which requires less chlorophyll to support photosynthetic requirements for growth. This lower chlorophyll concentration gives rise to high chlorophyll-specific photosynthetic rates. In other words, increasing P^{b}_{opt} with increasing SST. The empirical model developed by Behrenfeld and Falkowski (1997a) is parameterized from the observed relationship between median P^{b}_{opt} and temperature and is presented in eq. 7.

(8)

$$P^{b}_{opt} = -3.27 \times IO^{-8} T^{7} + 3.4132 \times lO^{-6} T^{6} - 1.348 \times 10^{-4} T^{5}$$
$$+ 2.462 \times 1\,0^{-3} T^{4} - 0.0205\, T^{3} + 0.0617\, T^{2} + 0.2749\, T + 1.2956.$$

MODIS level 1A products were downloaded from the NASA ocean color web portal http://oceancolor.gsfc.nasa.gov/. These products were then process to level 2 to obtain Chl-a and SST products. The images were processed using SeaWiFS Data Analysis System (SeaDAS) version 5.1.

3.3.8.1 CbPM Net Primary Production (NPP) calculations

MODIS remotely acquire particle backscatter at 443 nm, chlorophyll and the vertical attenuation coefficient at 490 nm data were used to obtain the Carbon-based Productivity Model (CbPM) NPP calculations. The CbPM concept uses carbon biomass (C_{phyto}) and growth rate (u) instead of chlorophyll and Pbopt as previously used by the VGPM to estimate NPP. This is based on the observation that that total particulate carbon concentration and C_{phyto} covary with light scattering properties (Behrenfeld and Boss, 2003 and 2006b). With the above information on surface phototrophic plankton carbon and growth rates, water column integrated NPP for the currently employed CbPM is simply:

$$\mathbf{NPP = C\ } u \mathbf{\ irradfunction\ z_{eu}} \quad (9)$$

where C is the carbon biomass, and is obtained through the following relationship.

$$\mathbf{C = 13000 * (bbp - 0.00035)} \quad (10)$$

The C relationship was described by Behrenfeld 2005 et al. (2005) and comes from a regression of monthly mean satellite-retrieved values of bbp(443) and Chl. The phototrophic plankton growth rate (u) is obtained from the following relationship.

$$U = u\mathbf{(max)\ f(N,T)\ g(Ig)} \quad (11)$$

where the factor for the suppression of growth rate by nutrient and temperature stress is

$$\mathbf{f(N,T) = (Chl : C)\ observed\ /\ (Chl : C)\ max} \quad (12)$$

and the light limitation factor is calculated as follows from the

$$\mathbf{g(Ig) = 1 - exp^{(-3Ig)}} \quad (13)$$

median mixed layer light level parameter.

$$\mathbf{Ig = irradiance\ /\ day\ lenght\ exp^{(-k490\ *\ mix\ layer\ depth\ /\ 2.0)}} \quad (14)$$

The chl to Carbon maxima is obtained through the following relationship,

$$\mathbf{(Chl : C)\ max = 0.022 + (0.045\text{-}0.022)\ *\ exp^{(-3.0\ *\ Ig)}} \quad (15)$$

and finally the euphotic depth at 1% light level is z_{eu} is calculated using the Morel and Berthon (1989) Case I model. This model estimates z_{eu} from surface chlorophyll concentrations and is based on empirical equations to fit field data.

3.3.9 Bio-optical data

3.3.9.1 *Chlorophyll-specific absorption coefficient of phototrophic plankton*

Particulate absorption samples were collected on 0.7 μm GF/F filters, which were placed on a drop of distilled water and the absorption of the total particulate ap(λ) (relative to a blank filter saturated with distilled water) was measured with Perkin Elmer Lambda 18 UV/VIS Spectrometer fitted with an integrating sphere. Methanol extractable pigments were removed by slowly passing hot methanol through the filter pad (Roesler et al., 1989). The absorption spectrum of this pad was measured to determine the detritus absorption coefficient, ad(λ). Optical density measurements were divided by the geometrical path length (volume filtered divided by clearance area of the filter) and multiplied by a factor of 2.3 (conversion factor for transforming decimal logarithms to natural logarithms) to obtain the absorption coefficient. The value of the absorption coefficient at 750 nm was subtracted from the values at all other wavelengths, as a rudimentary correction for errors arising from scattering by the phototrophic plankton cells. The measurements were corrected for path-length amplification, β factor, using the method of Bricaud and Stramski (1990). The difference between the particulate and detritus spectra, before and after the methanol extraction, is considered the *in vivo* phototrophic plankton absorption, $a_{ph}(\lambda)$. The pigment specific absorption coefficient of phototrophic plankton , $a_{ph}^*(\lambda)$ was calculated by dividing absorption by the chlorophyll-a concentration obtained fluorometrically.

3.3.9.1 *Slope of normalized absorption curves*

To evaluate changes in the shape of the a_{ph} spectra from 488 to 532 nm, we normalized the absorption data to 676 nm. The slopes of the normalized absorption curves from 488 to 532 nm (Eisner et al., 2003) were computed as:

$$a_{ph}\ \text{slope} = \frac{(a_{ph}\,488 - a_{ph}\,532)}{(a_{ph}\,676(488 - 532\ \text{nm}))} \qquad (16)$$

The slope of the a_{ph} spectra from 490 to 530 nm (normalized to 676 nm) has been found to be steeper in high-light compared to low-light adapted cultures (Johnsen et al., 1994). Such a_{ph} spectral variations are due to physiological changes in cellular pigment ratios and pigment packaging. Under high light, increases in photoprotective carotenoids, decreases in photosynthetic carotenoids, and a reduction in pigment packaging may cause the a_{ph} spectral slopes to become steeper, while the reverse is true for low-light conditions.

3.3.9.1 *The 4th derivative analysis of absorption curves*

Analysis of the absorption spectra of phototrophic plankton included a derivative analysis to detect and determine quantitatively the position and intensity of weak absorption bands. The derivative of a curve, simply its slope at a given point, provides information regarding the convexity and concavity of a given absorption curve. It is useful for separating the secondary absorption peaks and shoulders produced by algal pigments in regions of overlapping absorption. The minima of the 2nd and the maxima of the 4th derivative occur close to or at wavelengths where there are absorption peaks attributable to pigments. Bidigare et al. (1989) found that while the spectrum for the 2nd derivative is very useful for qualitative identification of pigments, its magnitude does not provide a reliable measure of the concentration of photosynthetic pigments. This problem arises from the overlapping of pigments, that with a 4th derivative analysis was found to be resolved providing better information on pigment peaks and concentration. For the analysis herein a 4th derivative was performed following a Savitzky-Golay smoothing of 20 points.

3.4 Results

The FRRF based carbon fixation and ^{14}C estimates significantly correlated (r = 0.91, n= 9) with a the slope of 0.82 (Figure 3.2a) . A series of field measurements performed during Oripex 7 and Oripex 8 were used for this correlation. These measurements correspond to surface samples obtained through a gradient from the area of the Gulf of Paria to samples close to the island of Puerto Rico at station CaTS. Statistically the distribution of the estimates between the methods showed FRRF values to be higher than the observed estimates for ^{14}C. The minimum and maximum observed estimates by ^{14}C were 1.256 and 4.58 mg C/(mg chla hr) for these samples, FRRF estimates showed values that ranged from 1.33 to 4.70 mg C/(mg chla hr). The observed medians are 3.07 and 3.17 mg C/ (mg chla hr) respectively. When analyzed by geographical location (Figure 3.2b) the production estimates increased at latitudes close to the origin of the Orinoco River plume. The correlation between ^{14}C and its position against the gradient from the plume origin showed a low negative relationship (r = -0.46), when compared to latitude the FRRF estimates showed a lower relationship (r = 0.38).

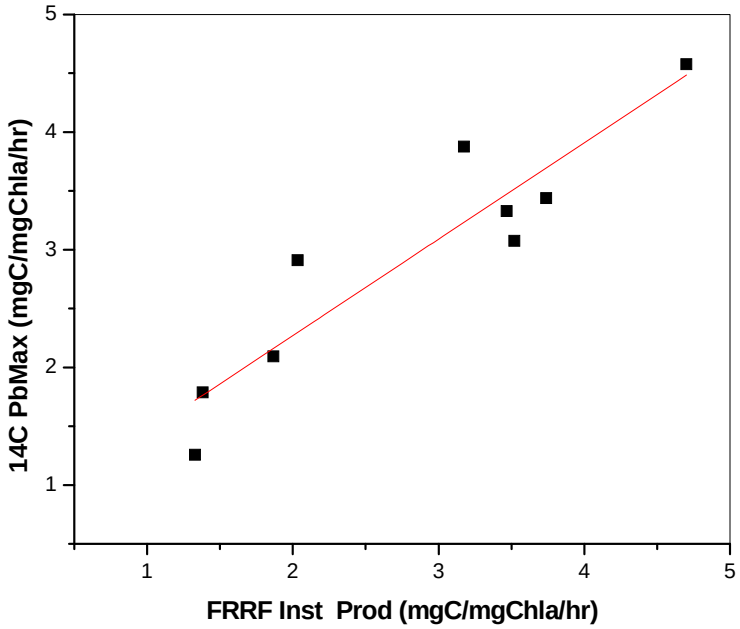

Figure 3.2a. Primary production obtained from ^{14}C incubations and Fast Repetition rate Fluorometry during Oripex 7. The correlation showed an r of 0.91.

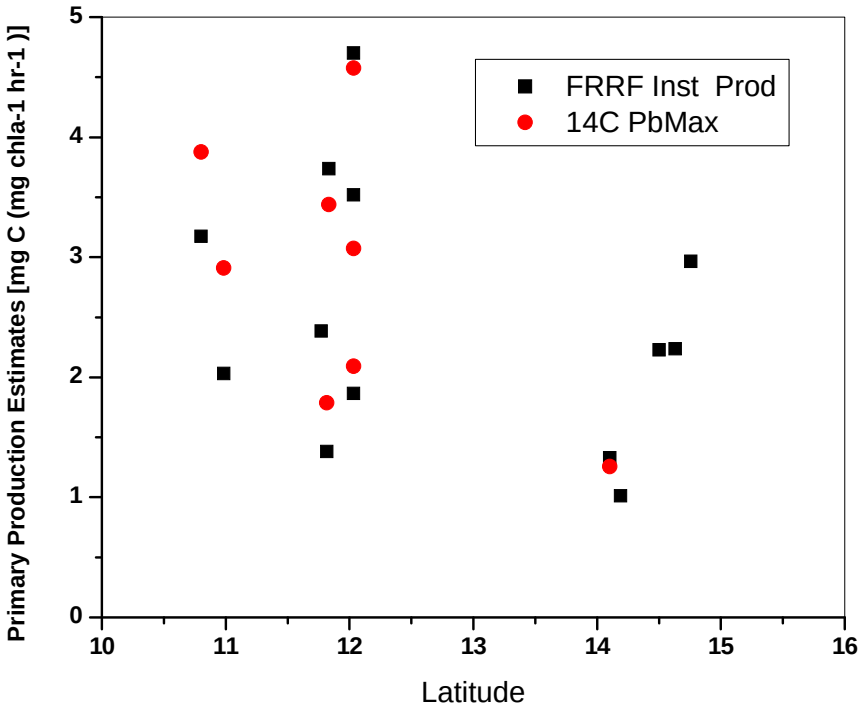

Figure 3.2b. Primary production estimates from ^{14}C and FRRF per sampled latitudes during Oripex 7, Oripex 8 and Cavortex 6. The correlation between ^{14}C and sampled latitude showed an inverse relationship and a r of - 0.46.

The uncertainties of FRRF primary production estimates were tested using Monte Carlo (MC) approximations (Figure 3.3, Table 3.1a, 3.1b). The variability in the estimates is rooted on the complexity of the models and the different variables involved, in order to generate a level of confidence in these production estimates, some estimate of error is needed. The estimates based on FRRF and ^{14}C were within the 95 % confidence intervals (CI) widths. The MC estimates (Table 3.1a, 3.1b) based on 1000 interactions per sample displayed that the means of the FRRF estimate and the MC approximation means varied from 1 % to 32% ; when correlated the means showed a r = 0.85 at a P-value of 0.05 (n = 32) (Figure 3.4). The lowest error was observed for the estimate was for the stations sampled during Oripex 7 at waters close to the Orinoco River plume. Higher error was observed at stations sampled in blue waters. The highest confidence interval difference was observed for the samples of CaTS and an inshore sample taken at the dock of Magueyes Island on the south coast of Puerto Rico (CI ranged 0.835 to 12.402 and 2.89 and 12.32 respectively).

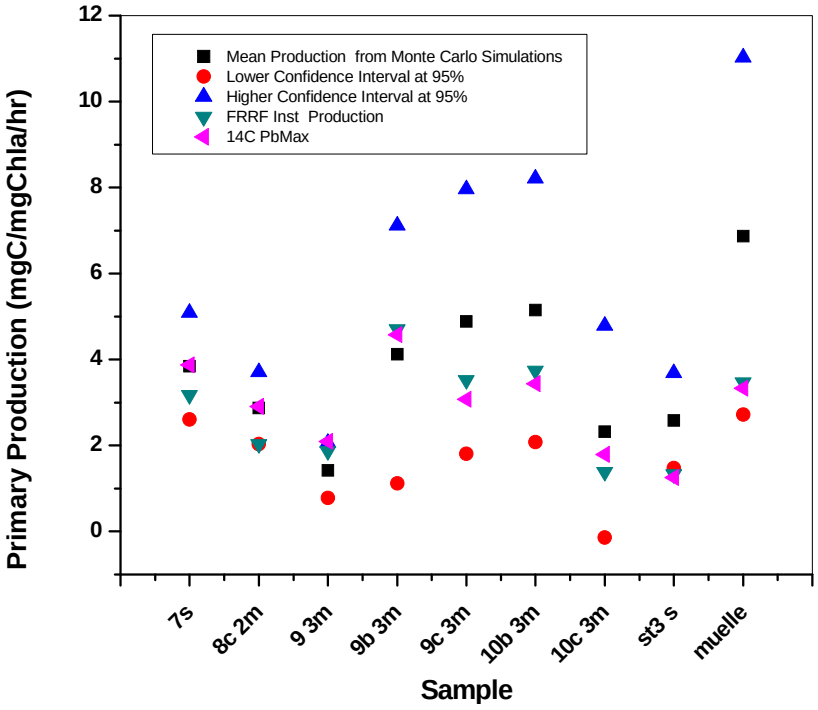

Figure 3.3. Primary production obtained from of the Fast Repetition rate Fluorometry and Monte Carlo Simulations and ^{14}C incubations. Confidence intervals show the extend of data distribution for Monte Carlo Simulations.

Phototrophic plankton bio-optical characteristics are summarized on Table 3.2. The chlorophyll specific absorption coefficient increased from lower latitudes to higher latitudes (Figure 3.5) but this relationship was moderately loose (r = 0.64). The highest chlorophyll specific absorption coefficient in the data set was 0.166 m^{-1} and the lowest 0.022 m^{-1} with an average of 0.089 m^{-1} The chlorophyll specific absorption coefficient at 440 showed values that ranged 0.022 - 0.163 with a mean value of 0.09 m^{-1} . Waters closed to the river plume displayed lower values of the absorption coefficient maxima than those at higher latitudes far from the river influence. The highest chlorophyll concentration was observed at the lowest latitudes close to the river plume also (Figure 3.6). An exponential relationship was observed between the parameters (r= 0.64). The ratio of absorption coefficient at 676 to 440 also showed values higher

at the lowest latitudes with the highest 0.831 close to the river plume origin0.41) between the parameters. The ratio of absorption coefficient at 676 to 440 also showed values higher at the lowest latitudes with the highest 0.831 close to the river plume origin (Dragon's Mouth between Trinidad and Venezuela) the lowest (0.17) was observed in oceanic samples during Cavortex 6.

Table 3.1a. Summary of primary production estimates for surface samples during Oripex 7 and 8.

Station	*Long*	*Lat*	*K_d PAR*	*Pmin from Monte Carlo Simulations*	*Pmax from Monte Carlo Simulations*	*Mean Production from Monte Carlo Simulations*	*Standard Deviation from Monte Carlo Simulations*	*Variance from Monte Carlo Simulations*	*Lower Confidence Interval at 95%*	*Higher Confidence Interval at 95%*	*FRRF Estimated Production [mgC(mgChla)$^{-1}$ hr^{1}]*	*$^{14}C\ P^{b}_{Max}$ [mgC(mgChla)$^{-1}$ hr^{1}]*
Ori7 st7s	-61.68	10.80	0.31	2.57	5.26	3.85	0.63	0.39	2.60	5.08	3.17	3.87
Ori 7 st8c 2m	-61.66	10.83	0.36	1.98	3.86	2.87	0.43	0.18	2.03	3.71	2.03	2.91
Ori 7 9 3m	-61.88	12.03	0.10	0.77	2.22	1.422	0.32	0.11	0.78	2.06	1.86	2.09
Ori 7 9b 3m	-61.90	12.03	0.10	1.35	8.05	4.12	1.53	2.34	1.12	7.11	4.70	4.57
Ori 7 9c 3m	-61.90	12.03	0.10	2.09	8.06	4.89	1.57	2.47	1.80	7.96	3.51	3.07
Ori 7 10b 3m	-61.48	11.83	0.09	2.14	9.53	5.15	1.56	2.45	2.08	8.21	3.73	3.43
Ori 7 10c 3m	-61.50	11.81	0.09	0.23	5.38	2.32	1.26	1.58	0.14	4.78	1.38	1.78
Ori 8 st3 s	-62	14.10	0.18	1.50	3.93	2.58	0.56	0.32	1.47	3.68	1.32	1.25
Dock	-67.04	17.96	0.11	2.90	12.32	6.87	2.12	4.49	2.71	11.02	3.46	3.32

Table 3.1b. Production estimates and Monte Carlo Simulation estimates for sampled stations across the Eastern Caribbean.

Station & Expedition	*Pmin from Monte Carlo Simulations*	*Pmax from Monte Carlo Simulations*	*Mean Production from Monte Carlo Simulations*	*Standard Deviation from Monte Carlo Simulations*	*Variance from Monte Carlo Simulations*	*Lower Confidence Interval at 95%*	*Higher Confidence Interval at 95%*	*Quantum yield of Carbon Fixation* $mol\ C\ (mol\ quanta)^{-1}$	*FRRF Estimated Production* $mgC(mgChla)^{-1}\ hr^{1}$	$^{14}C\ P^{b}_{Max}$ $mgC(mgChla)^{-1}\ hr^{1}$
Oripex 7										
7s	**2.57**	**5.27**	**3.85**	**0.63**	**0.40**	**2.61**	**5.09**	**1.58**	**3.17**	**3.88**
7 13m	**0.05**	**0.09**	**0.07**	**0.01**	**0.00**	**0.05**	**0.09**	**1.38**	**0.04**	**--**
7 50m	**0.01**	**0.02**	**0.02**	**0.00**	**0.00**	**0.01**	**0.02**	**0.75**	**0.02**	**--**
8 2m	**2.92**	**6.23**	**4.49**	**0.74**	**0.55**	**3.03**	**5.94**	**1.98**	**2.89**	**--**
8 48 m	**0.28**	**0.53**	**0.40**	**0.07**	**0.00**	**0.27**	**0.53**	**1.72**	**0.23**	**--**
8b 2m	**4.40**	**8.59**	**6.42**	**1.05**	**1.09**	**4.37**	**8.47**	**2.27**	**3.58**	**--**
8b 9m	**2.82**	**4.79**	**3.78**	**0.51**	**0.26**	**2.77**	**4.78**	**2.01**	**3.14**	
8b 15 m	**4.64**	**8.52**	**6.54**	**0.95**	**0.90**	**4.68**	**8.39**	**2.58**	**3.91**	**--**
8c 2m	**1.98**	**3.86**	**2.87**	**0.43**	**0.18**	**2.03**	**3.71**	**--**	**2.03**	**2.91**
9 3m	**0.77**	**2.22**	**1.42**	**0.33**	**0.11**	**0.78**	**2.06**	**0.48**	**1.87**	**2.09**
9 40m	**1.89**	**3.88**	**2.84**	**0.51**	**0.26**	**1.83**	**3.85**	**1.91**	**2.14**	**--**
9 70 m	**0.48**	**0.70**	**0.59**	**0.05**	**0.00**	**0.49**	**0.69**	**1.59**	**0.44**	**--**
9b 3m	**1.35**	**8.05**	**4.12**	**1.53**	**2.34**	**1.12**	**7.12**	**1.16**	**4.70**	**4.58**
9b 25m	**2.48**	**4.25**	**3.33**	**0.44**	**0.20**	**2.46**	**4.20**	**2.12**	**2.51**	**--**
9b 80m	**0.08**	**0.15**	**0.11**	**0.02**	**0.00**	**0.08**	**0.14**	**1.28**	**0.09**	**--**
9c 3m	**2.10**	**8.06**	**4.89**	**1.57**	**2.47**	**1.81**	**7.96**	**1.29**	**3.52**	**3.07**
9c 30m	**3.61**	**6.98**	**5.22**	**0.86**	**0.74**	**3.53**	**6.91**	**2.14**	**3.52**	**--**
9c 47	**1.65**	**3.39**	**2.47**	**0.43**	**0.18**	**1.64**	**3.31**	**1.64**	**1.64**	**--**
10b 3m	**2.14**	**9.54**	**5.15**	**1.56**	**2.45**	**2.08**	**8.21**	**1.67**	**3.74**	**3.44**
10 b dcm	**2.46**	**4.16**	**3.30**	**0.47**	**0.22**	**2.38**	**4.22**	**2.29**	**2.26**	**--**
10c 3m	**0.24**	**5.38**	**2.32**	**1.26**	**1.58**	**-0.14**	**4.79**	**1.09**	**1.38**	**1.79**
10 c dcm	**0.90**	**2.10**	**1.49**	**0.29**	**0.09**	**0.92**	**2.07**	**2.12**	**0.92**	**--**
0ripex 8										
st3 s	**1.50**	**3.93**	**2.58**	**0.56**	**0.32**	**1.48**	**3.68**	**--**	**1.33**	**1.26**
CaTS	**0.84**	**12.40**	**5.07**	**2.60**	**6.73**	**0.01**	**10.16**	**--**	**3.50**	**--**
Magueyes Dock										
Muelle	**12.32**	**6.87**	**2.12**	**4.49**	**2.72**	**11.03**	**--**	**3.47**	**3.33**	**12.32**
Cavortex 6										
st3bs	**2.65**	**1.37**	**0.45**	**0.20**	**0.48**	**2.25**	**1.33**	**2.23**	**--**	**2.65**
st4s	**3.65**	**2.05**	**0.63**	**0.40**	**0.82**	**3.29**	**1.21**	**2.24**	**--**	**3.65**
st5s	**3.28**	**2.13**	**0.52**	**0.27**	**1.11**	**3.15**	**1.45**	**2.96**	**--**	**3.28**
st6s	**4.48**	**2.55**	**0.74**	**0.54**	**1.11**	**4.00**	**1.51**	**2.76**	**--**	**4.48**
ST16S	**4.93**	**3.40**	**0.62**	**0.39**	**2.18**	**4.62**	**1.64**	**3.49**	**--**	**4.93**
ST17S	**4.25**	**3.16**	**0.45**	**0.20**	**2.28**	**4.04**	**--**	**3.51**	**--**	**4.25**
st21s	**4.46**	**3.36**	**0.49**	**0.24**	**2.39**	**4.33**	**--**	**2.82**	**--**	**4.46**

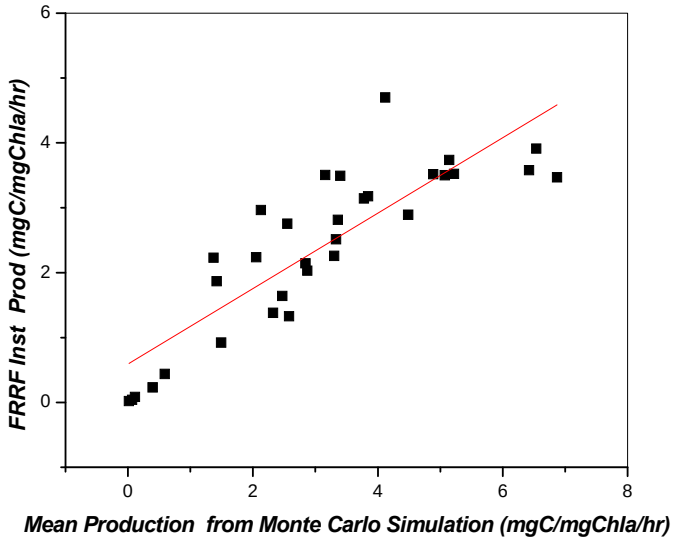

Figure 3.4. Primary production obtained from of the Fast Repetition rate Fluorometry and Monte Carlo Simulations. The correlation showed an r of 0.85 and n = 32.

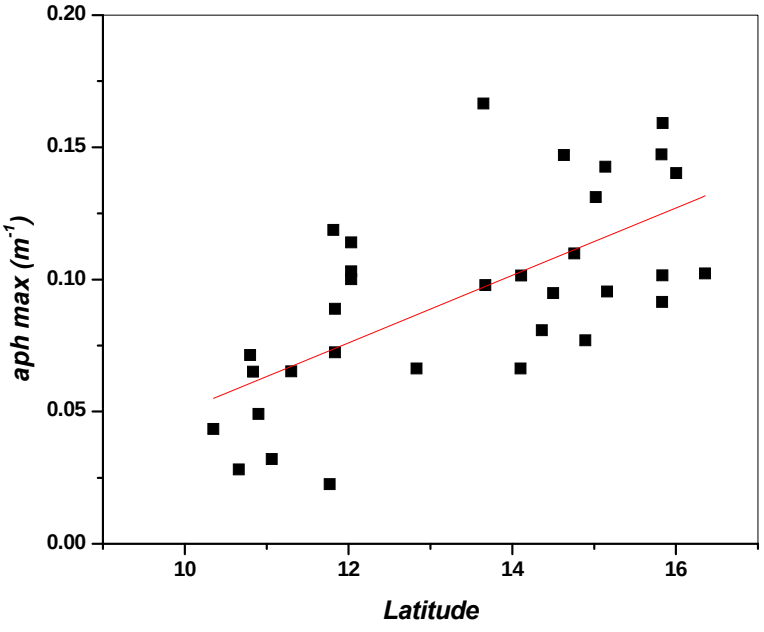

Figure 3.5. Phototrophic plankton absorption coefficient maxima at sampled latitudes during Oripex 7, Oripex 8 and Cavortex 6. The correlation showed a direct relationship (r = 0.64).

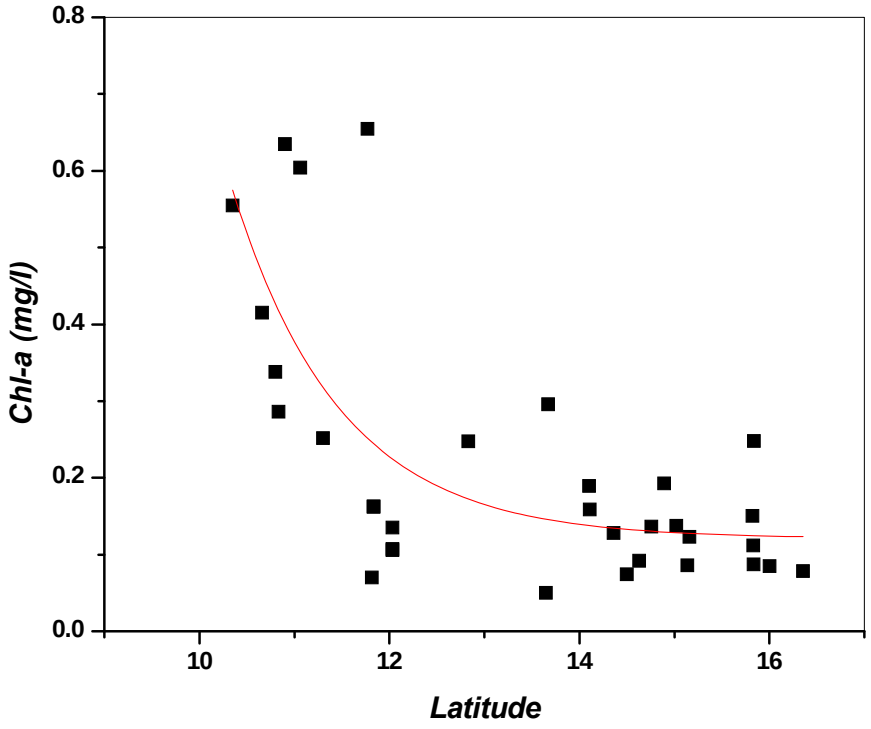

Figure 3.6. Chlorophyll-a concentration at sampled latitudes during Oripex 7, Oripex 8 and Cavortex 6. The correlation showed an exponential relationship (r =0.83).

The slope of the specific absorption spectra displayed values that ranged from - 0.016 to -0.0007 (Table 3.2). The highest slopes were observed at stations far from the influence of the river plume, sampled during Cavortex 6 (Figure 3.7), indicating less packaging. When compared to chlorophyll concentration the absorption slope demonstrated an exponential (r= 0.72) relationship (Figure 3.8) with higher slopes observed at low chlorophyll concentrations. The relationship of the slope with the absorption coefficient ratio 676/440 displayed an inverse relationship (r= 0.83). The slope decreased with increasing ratio (Figure 3.9). An increase in the ratio implies higher chlorophyll concentration. Similarly, the slopes also have the same relationship with the quantum yield for carbon fixation. Although a low relationship was observed (r= 0.48) the quantum yield was favorably affected when the absorption slopes decreased (Figure 3.10). Lower slopes due to packaging are indicative of photosynthetically active carotenoids (Eisner et. al., 2003), that in our case maybe favoring the quantum yield for carbon fixation.

Table 3.2 Phototrophic plankton Bio-optical characteristics and production estimates summary at the sampled stations.

Station	*A674/443*	*A674/490*	*Average abs*	*Abs 412*	*Abs 440*	*Chl-a*	*Fv/Fm*	*σ PSII*	*aph Slope*	*aph max*	*Quantum yield*	*FRRF Inst Prod mgC(mg Chla)$^{-1}$ hr^{1}*	*14C PbMax mgC(mgC hla)$^{-1}$ hr^{1}*
Oripex 7													
7s	**0.60**	**0.98**	**0.03**	**0.06**	**0.07**	**0.34**	**0.45**	**501.63**	**-0.01**	**0.07**	**1.58**	**3.17**	**3.88**
7 13m	**0.45**	**0.55**	**0.04**	**0.07**	**0.08**	**0.37**	**0.50**	**435.81**	**-0.02**	**0.08**	**1.38**	**0.04**	**--**
7 50m	**0.39**	**0.52**	**0.06**	**0.12**	**0.11**	**0.15**	**0.41**	**613.70**	**-0.02**	**0.12**	**0.75**	**0.02**	**--**
8 2m	**0.59**	**0.89**	**0.03**	**0.06**	**0.06**	**0.29**	**0.47**	**501.64**	**-0.01**	**0.07**	**1.98**	**2.89**	**--**
8 48 m	**0.51**	**0.68**	**0.03**	**0.06**	**0.07**	**0.31**	**0.48**	**577.92**	**-0.02**	**0.07**	**1.72**	**0.23**	**--**
8b 2m	**0.56**	**0.85**	**0.02**	**0.05**	**0.05**	**0.63**	**0.58**	**608.18**	**-0.01**	**0.05**	**2.27**	**3.58**	**--**
8b 9m	**0.54**	**0.68**	**0.03**	**0.06**	**0.06**	**0.47**	**0.49**	**437.23**	**-0.02**	**0.07**	**2.01**	**3.14**	
8b 15 m	**0.51**	**0.74**	**0.03**	**0.05**	**0.06**	**0.54**	**0.40**	**502.85**	**-0.02**	**0.06**	**2.58**	**3.91**	**--**
8c 2m	**--**	**--**	**--**	**--**	**--**	**--**	**0.40**	**400.00**	**--**	**--**	**--**	**2.03**	**2.91**
9 3m	**0.33**	**0.59**	**0.04**	**0.09**	**0.10**	**0.14**	**0.35**	**606.69**	**-0.03**	**0.10**	**0.48**	**1.87**	**2.09**
9 40m	**0.46**	**0.75**	**0.03**	**0.06**	**0.07**	**0.30**	**0.44**	**612.97**	**-0.02**	**0.07**	**1.91**	**2.14**	**--**
9 70 m	**0.52**	**0.72**	**0.04**	**0.07**	**0.08**	**0.26**	**0.45**	**571.82**	**-0.02**	**0.08**	**1.59**	**0.44**	**--**
9b 3m	**0.25**	**0.46**	**0.04**	**0.09**	**0.10**	**0.11**	**0.41**	**742.56**	**-0.04**	**0.10**	**1.16**	**4.70**	**4.58**
9b 25m	**0.51**	**0.72**	**0.03**	**0.07**	**0.07**	**0.28**	**0.53**	**483.77**	**-0.02**	**0.08**	**2.12**	**2.51**	**--**
9b 80m	**0.38**	**0.46**	**0.06**	**0.10**	**0.13**	**0.06**	**0.55**	**775.79**	**-0.04**	**0.14**	**1.28**	**0.09**	**--**
9c 3m	**0.27**	**0.52**	**0.04**	**0.10**	**0.11**	**0.11**	**0.41**	**571.37**	**-0.04**	**0.11**	**1.29**	**3.52**	**3.07**
9c 30m	**0.57**	**0.89**	**0.03**	**0.05**	**0.06**	**0.40**	**0.44**	**554.09**	**-0.02**	**0.07**	**2.14**	**3.52**	**--**
9c 47	**0.44**	**0.61**	**0.03**	**0.07**	**0.09**	**0.33**	**0.46**	**656.43**	**-0.03**	**0.09**	**1.64**	**1.64**	**--**
10b 3m	**0.44**	**0.63**	**0.03**	**0.06**	**0.07**	**0.16**	**0.40**	**406.59**	**-0.02**	**0.07**	**1.67**	**3.74**	**3.44**
10 b dcm	**0.46**	**0.63**	**0.03**	**0.05**	**0.07**	**0.40**	**0.42**	**604.72**	**-0.03**	**0.07**	**2.29**	**2.26**	**--**
10c 3m	**0.38**	**0.65**	**0.05**	**0.11**	**0.11**	**0.07**	**0.47**	**570.91**	**-0.03**	**0.12**	**1.09**	**1.38**	**1.79**
10 c dcm	**0.43**	**0.60**	**0.03**	**0.06**	**0.08**	**0.32**	**0.45**	**612.96**	**-0.03**	**0.08**	**2.12**	**0.92**	**--**
11 surf	**0.19**	**0.36**	**0.05**	**0.14**	**0.16**	**0.05**	**0.32**	**588.57**	**-0.05**	**0.17**	**0.78**	**--**	**--**
11 dcm	**0.49**	**0.69**	**0.03**	**0.05**	**0.07**	**0.14**	**0.41**	**599.05**	**-0.03**	**0.07**	**2.12**	**--**	**--**
Oripex 8													
st 2 s	**0.34**	**0.51**	**0.04**	**0.09**	**0.10**	**0.08**	**--**	**--**	**-0.04**	**0.10**	**--**	**--**	**--**
St2 dcm	**0.60**	**0.75**	**0.03**	**0.05**	**0.07**	**0.33**	**--**	**--**	**-0.02**	**0.07**	**--**	**--**	**--**
st3 s	**0.46**	**0.73**	**0.03**	**0.06**	**0.06**	**0.19**	**--**	**--**	**-0.02**	**0.07**	**--**	**1.33**	**1.26**
St6 s	**0.42**	**0.58**	**0.03**	**0.06**	**0.07**	**0.25**	**--**	**--**	**-0.02**	**0.07**	**--**	**--**	**--**
St6 dcm	**0.48**	**0.59**	**0.03**	**0.06**	**0.07**	**0.16**	**--**	**--**	**-0.03**	**0.07**	**--**	**--**	**--**
St 10 dcm	**0.77**	**1.01**	**0.02**	**0.03**	**0.03**	**0.60**	**--**	**--**	**-0.01**	**0.03**	**--**	**--**	**--**
St 13 s	**0.75**	**1.04**	**0.01**	**0.02**	**0.03**	**0.42**	**--**	**--**	**-0.01**	**0.03**	**--**	**--**	**--**
st4	**--**	**--**	**--**	**--**	**--**	**--**	**--**	**--**	**--**	**--**	**--**	**1.01**	**--**
st8s	**0.83**	**1.10**	**0.01**	**0.02**	**0.02**	**0.65**	**0.30**	**836.17**	**0.00**	**0.02**	**--**	**2.38**	**--**
CaTS	**--**	**--**	**--**	**--**	**--**	**--**	**--**	**--**	**--**	**--**	**--**	**3.50**	**--**
Muelle	**--**	**--**	**--**	**--**	**--**	**--**	**--**	**--**	**--**	**--**	**--**	**3.47**	**3.33**

Table 3.2 Continued

Station & Expedition	*A674/443*	*A674/490*	*Average abs*	*Abs 412*	*Abs 440*	*Chl-a*	*Fv/Fm*	*σPSII*	*aph Slope*	*aph max*	*Quantum yield*	*FRRF Inst Prod mgC(mgChla)$^{-1}$ hr^{1}*	*14C PbMax mgC(mgChla)$^{-1}$ hr^{1}*
Cavortex 6													
st2s	0.36	0.55	0.05	0.11	0.14	0.09	0.34	670.55	-0.03	0.14	--	--	--
st2dcm	0.49	0.60	0.05	0.08	0.10	0.27	0.34	604.94	-0.03	0.10	--	--	--
st3bs	0.34	0.60	0.03	0.07	0.09	0.07	0.42	280.47	-0.04	0.09	1.33	2.23	--
st4s	0.29	0.48	0.05	0.11	0.14	0.09	0.32	496.82	-0.04	0.15	1.21	2.24	--
st4dcm	0.49	0.59	0.05	0.09	0.11	0.21	0.53	586.14	-0.03	0.11	--	--	--
st5s	0.37	0.55	0.05	0.09	0.11	0.14	0.34	562.41	-0.03	0.11	1.45	2.96	--
st5dcm	0.48	0.61	0.04	0.06	0.09	0.19	0.54	509.03	-0.03	0.09	--	--	--
st6s	--	--	--	--	--	--	--	--	--	--	1.51	2.76	--
st6dcm	0.54	0.71	0.03	0.05	0.08	0.19	0.44	566.42	-0.02	0.08	--	--	--
st7s	0.17	0.33	0.04	0.07	0.13	0.14	0.33	573.24	-0.04	0.13	--	--	--
st8s	0.26	0.37	0.03	0.07	0.10	0.12	0.30	607.34	-0.06	0.10	--	--	--
st8bdcm	0.63	0.87	0.04	0.06	0.08	0.28	0.53	597.18	-0.02	0.08	--	--	--
st10s	0.47	0.64	0.03	0.06	0.08	0.13	--	--	-0.03	0.08	--	--	--
st12s	0.37	0.50	0.04	0.08	0.10	0.16	--	--	-0.03	0.10	--	--	--
st13d	0.53	0.72	0.05	0.08	0.10	0.30	--	--	-0.02	0.10	--	--	--
st15s	0.34	0.55	0.05	0.11	0.14	0.09	0.46	555.60	-0.03	0.14	--	--	--
st15d	0.60	0.72	0.04	0.05	0.08	0.21	0.48	636.74	-0.03	0.08	--	--	--
ST16S	0.45	0.74	0.03	0.07	0.09	0.11	0.38	527.63	-0.03	0.09	1.64	3.49	--
ST16D	0.59	0.68	0.04	0.05	0.07	0.28	0.61	453.29	-0.03	0.08	--	--	--
ST17S	0.32	0.56	0.05	0.11	0.15	0.15	0.41	442.88	-0.03	0.15	--	3.51	--
ST17D	0.54	0.68	0.05	0.08	0.10	0.27	0.59	466.72	-0.03	0.11	--	--	--
st21s	--	--	--	--	--	--	--	--	--	--	--	2.82	--
ST21D	0.36	0.65	0.06	0.12	0.16	0.25	0.54	509.57	-0.03	0.16	--	--	--
ST23S	0.32	0.50	0.03	0.05	0.10	0.09	--	--	-0.04	0.10	--	--	--
ST23D	0.54	0.64	0.04	0.07	0.09	0.27			-0.03	0.09	--	--	--

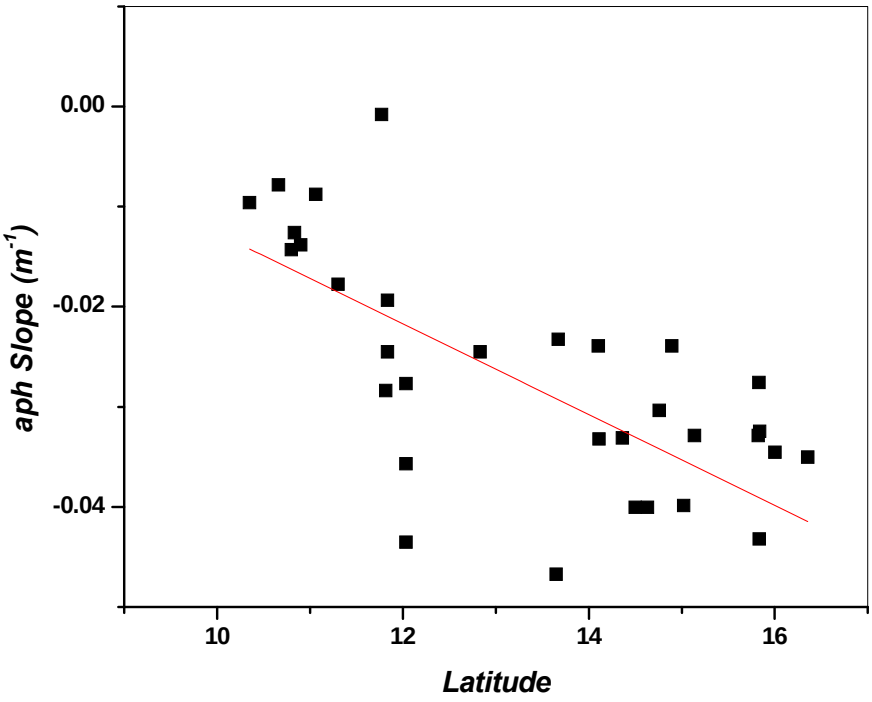

Figure 3.7. The absorption slope at sampled latitudes during Oripex 7, Oripex 8 and Cavortex 6. The correlation showed an inverse relationship (r =-0.66).

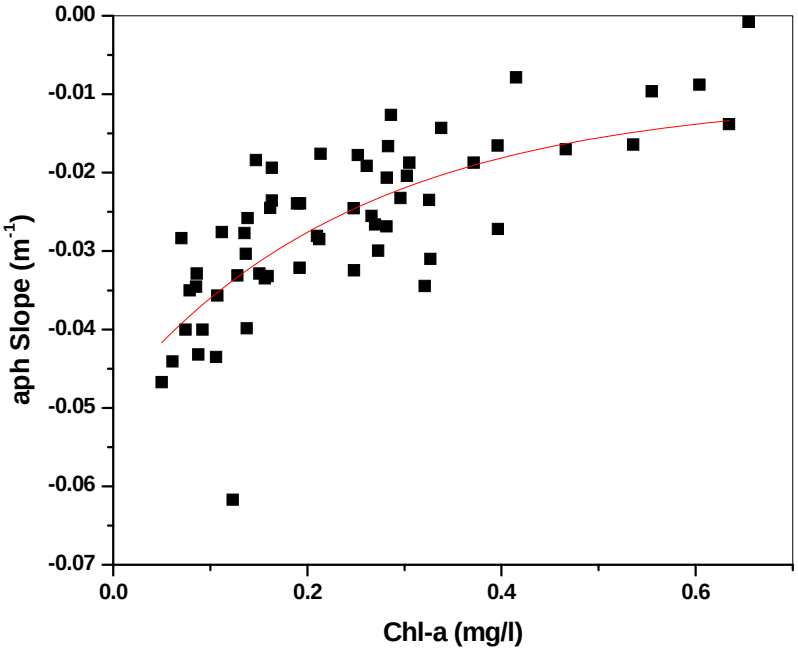

Figure 3.8 The slope of absorption spectra and chlorophyll relationship through the sampled areas. The slope denotes the physiological changes in cellular pigment ratios and pigment packaging. The correlation between both parameters showed a r of 0.72.

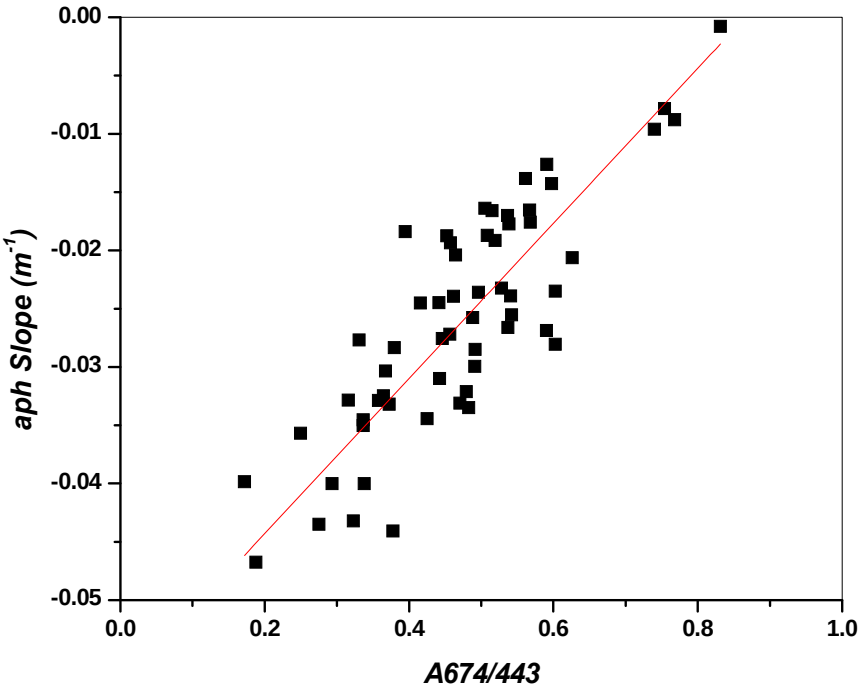

Figure 3.9. Phototrophic plankton absorption coefficient slope and its relationship to absorption ratio 674/443. A direct relationship was observed (r = 0.83).

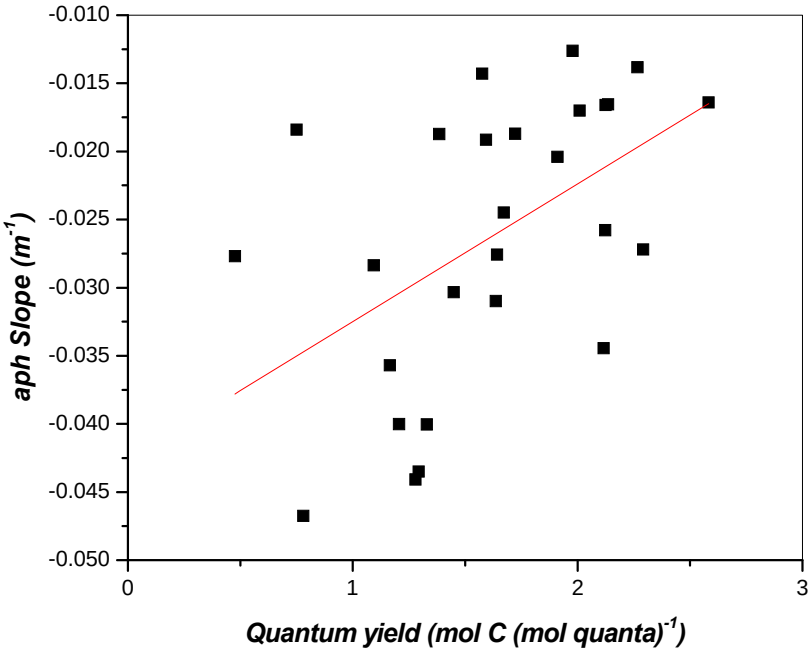

Figure 3.10. Quantum yield for photosynthesis obtained from FRRF and its relationship to phototrophic plankton absorption slope. The correlation between both parameters showed a r of 0.69.

The quantum yield for carbon fixation based on FRRF measurements, also covaried inversely with the specific absorption maxima, decreasing as the absorption increased (r= 0.77) (Figure 3.11). On the contrary, when related to the absorption coefficient ratio 676/440, it displayed a positive correlation increasing with the ratio (r = 0.70) (Figure 3.12). It also increased with chlorophyll concentration resulting in a similar positive correlation (r= 0.71) (Figure 3.13).

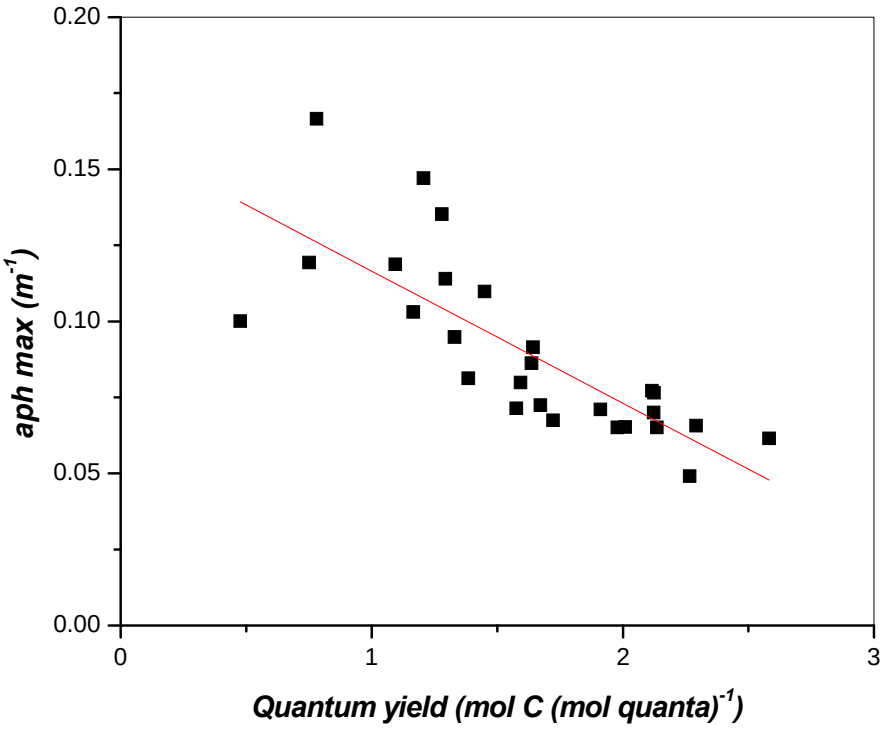

Figure 3.11. Quantum yield for photosynthesis obtained from FRRF and its relationship to phototrophic plankton absorption maxima. The correlation between both parameters showed a r of 0.77.

A fourth derivative analysis of sea surface samples denoted the absorption peaks for chlorophyll-a and accessory pigments (Figures 3.14 and 3.15). In general the samples show consistent peaks around the areas typical for chlorophyll absorption, around 440 nm and 676 nm. Accessory pigments regions denoted pigments peaks at around 467, 490,536, 585 and 636 among others. The region of 467 has been previously related to the pigment chlorophyll-c, fucoxanthin and other xanthophylls (Aguirre-Gomez et al, 2001; Bidigare et al, 1988;

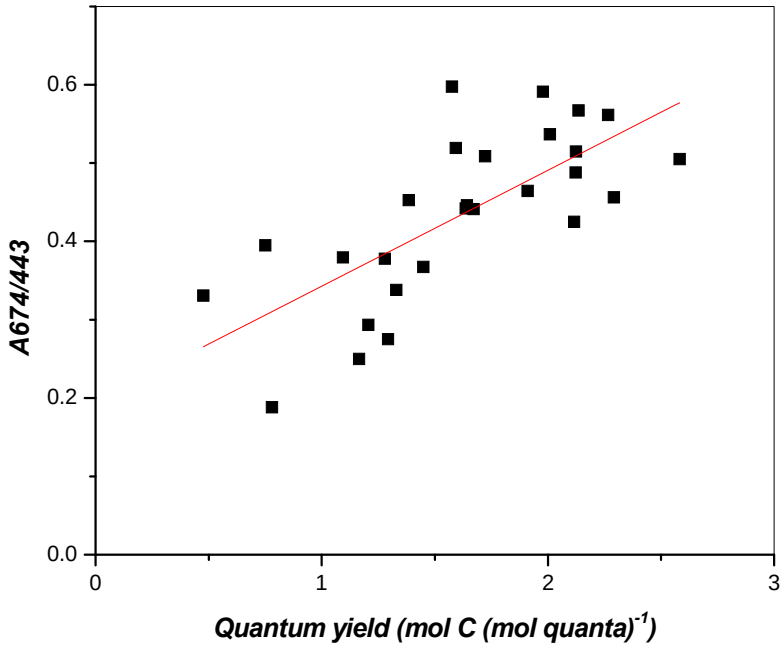

Figure 3.12. Quantum yield for photosynthesis obtained from FRRF and its relationship to phototrophic plankton absorption ratio 674/443. The correlation between both parameters showed a r of 0.70.

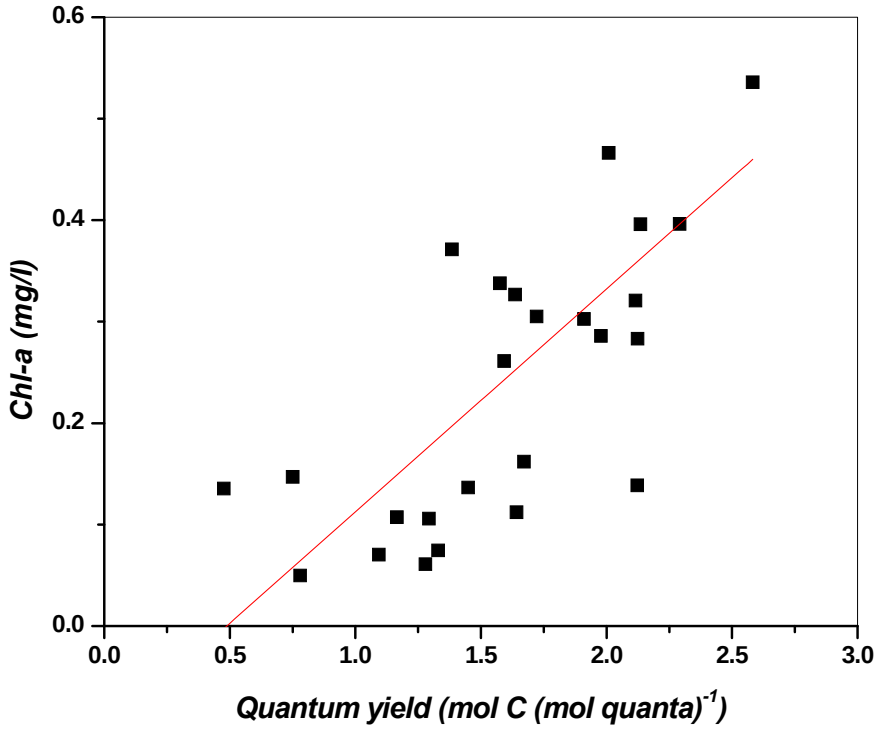

Figure 3.13. Quantum yield for photosynthesis obtained from FRRF and its relationship to chlorophyll concentration during the study. The correlation between both parameters showed a r^2 of 0.51.

Millie et al. 1997). The 490 nm peak is related to areas of absorption by carotenoids. Hoepffner and Sathyendranath (1991) concluded that the peaks found at 489 and 536 may correspond to a mixture of carotenes and xanthophylls rather than to separate groups. The region between 530-555 may be attributed also to fucoxanthin (Aguirre-Gomez et al, 2001). The region of 636 nm has been related with chlorophyll c and b (Bidigare, 1990). In general different regions show distinct derivative absorption peaks, those close to the river front (the Dragon's Mouth) differing from those far into the Caribbean (Figures 3.14 and 3.15) These spectra comprise the sum of the spectra of all natural phototrophic plankton populations present thus making it difficult to attribute the observed spectra to a single taxonomic group. Flow cytometry analysis of Cavortex 6 samples showed oceanic populations to be comprised mainly by *Prochlorococcus spp*. These populations are characterized by the presence of the chemotaxonomic markers divinyl chlorophyll-a (Chl-a_2) and divinyl chlorophyll-b (Chl-b_2 (Goerike and Repettla, 1993). The absorption peaks of these pigments in acetone are 442, 622 and 668 for Chl-a_2, and 478, 602 and 658 for Chl-b_2 (Goerike and Repetta, 1993). In our case absorption by Chl-a_2 is part of the total Chl-a absorption peak, Absorption peaks close to 622 are observed in the Cavortex 6 samples. the 668 peak is probably expressed with the observed 670 nm peaks. The 602 nm peak of Chl-b_2 is observed in some of these samples. Analysis of pigments through HPLC performed by Helena Antoun (personal communication) for of the samples stations confirm the presence of divinyl chlorophyll-a during Cavortex 6. She also reports the presence of the photoprotective carotenoid (PPC) diadinoxanthin in some of the stations (for Cavortex 6 and Oripex 8) both at surface and at deep chlorophyll maximum denoting stress due to high irradiances. The pigments zeaxanthin and *B*-Carotene were also present at all stations. These pigments along with violaxanthin and alloxanthin, comprise the pigments associated with the xanthophylls cycle that protects the photosynthetic apparatus during exposure and high irradiances. The photosynthetic carotenoids (PSC) involved in the assimilation of energy for photosynthesis are peridinin, fucoxanthin, 19'-hexanoyloxyfucoxanthin and19'-butanoyloxyfucoxanthin.She reports a gradual increase in the PSC fucoxanthin from open ocean waters toward the highest concentrations close to the Gulf of Paria.

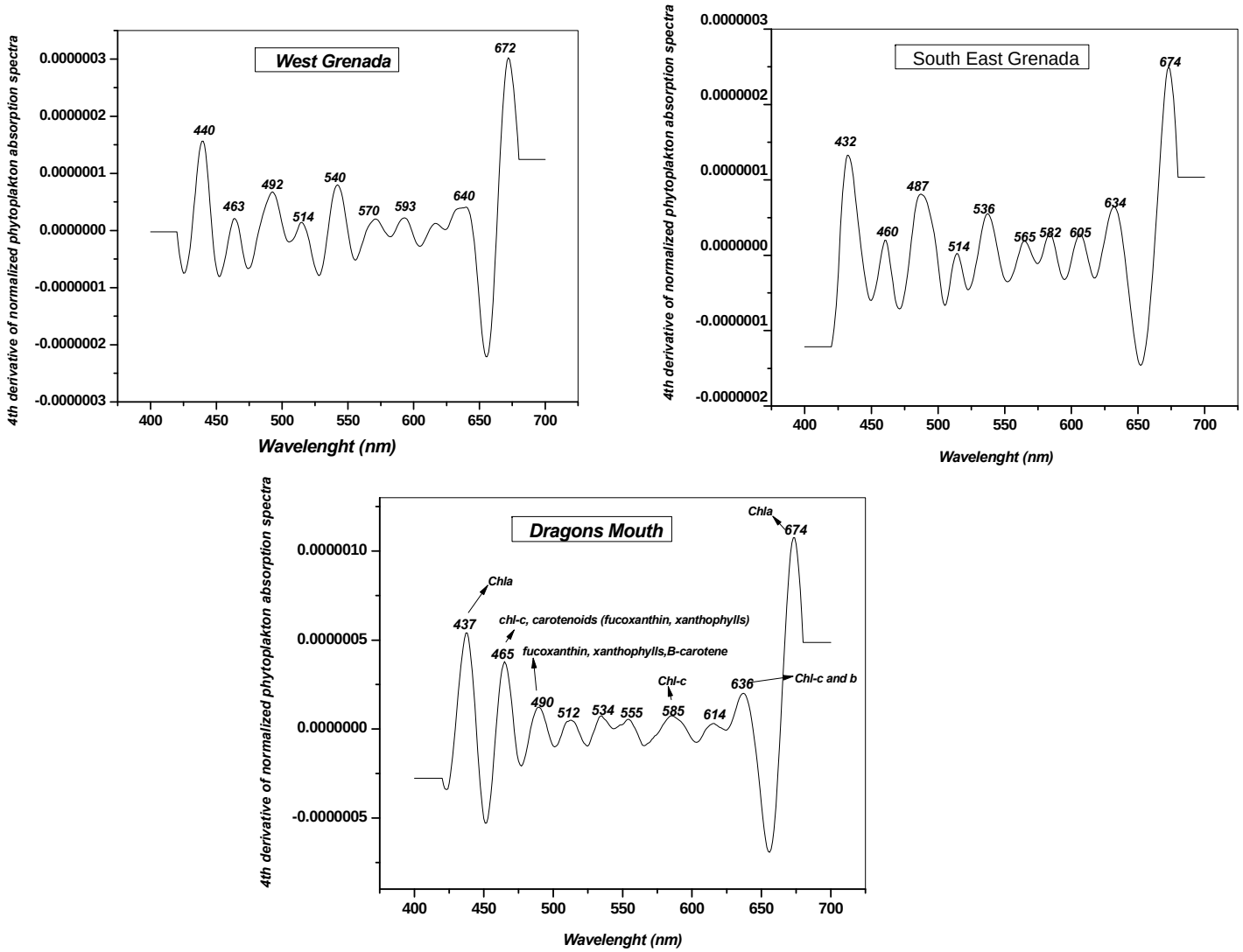

Figure 3.14 Fourth derivative analysis of phototrophic plankton absorption spectra at surface for stations sampled during Oripex 7.

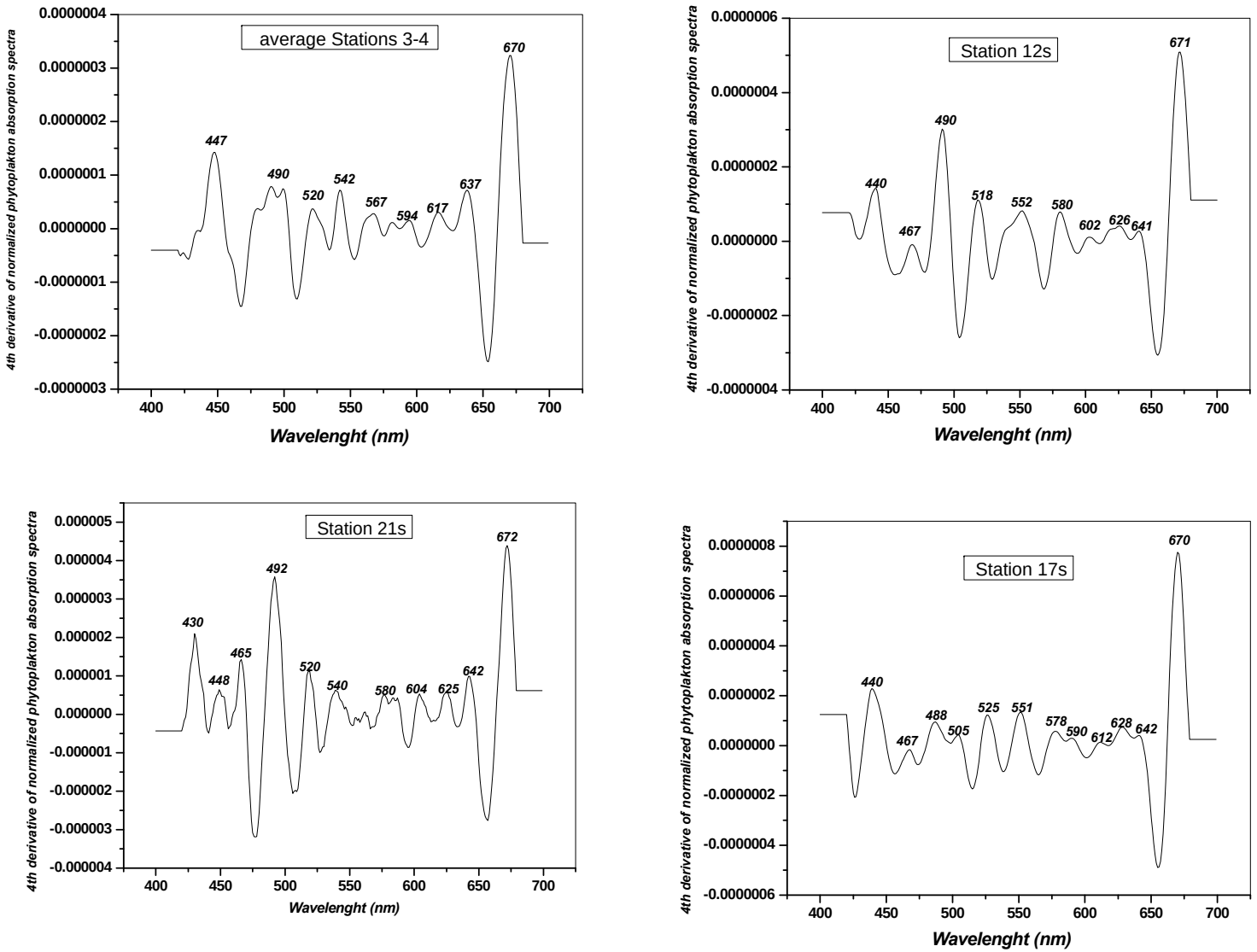

Figure 3.15. Fourth derivative analysis of phototrophic plankton absorption spectra at surface for stations sampled during Cavortex 6.

Table 3.3. Satellite derived Net Primary Production estimates through VGPM and CbPM models during Oripex 8.

	Longitude	Latitude	MODIS VGPM (Mg C m^{-2} d^{-1})	Log Transformed MODIS VGPM (1km) (Mg C m^{-2} d^{-1})	FRRF Modeled NPP (Mg C m^{-3} d^{-1})	Log Transformed FRRF NPP (Mg C m^{-2} d^{-1})	MODIS CbMP NPP (Mg C m^{-2} d^{-1})	Log Tansformed CbPM npp (Mg C m^{-2} d^{-1})
1	-67.01	17.61	175.98	2.25	186.94	2.27	75.21	1.88
2	-66.96	17.58	182.26	2.26	146.82	2.17	79.50	1.90
3	-66.93	17.57	181.54	2.26	169.01	2.23	77.96	1.89
4	-66.92	17.56	182.81	2.26	183.32	2.26	79.47	1.90
5	-66.90	17.54	185.40	2.27	227.61	2.36	79.73	1.90
6	-66.89	17.54	185.40	2.27	190.03	2.28	79.73	1.90
7	-66.83	17.51	192.19	2.28	138.42	2.14	83.22	1.92
8	-66.80	17.49	201.87	2.31	200.78	2.30	82.23	1.92
9	-66.76	17.47	204.52	2.31	211.65	2.33	83.31	1.92
10	-66.67	17.42	260.66	2.42	236.39	2.37	96.23	1.98
11	-66.57	17.37	234.84	2.37	192.15	2.28	93.21	1.97
12	-66.51	17.33	249.63	2.40	186.60	2.27	95.17	1.98
13	-66.40	17.27	232.27	2.37	187.18	2.27	96.10	1.98
14	-66.36	17.25	243.55	2.39	222.85	2.35	101.51	2.01
15	-66.32	17.23	252.29	2.40	187.77	2.27	105.38	2.02
16	-66.30	17.22	251.72	2.40	250.34	2.40	108.42	2.04
17	-66.26	17.20	250.02	2.40	166.46	2.22	104.86	2.02
18	-66.25	17.19	237.95	2.38	231.63	2.36	95.86	1.98
19	-66.23	17.18	218.94	2.34	252.87	2.40	91.61	1.96
20	-66.22	17.17	218.94	2.34	308.16	2.49	91.61	1.96
21	-62.60	14.85	585.16	2.77	570.09	2.76	268.29	2.43
22	-62.59	14.84	585.16	2.77	268.57	2.43	268.29	2.43
23	-62.58	14.82	586.64	2.77	250.07	2.40	276.24	2.44
24	-62.57	14.81	608.71	2.78	305.85	2.49	271.84	2.43

	Longitude	Latitude	MODIS VGPM ($Mg\ C\ m^{-2}\ d^{-1}$)	Log Transformed MODIS VGPM (1km) ($Mg\ C\ m^{-2}\ d^{-1}$)	FRRF Modeled NPP ($Mg\ C\ m^{-3}\ d^{-1}$)	Log Transformed FRRF NPP ($Mg\ C\ m^{-2}\ d^{-1}$)	MODIS CbMP NPP ($Mg\ C\ m^{-2}\ d^{-1}$)	Log Tansformed CbPM npp ($Mg\ C\ m^{-2}\ d^{-1}$)
25	-62.56	14.80	604.34	2.78	317.94	2.50	261.45	2.42
26	-62.56	14.79	604.34	2.78	377.60	2.58	261.45	2.42
27	-62.55	14.78	613.48	2.79	465.16	2.67	285.64	2.46
28	-62.54	14.77	601.64	2.78	499.36	2.70	291.89	2.47
29	-62.53	14.76	601.16	2.78	493.86	2.69	270.11	2.43
30	-62.52	14.75	601.16	2.78	540.11	2.73	270.11	2.43
31	-62.51	14.74	580.26	2.76	544.89	2.74	260.87	2.42
32	-62.50	14.72	544.66	2.74	469.55	2.67	234.31	2.37
33	-62.36	14.55	528.05	2.72	440.72	2.64	295.47	2.47
34	-62.34	14.53	470.57	2.67	488.79	2.69	277.18	2.44
35	-62.25	14.41	219.32	2.34	236.70	2.37	215.20	2.33
36	-62.24	14.39	187.86	2.27	243.50	2.39	205.07	2.31
37	-62.19	14.34	191.22	2.28	230.70	2.36	199.52	2.30
38	-62.15	14.29	295.91	2.47	217.59	2.34	218.84	2.34
39	-62.12	14.25	418.68	2.62	218.20	2.34	255.61	2.41
40	-62.09	14.22	513.69	2.71	245.66	2.39	255.61	2.41
41	-62.08	14.19	821.70	2.91	280.72	2.45	255.61	2.41
42	-62.05	14.16	1404.66	3.15	241.28	2.38	255.62	2.41
43	-62.03	14.14	1500.01	3.18	344.82	2.54	422.21	2.63
44	-62.00	14.14	--	--	506.68	2.70	210.90	2.32
45	-61.99	14.14	--	--	311.44	2.49	210.90	2.32
46	-61.97	14.14	--	--	175.47	2.24	208.97	2.32
47	-61.92	14.14	--	--	324.78	2.51	208.47	2.32
48	-61.90	14.15	562.08	2.32	195.84	2.29	208.47	2.32
49	-61.85	14.15	483.22	2.34	205.91	2.31	208.47	2.32
50	-61.79	14.16	531.62	2.37	212.28	2.33	213.95	2.33

Table 3.3. Continued.

Samples	Longitude	Latitude	MODIS VGPM (Mg C m^{-2} d^{-1})	Log Transformed MODIS VGPM (1km) (Mg C m^{-2} d^{-1})	FRRF Modeled NPP (Mg C m^{-3} d^{-1})	Log Transformed FRRF NPP (Mg C m^{-2} d^{-1})	MODIS CbMP NPP (Mg C m^{-2} d^{-1})	Log Tansformed CbPM npp (Mg C m^{-2} d^{-1})
51	-61.75	14.16	534.63	2.38	218.39	2.34	218.02	2.34
52	-61.73	14.16	509.14	2.37	286.96	2.46	223.14	2.35
53	-61.71	14.16	509.14	2.37	108.37	2.03	223.14	2.35
54	-61.67	14.17	506.28	2.39	227.60	2.36	220.34	2.34
55	-61.63	14.17	563.85	2.42	308.94	2.49	245.74	2.39
56	-61.59	14.17	665.37	2.49	495.17	2.69	307.51	2.49
57	-61.57	14.18	713.64	2.51	290.70	2.46	328.82	2.52
58	-61.54	14.18	818.31	2.54	623.26	2.79	327.79	2.52
59	-61.51	14.18	798.13	2.52	430.77	2.63	403.02	2.61
60	-61.48	14.19	603.72	2.41	201.47	2.30	246.23	2.39
61	-61.45	14.19	445.51	2.28	117.36	2.07	158.51	2.20
62	-61.00	12.74	214.71	2.33	362.63	2.56	83.28	1.92
63	-61.01	12.73	214.71	2.33	188.98	2.28	83.28	1.92
64	-61.01	12.72	210.15	2.32	416.38	2.62	83.20	1.92
65	-61.01	12.71	210.15	2.32	193.22	2.29	83.20	1.92
66	-61.01	12.70	210.15	2.32	189.19	2.28	83.20	1.92
67	-61.02	12.69	202.21	2.31	127.38	2.11	79.68	1.90
68	-61.02	12.68	193.58	2.29	312.25	2.49	79.85	1.90
69	-61.02	12.67	191.64	2.28	235.41	2.37	79.86	1.90
70	-61.02	12.66	193.42	2.29	291.50	2.46	79.06	1.90
71	-61.03	12.64	193.42	2.29	212.36	2.33	79.06	1.90
72	-61.03	12.63	193.63	2.29	379.66	2.58	83.53	1.92
73	-61.03	12.62	193.63	2.29	179.86	2.25	83.53	1.92
74	-61.04	12.61	195.24	2.29	257.12	2.41	87.74	1.94
75	-61.04	12.60	195.24	2.29	266.59	2.43	87.74	1.94
76	-61.04	12.59	194.70	2.29	234.61	2.37	92.01	1.96
77	-61.04	12.58	194.70	2.29	152.12	2.18	92.01	1.96
78	-61.05	12.57	190.66	2.28	260.52	2.42	91.03	1.96
79	-61.05	12.55	190.66	2.28	231.91	2.37	91.03	1.96
80	-61.05	12.54	189.88	2.28	300.58	2.48	92.05	1.96
81	-61.15	12.16	220.40	2.34	149.41	2.17	171.96	2.24
82	-61.15	12.16	220.40	2.34	226.23	2.35	171.96	2.24
83	-61.15	12.14	220.50	2.34	256.74	2.41	174.21	2.24

Satellite derived primary production estimates

Satellite derived production estimates based on the vertically generalized production model (VGPM) from MODIS level 3 products resulted in estimates that displayed some degree of correlation (r= 0.51, n = 18) (Figure 3.16) with FRRF daily integrated estimates obtained from transects sampled during Oripex 8. MODIS level 2 products of temperature and chlorophyll concentration (Figures 3.17 and 3.18 respectively) were then used to create higher resolution VGPM estimates at a 1 km resolution. These new estimates when analyzed against FRRF measurements also showed low correlations (r= 0.46, n= 83) (Figure 3.19). Carbon based production (CbMP) estimates were performed from MODIS level 3 data, these estimates also demonstrated low correlation with *in situ* FRRF estimates (r= 0.40, n= 18) (Figure 3.20). When MODIS level 2 data (bbp 553, Chlorophyll concentration and K 490) was used the estimates correlation increased (Figure 3.21) (r= 0.55, n= 83). The VGPM and CbPM estimates showed a high degree of correlation (r= 0.84, n= 83) (Figure 3.22) , demonstrating a 30 % error between these estimates. Lower estimates were observed for CbPM (a minimum value 75 mg C m^{-2} d^{-1}) than the other estimates (Table 3.3). Observed average NPP was 173 mg C m^{-2} d^{-1} compared to 279 mg C m^{-2} d^{-1} and 378 mg C m^{-2} d^{-1} for FRRF based and VGPM respectively. The observed standard deviation was greater for the VGPM (250 mg C m^{-2} d^{-1}) and lower for CbPM (90 mg C m^{-2} d^{-1}); 123 mg C m^{-2} d^{-1} for FRRF. These satellite estimates when analyzed against geographical position (Figure 3.23, eg. CbPM) were observed to vary accordingly with the river plume front, lower production estimates for all the models agree with waters out of the influence of the river front (Figure 24). The highest values are observed for data sampled around the latitude 14˚ close to the islands of St Lucia and Martinique. Lower values were observed for the transect close to the island of Puerto Rico at latitude 17˚, and those of clear blue waters off the eastern coast of the island Grenada at latitude 12˚(Table 3.3).

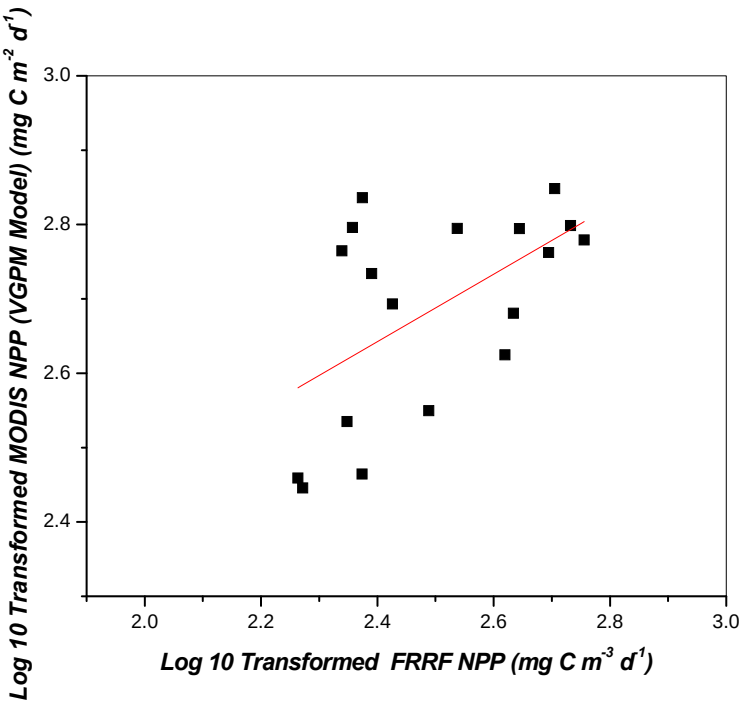

Figure 3.16 Modeled net primary production from remote sensed data (MODIS) and in-situ measurements from FRRF. The correlation between both parameters showed a r^2 of 0.51.

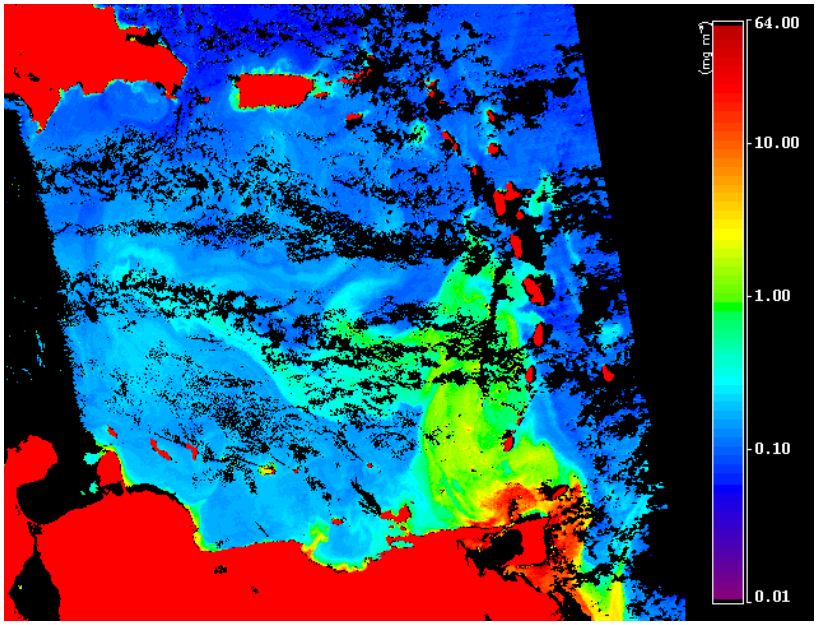

Figure 3.17. MODIS aqua Chlorophyll level 2 product for September 20, 2006.

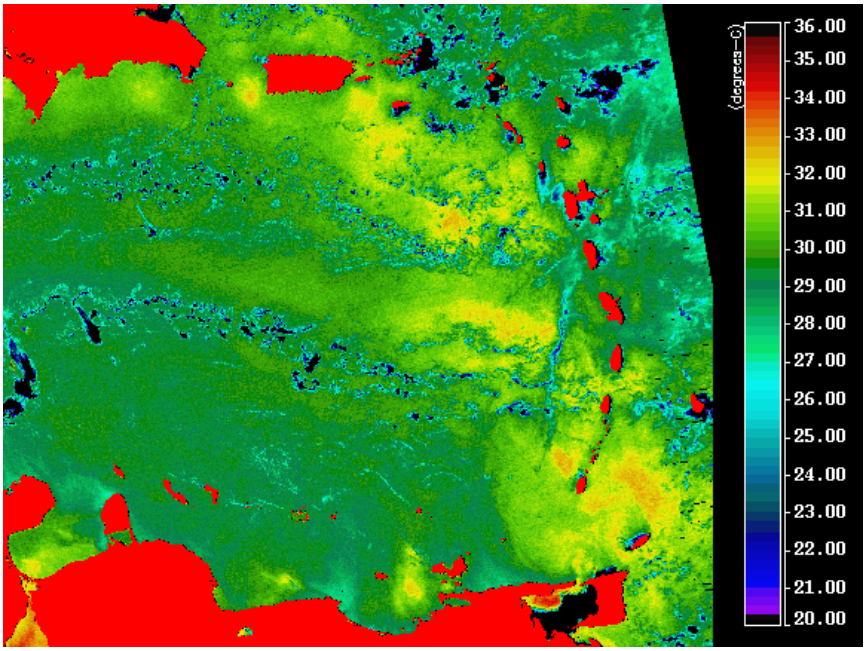

Figure 3.18 MODIS Aqua SST level 2 product for September 20, 2006.

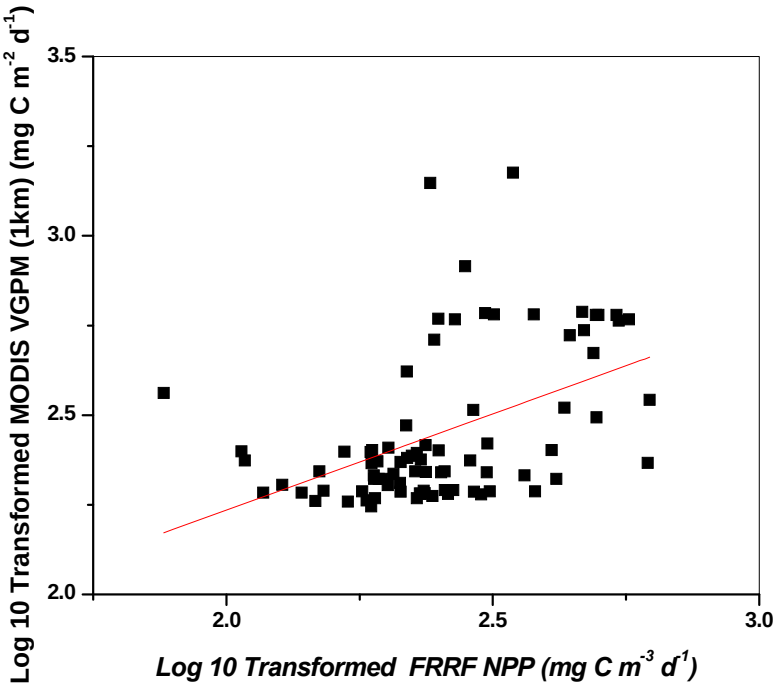

Figure 3.19 Modeled net primary production from remote sensed data (MODIS) at a 1 km resolution and in-situ measurements from FRRF. The correlation between both parameters showed a r of 0.46 with an n= 83.

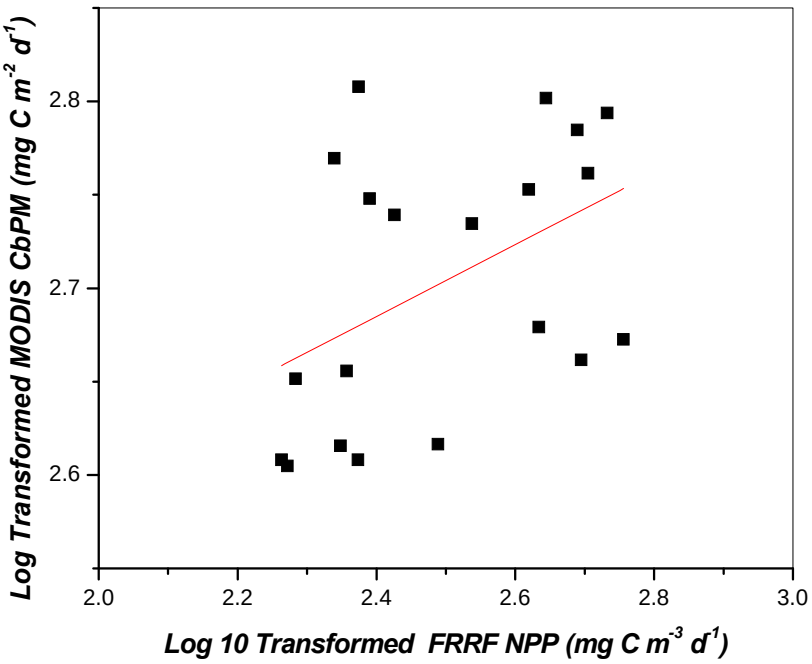

Figure 3.20 Carbon based modeled net primary production from MODIS level 3 remote sensed data and in-situ measurements from FRRF. The correlation between both parameters showed a r of 0.40, n= 18.

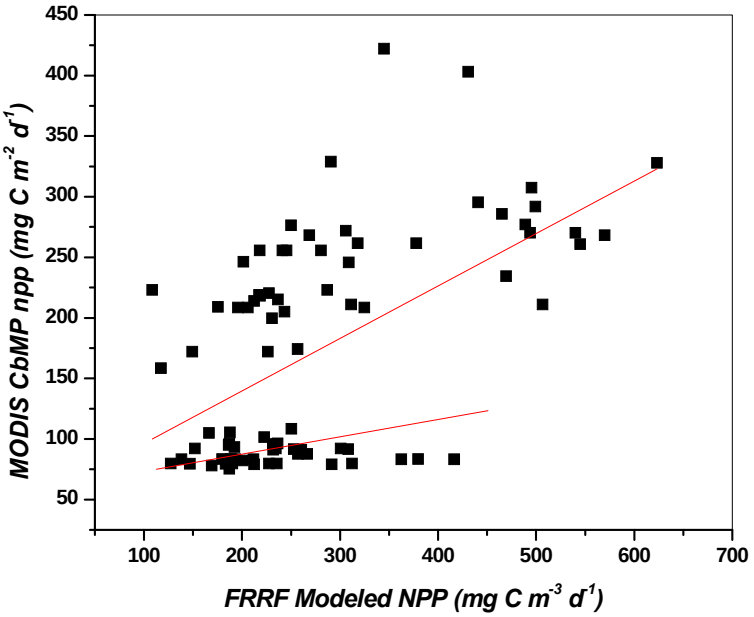

Figure 3.21 Carbon based modeled net primary production from MODIS level 2 remote sensed data and in-situ measurements from FRRF. The correlation between both parameters showed a r of 0.55, n= 83. The correlation for the observed low values is r = 0.32 and for the observed higher values is r = 0.51.

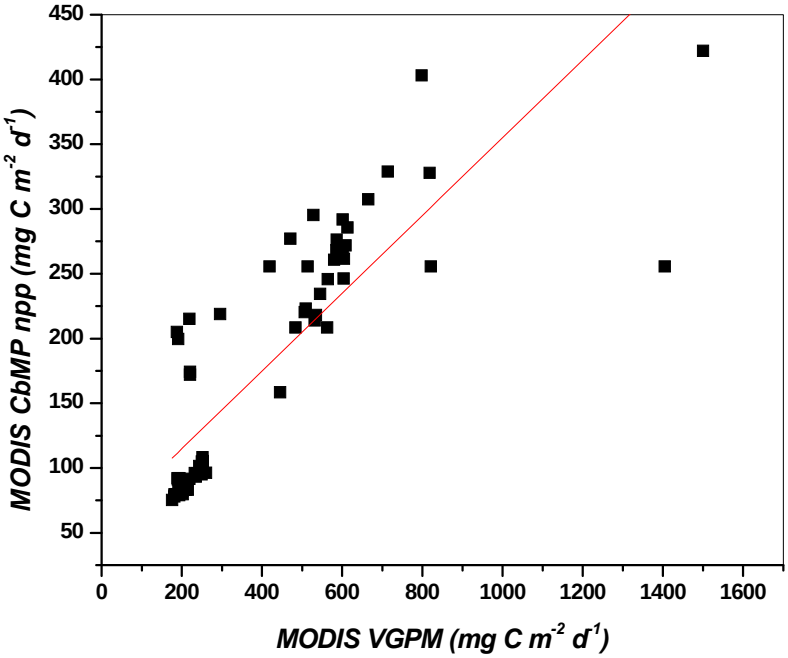

Figure 3.22 Carbon based and VGPM modeled net primary production from MODIS level 2 remote sensed data . The correlation between both parameters showed a r^2 of 0.84, n=83.

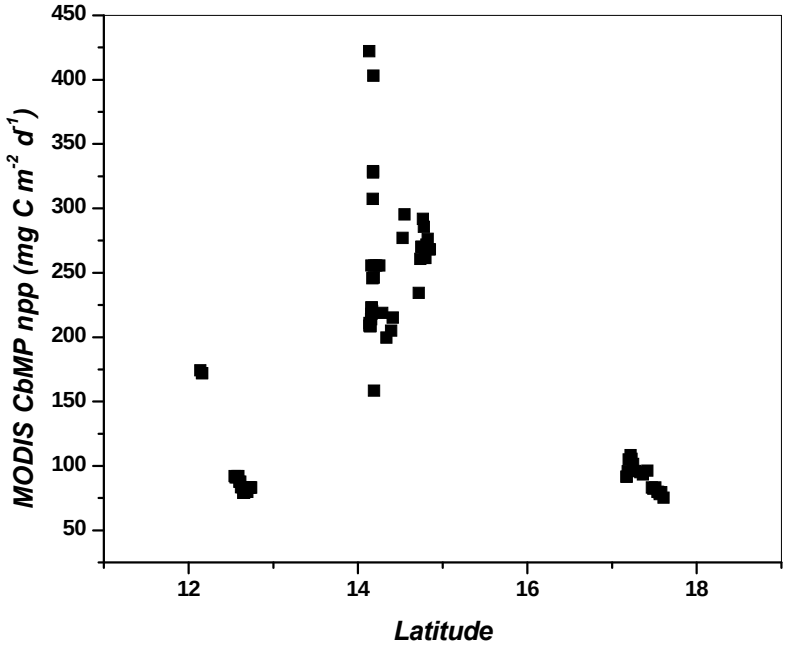

Figure 3.23. Carbon based modeled net primary production from MODIS level 2 remote sensed data per latitude.

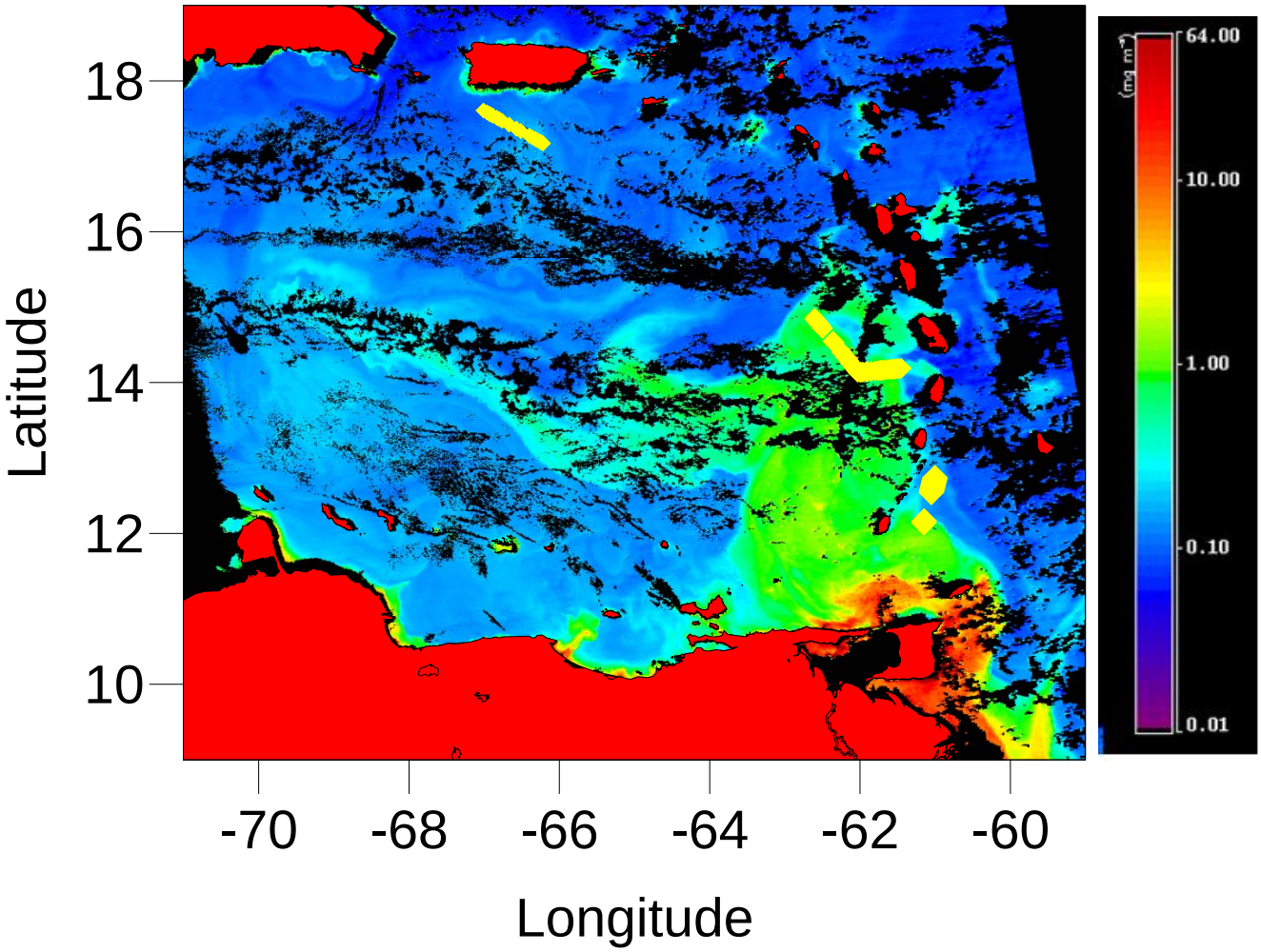

Figure 3.24 MODIS level 2 chlorophyll-a concentration image of September 20, 2006, denoting the extend of the river front. In yellow the transects sampled during Oripex 8, used to analyze its relationship with satellite based estimates of net primary production.

Natural fluorescence estimates of net primary production were performed during Cavortex 2, these estimates demonstrated a high degree of relationship to FRRF estimates ((r= 0.92, n= 407) (Figure 3.25). FRRF modeled production by depth for the zone (Figure 3.26) was observed to vary according to biogeophysical eddy features. This area visited during Cavortex 2 comprised a zone where a cyclonic-anticyclonic eddy pair

interacted. The cyclonic portion had a center (Figure 3.27) close to longitude 66.38 W and was sampled at station 3. This portion showed the highest FRRF net integrated primary production estimated at 426 mg C m-^{3} d^{-1} while the natural fluorescence based integrated modeled production reported 60 mg C m-^{3} d^{-1}. Comparable net primary production was observed at the center of the anti-cyclonic area sampled during station 6. with FRRF based NPP of 413 mg C m-^{3} d^{-1} and natural fluorescence based NPP of 68 mg C m-^{3} d^{-1}. The lowest integrated production in the region was observed for station 5 localized in the area of interaction between eddies with FRRF based integrated NPP of 165 mg C m-^{3} d^{-1} and 47 mg C m-^{3} d^{-1} for natural fluorescence.

Satellite acquired diffuse attenuation coefficient at 490nm (K490) obtained from MODIS Aqua (Figure 3.28) denotes higher attenuation in waters under the influence of the river plume during Oripex 8. Higher attenuation is observed for stations sampled during the transect of September 20. *In-situ* attenuations coefficients for the station sampled during Oripex 7 (Table 1) show higher light attenuation for stations closer to the Dragon's Mouth.

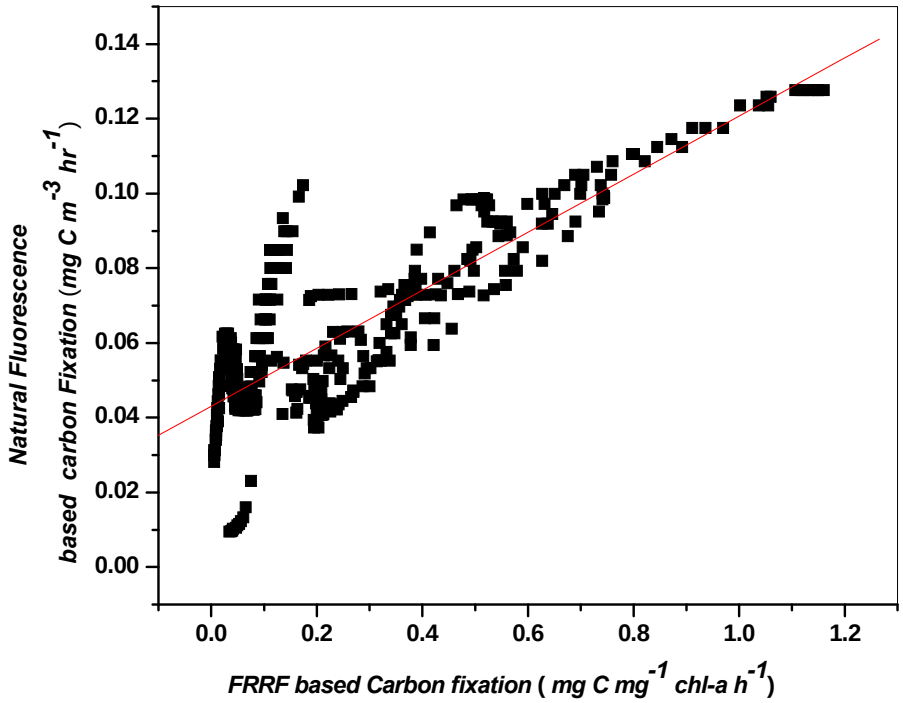

Figure 3.25. Primary production obtained from of Fast Repetition rate Fluorometry and its relation to natural fluorescence derived production during Cavortex 2. The correlation showed an r of 0.92.

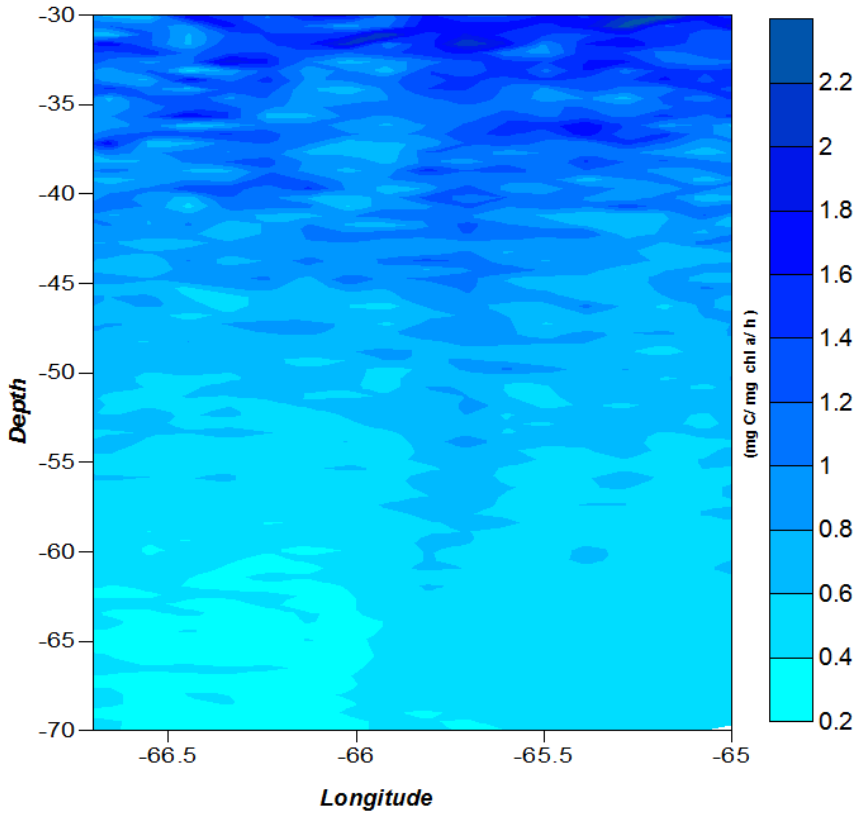

Figure 3.26. Modeled net primary production from FRRF-based measurements during Cavortex 2 through an eddy pair.

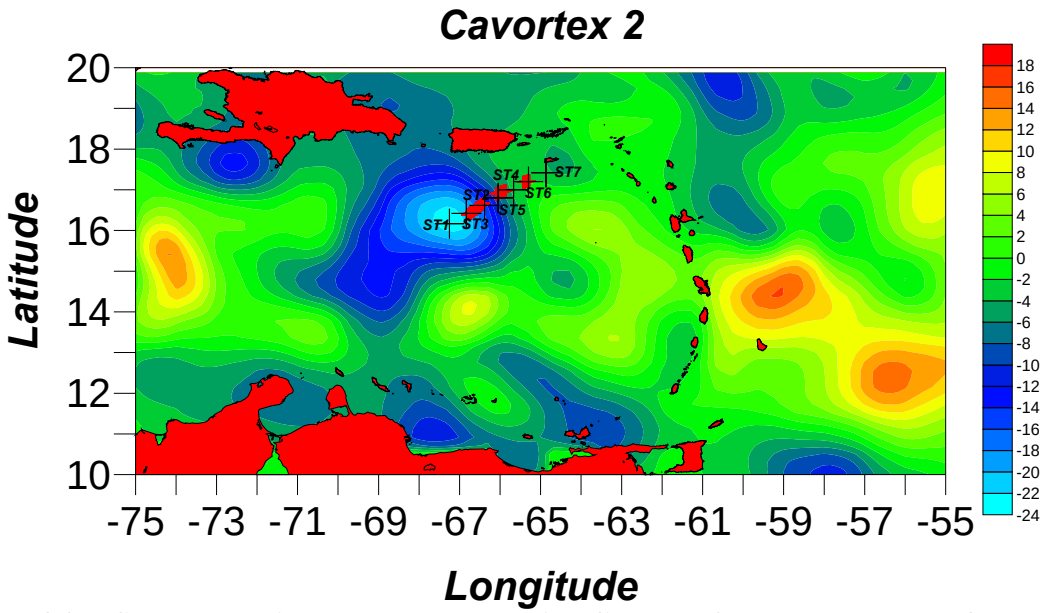

Figure 3.27. Sampled stations and transect during Cavortex 2 over Jason sea surface anomaly obtained from AVISO live access server (LAS). These altimeter products were produced by Ssalto/*Duacs* and distributed by *Aviso*, with support from *Cnes*.

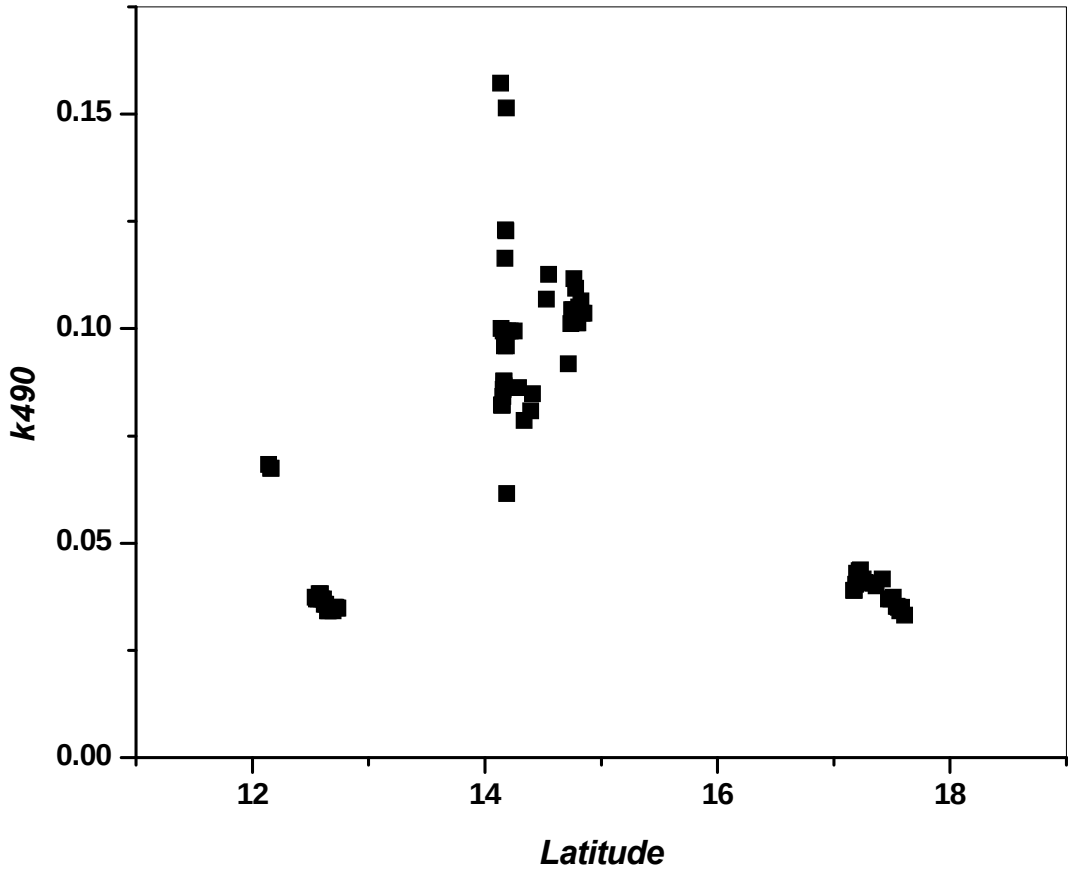

Figure 3.28. MODIS Aqua derived diffuse attenuation coefficient at 490 nm (kd490) for sampled stations from transects during Oripex 8.

3.5 Discussion

FRRF-based Productivity estimates vs ^{14}C

FRRF-based productivity estimates produced a strong linear relationship with independent measurements of ^{14}C for data collected throughout the Eastern Caribbean Sea. The observed slope (0.82) ranged within those reported by Melrose et al. (2006) ranging between 0.23 and 1.04. The squared correlation coefficient (r= 0.91) for our data set compares favorably to those observed elsewhere. It is comparable to the ones reported by Kolber and Falkowski (1993)(r= 0.93) and Melrose et al. (2006)(r > 0.95); and better than that observed by Sugget et al. (2003)(r= 0.77). These observations are considerably close, even within the sources of uncertainties associated with estimates by FRRF owing to the biogeochemical variability throughout the areas sampled. The sources of uncertainties in FRRF measurements include the taxon-related variability in the photosynthetic efficiency (*Fv/Fm*) parameter as it changes with species assemblages (Corno et al., 2008; Kobliz˘ek et al. 2001). The *Fv/Fm* ratio has been used to diagnose nutrient limitation in natural waters but it has been found not to be a robust diagnostic indicator in culture experiments (Parkhill et al., 2001). In steady, low nutrient conditions, cells adapted and exhibited a high *Fv/Fm* ratio while growth remained low. In cultures, the *Fv/Fm* was low only when the cells were subject to short term nutrient starvation. This would cause the Kolber & Falkowski (1993) model to detect changes in the growth rates of cells acclimated to low nutrient zones. Furthermore, another problem present is the signal originated by phaeophytin. Phaeophytin is produced when Chl-*a* is digested by grazers, such as zooplankton. If the quantity of phaeophytin accounts for more than 30% of the total pigment present in a sample, it will lead to a reduction in the measured *F*v/*F*m ratio, and an underestimation of primary productivity (Fuchs et al., 2002). Similarly to *Fv/Fm,* the absorption cross section of photosystem II (σPSII) also exhibits intrinsic variations as a function of light, nutrients, temperature and species composition that ultimately will affect the production estimates. The rate of PSII reaction centers closure per absorbed photon of light, as determined by σPSII, is a measure of the ‘‘functional size’’ of the pigment antenna or an index of its ability to close the functional reaction centers. While a large σ_{PSII} value means large antenna relative to a small number of PSII

reaction centers (such as under nutrient depletion), a small σPSII value corresponds to a small antenna relative to a large number of PSII reaction centers (typical of high nutrient availability; Kolber and Falkowski 1993). Despite these uncertainties, our estimates are similar to those observed by the ^{14}C method. This method, although considered here as reference value for production estimates, is itself subject to errors. Some potential sources of error, for instance, are the contamination of samples with trace metals or nutrients; and the nature of the process for short term incubations under artificial light leading to uncertainties in whether the resulting estimates account for net or gross primary production (Carpenter and Lively, 1980). However, these shortcomings are well known and, because of the widespread distribution of the ^{14}C technique data, these are considered here as reference values of primary production. Our analysis with Montecarlo approximations was intended to constrain the uncertainties in the FRRF estimates that arose from the variability described above. Less error in the estimates was observed for those stations in the river side of the front in the area of the Gulf of Paria. Apparently, the relatively homogeneous conditions (nutrient and light availability) favor less variability in the FRRF-based estimates than in oligotrophic zones. One technical limitation of the FRRF technique that must be considered is the poor sensitivity of this instrument at low chlorophyll-a concentrations (decrease in the signal to noise ratio, which makes it difficult to interpret the fluorescence signal). However, Corno et al. (2006) highlighted the positive potential for this instrument to detect changes in productivity in Hawaiian oligotrophic waters. Our estimates, both FRRF and ^{14}C for these waters, despite the high variability foreseen by Montecarlo approximations, demonstrated close affinity thus validating the observations of Corno et al. (2006).

Chlorophyll-specific absorption coefficient

Variability in the magnitude and shape of chlorophyll specific absorption (a_{ph}) coefficients is caused by variations in the package effect and in the relative abundance of Chl-a and accessory pigments (Sathyendranath et al., 1987; Fujiki and Taguchi, 2002). Peak absorption values for a_{ph} are located at about 400 and 675 nm. In the case of $a_{ph}(675)$, the variability due to pigment composition is minimal as absorption in this region is primarily from Chl-a. In contrast, the portion around 440 nm is influenced by

accessory pigments; pigments other than chlorophyll that capture light photons either for photosynthesis or photoprotection. Thus, variations in a_{ph} *(440)* may result from the combined influences of packaging effect of total cellular pigment content as well as cell pigment composition (Bricaud et al., 1995). Our data shows higher absorption values in samples gathered in eastern Caribbean blue waters (low Chl-a) in contrast to those from high Chl-a waters close to the Orinoco river source. This higher a_{ph} *(440)* at higher latitudes in clear waters with K_d approximately 0.05 m^{-1}(Figure 28) is probably due to an increase of photoprotective accessory carotenoids (PPC) in cells acclimated to higher irradiance. Waters close to the river plume source, should contain more river originated dissolved materials and therefore, decreased irradiance. In effect, observed k_d were mostly below 0.1 m^{-1} (Figure 3.28 and Table 3.1a). As cells become shade-adapted, the cellular concentration of absorbing pigments increases (Falkowski and LaRoche, 1991). The increase in intracellular pigment concentration could in turn lead to an increase in the flattening effect and a corresponding decrease in specific absorption (Geider et al., 1986). The flattening effect or flattening of the peaks occurs when the increase of pigments within the discrete packages in chloroplasts lessens the effectiveness with which they collect light, hence lowering the specific absorption (Kirk, 2004).

The ratio a_{676}/a_{440}, indicative of the proportion of the variability due to chlorophyll, suggests a lesser contribution of chlorophyll to the 440 nm peak at the Cavortex 6 oceanic samples (the observed K_d was approximately 0.05). Thus, the observed high absorption coefficients in the 440 nm region are probably the action of increased PPC, in adaptation to higher irradiances. While in samples influenced by the river plume, the ratio indicated higher chlorophyll contribution to $a_{ph}(440)$, and possibly increased photosynthetic accessory carotenoids (PSC), reducing the specific absorption.

The ratio of photoprotective carotenoids to photosynthetic carotenoids (PPC:PSC) represented in this study by the slope of a_{ph} , suggests that less packaging is associated with a lesser action of chlorophyll and probably an increase in the action of PPC. Under high irradiances the increase in PPC and the decrease of PSC causes the a_{ph} spectral slope to become steeper. The decrease in packaging then causes an increase in the absorption in the 440 nm region. Our data suggests that this increase in absorption does not contribute to higher efficiency in the quantum yield of carbon fixation. The lowest value for

maximum quantum yield of carbon fixation (φ_{max}) was observed in samples with the higher a_{ph} slope,which as previously discussed, had the highest a_{ph} *(440).* and reflects energy that as absorbed but not used for carbon fixation. This energy is then dissipated by PPC as a mechanism for photoprotection. PPCs help prevent damage to chloroplasts from excess light energy by modifying chlorophyll –chlorophyll interactions and reducing the efficiency of energy transfer among photosynthetically active pigments (Frank et al. 2001) as has been observed in the northeast tropical Atlantic (Babin et al., 1996), in the Arabian Sea (Marra et al., 2000) and in the Southern Ocean (Vaillancourt et al., 2003). Prieto et al. (2008) also demonstrated in a study near the continental shelf break in the NW Atlantic Ocean that when the proportion of photoprotective carotenoids increases, photosynthetic efficiency decreases. The role of pigment concentration and PSC pigments in transferring energy to the chlorophyll pigment protein complexes of the reaction center was addressed by Sugget et al. (2004). They questioned the traditional assumption that the photosynthetically active pigments transfer absorbed light with 100% efficiency and are completely associated to PSII. PPCs have the lowest transfer efficiencies, with minimum values of 20% (Rabinowitch and Govindjee, 1969).

Another aspect to consider is that the changes in a_{ph} slope can reflect physiological changes at the cellular level or indicate a shift in species composition with different light tolerance or nutrient requirements. At low species diversity, changes in the shape of the $\boldsymbol{a_{ph}}$ spectrum indicate physiological acclimation rather than taxonomic diversity. Variations in nutrient concentration can also promote changes in physiology (Geider et al., 1993) and species successions that influence the relative pigment concentrations of the assemblage. The effect of the Orinoco river plume should maintain the available surface N, otherwise considered as a limiting factor for these oligotrophic waters thus having an effect on species assemblages. Observations by Corredor et al. (2003) and Muller –Karger et al. (1989) establish that within the Orinoco River plume "N is recycled many times before being exported". The analysis of the $\boldsymbol{a_{ph}}$ spectra through fourth derivative methods yielded absorption peaks that could be associated with distinctive pigments, but no conclusive differences were found that could be attributed to taxonomic variations. Fuentes-Figueroa (2007) during the Oripex 7 and 8 observed a decrease in the microphytoplankton biomass (also in the nano and picoplankton class

sizes) from areas close to the river source to areas close to the island of Puerto Rico. This reduction was suggested to be associated with reduction in dissolved organic carbon (Del Castillo et al. 1999) and the rate of photomineralization (Morell & Corredor 2001) or biomineralization of nutrients as waters become diluted. Mendez-Silvagnoli (2008) observed, for the same sampled regions in this study, higher CDOM slopes indicated photodegradation of the material originated from Amazon River plume waters in summer followed by the intrusion of Orinoco River plume water in the fall. Observations by Helena Antoun (personal communication) of HPLC pigments throughout the region report a gradual increase in the PSC fucoxanthin from open ocean waters toward the highest concentrations close to the Gulf of Paria. This increase suggests the expected increase in diatoms populations and the shift in phototrophic plankton species assemblages close to the river origin. Fucoxanthin is a PSC pigment therefore its increase indicates adaptations to lower irradiances, and validates the observation of lower a_{ph} slopes throughout the zone.

Fujiki and Taguchi (2002) noted that under high irradiances the cell size dependence of $a_{ph}\,(440)$ was weakened due to the effect of photoprotective pigments. They argue that, at all irradiances, cellular Chl-a per unit of volume of larger species was lower than that of small species, agreeing with Augusti, (1991 cited in Fujiki and Taguchi, 2002) who stated that large cell with longer path lengths, have reduced package effect which in turn prevents the lowering of specific absorption. Therefore size dependence of absorption is a robust characteristic of marine phototrophic plankton under low light. Fujiki and Taguchi (2002) demonstrated that at low irradiances the relationship between spectra and cell volume was statistically significant, but at high irradiances the relationship becomes weakened apparently due to increased PPC. Barlow et al (2002) studied pigment absorption characteristics along a meridional transect in the Atlantic Ocean and across a range of a range of oceanic provinces. Their data suggest that the effect of pigments on the variability of a_{ph} is due primarily to variations in absorption by PPC. The samples analyzed in this study were collected near the surface (approximately 3 m) therefore all samples could be considered within the same irradiance regime and the variations in the irradiance field could then be related to the effect of the *in-situ* inherent optical properties. The observed increase in the quantum yield of carbon

fixation could then be associated to a decrease in the proportion of PPC to PSC, and this probably constitutes an important factor molding the net primary production estimates of the zone. This factor should then be considered with equal contribution to productivity estimates as the traditional parameters of Chl-a concentration and the availability of nutrients through the zone, especially when considering satellite based estimates.

Satellite derived primary production estimates

Current models for determining primary production incorporate chlorophyll concentration as one of the parameters (e.g. Behrenfeld and Falkowski, 1997) with the intention to be used as satellite-retrievable pigment data at large geographical scales. The reality is that chlorophyll is a poor proxy for primary production and it only accounts for about 50% of the total pigment in most marine environments. As our analysis shows.PPC account for a significant proportion of pigment absorption in the eastern Caribbean, particularly in oligotrophic regions, making accurate chlorophyll concentration based determination of primary production difficult. The MODIS OC3M Chl-a algorithm incorporates the reflectance at the 443 and 488 nm bands within the area we have described as affected by the flattening effect. Consequently, the low correlation of MODIS derived VGPM net primary production estimates and *in situ* FRRF-based estimates is not surprising. The FRRF-based estimates, although normalized to biomass using chlorophyll-a concentrations, are performed considering the effective rate of light absorption or, as previously described here, as functional absorption cross-section of PSII (σ_{PSII}) which bringd these estimates closer to the reality of the active phototrophic plankton absorption spectra. σ_{PSII} is reduced at high irradiances by photoprotective mechanisms operating at multiple time scales, ranging from minute with action by the xanthophylls cycle (Olaizola et al. 1994) to hours with xanthophyll acclimation (Babin et al., 1996). Sugget et al. (2004) established that the ratio of absorption by photosynthetic to non photosynthetic pigments could be the strongest predictor of σ_{PSII} although it also can be affected by the taxonomy and physiological state of the algal community.

MODIS carbon based production estimates (CbPM) showed better correlation to the FRRF based estimates through the areas sampled. This C-based approach allows for

the separation of biomass and physiological changes in Chl-a. Behrenfeld et al. (2005) developed this methodology in which information contained in ocean color reflectance spectra on particulate backscattering is transformed to direct estimates of carbon. This assumption is based on evidence of a relationship between Chl-a and the particulate beam attenuation coefficient, cp, (Behrenfeld and Boss, 2003), which is most sensitive to particles with diameters of 0.5–20 mm in size (Stramski and Kiefer, 1991). This range commonly overlaps the size distribution of phototrophic plankton in the ocean. When combined with measurements of Chl-a, the Chl-a:cp ratio can closely track changes in photosynthetic competency (Behrenfeld and Boss, 2003, 2006). Consequently, CbPM estimates and FRRF-based ones must fluctuate in accordance, and in relation to changing biogeochemical conditions. Note here that these satellite based estimates both the VGPM and CbPM are based on MODIS satellite information with a resolution of 1 km and the FRRF estimates consider a small portion of the spatial area sampled by the satellite. Each cast profile used to model the FRRF production estimates corresponds to a half oscillation of the towed vehicle within a range of about 0.4 to 0.6 km. Therefore the differences in these estimates compared to those based on the absorption spectra also should consider the uncertainties caused by the spatial resolution sampled, and the variability in the inherent optical properties due to the impact of the river plume. Another consideration is that the model uses a scattering (b_{bp}) to carbon relationship that is based in an invariant particle size spectrum. This assumption holds over much of the ocean (Stramski and Kiefer, 1991) but is not always true; large diatom or coccolitophorids with silica and calcium carbonate exoskeletons contribute disproportionally to backscattering (Balch et al. 1999) which is a factor to consider throughout the Orinoco River plume. In addition, these organisms incorporate organic carbon through photosynthesis and particulate inorganic carbon into their calcareous plates further confusing the relationship between b_{bp} and C (Westberry et al., 2008). Nevertheless our estimates with both satellite methods and FRRF estimates co-varied and both reflected the extent of features characteristic of the Orinoco River Plume, measured *in situ* and remotely observed.

The production estimates derived from natural fluorescence varied closely with those modeled through FRRF at the stations visited during Cavortex 2, a relationship is comparable to other studies where ^{14}C was used (Garcia-Mendoza and Maske, 1996;). These estimates analyzed with data gathered on the interaction of an eddy pair, showed agreement with the expected higher production due to the flux of material to the surface in the cyclonic eddy portion and the apparent accumulation of material in the anti-cyclonic portion (as described in chapter 2 of this dissertation) . Even though the estimates covaried (r= 0.91) accordingly to the *in-situ* biogeochemical features, the difference between these estimates was large, the production estimates based on natural fluorescence underestimated that observed with the FRRF methodology.

Fluorescence and photosynthesis are only two of three possible outcomes of the absorbed energy; it is use for carbon fixation, is emitted as fluorescence or its lost as heat. Energy once absorbed normally goes through the process of PSII light reactions where it is transformed into the chemical energy necessary for the dark reactions and carbon fixation. Consequently, if an inverse relationship exists between the first two, the loss by heat must be negligible. Nevertheless, according to the observed PPC to PSC relationships, in most of eastern Caribbean beyond the influence of the river plume, absorption is largely influenced by PPC. Here, most of the absorbed energy must in fact be dissipated and not used for carbon fixation. This energy must considered to be lost in the form of heat, a process called thermal deactivation or non-radiative dissipation channeled through the xanthophyll cycle. Our estimates from oligotrophic waters thus should reflect lower fluorescence as their photosystems adapt to higher irradiances throughout the water column. The estimates based of FRRF fluorometry are based on the maximum potential for these photosystems to fluorescence, natural fluorescence only accounts for that minimal fluorescence as stimulated by the sun. Considering also that most of the FRRF measurements were performed at night, the photosynthetic potential of these cells should reflect a relaxed state. The bias between these measurements could be explained by this difference in the state of the photosynthetic potential. The FRRF fluorometry was developed to improve the variable fluorescence yield estimates by considering photochemical quenching, non-photochemical quenching, and the redox state of the acceptor and donor side of PS II.

Conclusions

The variable bio-optical and biophysical (FRRF) characteristics of phototrophic plankton populations in the eastern Caribbean Sea discussed here denote the complexity of biogeochemical processes of the zone. The periodic intrusion of the Orinoco River plume and, to lesser extent by the Amazon River, causes variablility of the bio-optical environment in these surface waters. The mechanisms suggested for fertilization derived from river originated materials such as photomineralization and biomineralization (Morell and Corredor, 2001), and the resulting inherent optical conditions, must account for higher carbon export through the zone. Our observations suggest such relationship as increased quantum yield of carbon fixation with changing environmental conditions. These conditions can be summarized first by nutrient release from the river originated materials, promoting an increase in the phototrophic plankton photosynthetic efficiency of surface waters. Second, the variability in irradiance regimes through the zone for surface waters prompting changes in absorption spectra, pigment composition and efficiency in the transfer of absorbed energy.

Hence considering that the ultimate goal is to properly quantify the rates of carbon assimilations and transport at global scales, our journey is far from over. Our current understanding of the parameters affecting photosynthesis is limited to small regions of the planet in which we are beginning to grasp the factors involved. The eastern Caribbean is one of these regions and we are only starting to understand its complexity.

General Conclusion

From this study it can be concluded that eastern Caribbean surface waters in general maintain conditions for increased phototrophic plankton photosynthetic efficiency (*Fv/Fm)* at least during the months of continental riverine influence. The dispersion of riverine material across the region delivers the necessary materials to liberate surface populations from micronutrient starvation influencing their photosynthetic potential. Satellite and *in-situ* primary production estimates confirm that primary production responds to the gradient generated by the Orinoco River plume. Advection of the river plumes by Caribbean mesoscale eddies may contribute to the diffusion and mixing of the materials through the zone and within the water column. Eddy pumping potential of cyclonic eddies also promotes baroclinic instabilities that favor the flux of refractive materials and with it micronutrients to relieve surface populations from starvation, as apparent from the relationship of *Fv/Fm* and the chlorophyll normalized particle beam attenuation. The optical conditions of surface waters through the region respond to continental runoff as evidentiated by the gradient in satellite surface attenuation coefficients at 490 nm (K490). These prevalent optical conditions then influence the photosynthetic potential for surface phototrophic plankton populations. Lower quantum yield for carbon fixation prevail in the clearest oceanic waters (Kd PAR= 0.05), even in the presence of higher specific absorption coefficients (a_{ph}). The increased a_{ph} slopes (488-532 nm) in these clear waters suggests the presence of photoprotective carotenoids responsible for the absorption of the energy not used for carbon fixation. On the contrary, waters influenced by the Orinoco River present lower a_{ph} at surface, consistent with increased packaging effect due to lower irradiances. These riverine influenced waters present lower a_{ph} slopes denoting increased influence of photosynthetic carotenoids that consequently favor higher quantum yield for carbon fixation. This in fact suggest that the region under the influence of continental runoff not only presents increased photosynthetic potential due to increased micronutrients (higher *Fv/Fm*), but is favored by higher efficiency in light absorption by the action of photosynthetic carotenoids. In summary our hypothesis, that the effect of the Caribbean mesoscale phenomena differentiates eastern Caribbean surface waters from the typical

oceanic oligotrophic environment towards one with phototrophic plankton communities rather more efficient in photosynthesis, is supported.

Cited Literature

Abbott, M.R., K.H. Brink, C.R. Booth, D. Blasco, M.S. Swenson, C.O. Davis, and L.A. Codispoti. 1995. Scales of variability of bio-optical processes as observed from near-surface drifters, J. Geophys. Res., 100, 13,345-13,367.

Abbott M. R. and Letelier R.M. 1999. Algorithm Theoretical Basis Document Chlorophyll Fluorescence (MODIS Product Number 20). 44 pp

Aiken, J., J. Fishwick, G. Moore & K. Pemberton. 2004. The annual cycle of phytoplankton photosynthetic quantum efficiency, pigment composition and optical properties in the western English Channel. *J. Mar. Biol. Ass. UK*. 84: 301-303.

Alfonso-Sosa, E. 2000. Variabilidad temporal de la producción primaria fitoplanctónica en la estación CaTS (*Caribbean Time Series Station*): Con énfasis en el impacto de la marea interna semidiurna sobre la producción. Disertación Ph.D. Universidad de Puerto Rico, Mayaguez, P.R.

Alfonso, E., López, J. M., Capella, J., Dieppa, A. y J. M. Morell. (submitted). Internal tide induced variations in primary productivity and optical properties in the Mona Passage, Puerto Rico. Deep-Sea Research.

Andersen R.A., Bidigare R.R., Keller M.D., Latasa M. 1996, A comparison of HPLC pigment signatures and electron microscopic observations for oligotrophic waters of the North Atlantic and Pacific Oceans, Deep Sea Res. II, 43 (2)–(3), 517–537.

Antoine, D., and A. Morel. 1996. Oceanic primary production. 2. Estimation at global scale from satellite (coastal zone color scanner) chlorophyll, Global Biogeochem. Cycles, 10, 57–69

Babin, M., A. Morel, H. Claustre, C. Bricaud, Z. Kolber, and P. G. Falkowski, 1996. Nitrogen- and irradiance-dependent variations of the maximum quantum yield of carbon fixation in eutrophic, mesotrophic and oligotrophic marine systems. Deep Sea Res. 43(8):1241-1272.

Babin, M., Morel, A., Falkowski, P.G., Claustre, H., Bricaud, A. and Z. Kobler, 1996. Nutrient- and light-dependent variations of the maximum quantum yield of carbon fixation in eutrophic, mesotrophic and oligotrophic systems. Deep Sea Research, 43, 1241-1272.

Balch, W. M., D. T. Drapeau, T. L. Cucci, R. D. Vaillancourt, K. A. Kilpatrick, and J. J. Fritz .1999. Optical backscattering by calcifying algae – Separating the contribution by particulate inorganic and organic carbon fractions, J. Geophys. Res., 104, 1541 – 1558.

Baums, I.B., Paris, C., Che´rubin, L.M. 2006. A dynamical filter in larval dispersal in a reef building coral. Limnology and Oceanography 51 (5), 1969–1981.

Behrenfeld, M.J., Bale, A.J., Kolber, Z.S., Aiken, J. and Falkowski, P.G. 1996. Confirmation of iron limitation of phytoplankton photosynthesis in the equatorial Pacific Ocean, Nature, 383, 508-511.

Behrenfeld, M. J., and E. Boss. 2006. Beam attenuation to chlorophyll concentration as alternative indices of phytoplankton biomass, J. Mar. Res., 64, 431– 451.

Behrenfeld, M. J., E. Boss, D. A. Siegel, and D. M. Shea, 2005. Carbonbased ocean productivity and phytoplankton physiology from space, Global Biogeochem. Cycles, 19, GB1006, doi:10.1029/2004GB002299.

Behrenfeld, M. J., and E. Boss. 2003. The beam attenuation to chlorophyll ratio: an optical index of phytoplankton photoacclimation in the surface ocean. Deep Sea Res., Part I, 50, 1537 – 1549

Behrenfeld, M.J., Falkowski, P.G. 1997. Photosynthetic rates derived from satellite-based chlorophyll concentration. Limnology andOceanograp hy 42, 1–20.

Behrenfeld, M.J. and Kolber, Z., 1998. Widespread iron limitation of phytoplankton in the south Pacific Ocean. Science 283, 840-843.

Behrenfeld, M.J., Prasil, O., Kolber, Z., Babin, M., Falkowski, P. 1998. Compensatory changes in Photosystem II electron turnover rates protect photosynthesis from photoinhibition. Photosynthesis Research, 58: 259-268.

Benitez-Nelson, C. R., R. Bidigare, T. D. Dickey, M.R. Landry,C. L. Leonard, S.L., Brown, F. Nencioli, Y. M. Rii, Kanchan, J.W. Becker, T.S. Bibby,W.Black, W. Cai, C.A. Carlson, F. Chen, V. S. Kuwahara, C.Mahaffey, P. M. McAndrew, P. McAndrew, M. S. Rappé, K.E. Selph, M.P. Simmons, Eun Jin Yang.2007. Mesoscale Eddies Drive Increased Silica Export in the Subtropical Pacific Ocean *Science* 316, 1017 (2007)

Bidigare, R. R. 1989. Photosynthetic pigment composition of the brown tide alga: Unique chlorophyll and carotenoid derivatives, p. 57-75. In E. Cosper et al. [eds.], Novel phytoplankton blooms. Springer.

Bidigare, R. and others. 1990. Evidence for phytoplankton succession and chromatic adaptation in the Sargasso Sea during spring 1985. Mar. Ecol. Prog. Se

Bonilla, J., Senior W., Jugden, J., Zafiriou, O. y Jones, R. 1993. Seasonal distribution of nutrients and primary productivity on the Eastern continental shelf of Venezuela as influenced by the Orinoco river. *J Geophys. Res*., 98(2C): 2245-2257.

Boss, E., R. Collier, G. Larson, K. Fennel, and W.S. Pegau, 2007. Measurements of spectral optical properties and their relation to biogeochemical variables and processes in Crater Lake National Park, OR. Hydrobiologia (2007), 574:149-159.

Boss, E. & W. S. Pegau, 2001. The relationship of light scattering at an angle in the backward direction to the backscattering coefficient. Applied Optics 40: 5503–5507

Boss, E., W. S. Pegau, W. D. Gardner, J. R. V. Zaneveld, A. H. Barnard, M. S. Twardowski, G. C. Chang & T. D. Dickey, 2001a. The spectral particulate attenuation and particle size distribution in the bottom boundary layer of a continental shelf. Journal of Geophysical Research 106: 9509–9516.

Boss, E., W. S. Pegau, M. Lee, M. S. Twardowski, E. Shybanov, G. Korotaev & F. Baratange, 2004. The particulate backscattering ratio at LEO 15 and its use to study particles composition and distribution. Journal of Geophysical Research 109, C0101410.1029/ 2002JC001514.

Boyd, P.W. and Abraham, E. 2001 Iron-mediated changes in phytoplankton photosynthetic competence during SOIREE Deep Sea Research II 48 2529 – 2550.

Boyd, P.W. (2002) The role of iron in the biogeochemistry of the Southern Ocean and equatorial Pacific: a comparison of in situ iron enrichments. Deep Sea Research II . 49:1803-1821

Bricaud, A., Babin, M., Morel, A. and H. Claustre, 1995. Variability in the chlorophyll-specific absorption coefficient of natural phytoplankton : analysis and parameterization. Journal of Geophysical Research, 100, C7, 13321-13332

Bricaud, A., A.L. Bedhomme, and A. Morel. 1988. Optical properties of diverse phytoplanktonic species: Environmental results and theoretical interpretation. Journal of Plankton Research. 10:851-873.

Bricaud, A., and D. Stramski. 1990. Spectral absorption coefficients of living phytoplankton and non-algal biogenous matter: a comparison between the Peru upwelling area and Sargasso Sea. *Limnology and Oceanography*, 35, 562-582.

Campbell L 2001. Flow cytometric analysis of autotrophic picoplankton. *In* Paul JH ed, Marine Microbiology: Methods in Microbiology, 30. Academic Press, San Diego: 317-343.

Canals-Silander, Miguel F**..** 2005. On the Three-Dimensional Structure of Caribbean Mesoscale Eddies. Master of Science Thesis. University of Puerto Rico, Mayaguez, P.R.

Carpenter EJ, Lively JS, 1980. Review of estimates of algal growth using 14C tracer techniques. In: Falkowski PG (ed) Primary productivity in the sea. Plenum Press, New York, p 161–178

Chamberlin, W. S., Booth C.R., Kiefer D. A., Morrow J. H., Murphy, R.C. 1990. Evidence for a simple relationship between natural fluorescence, photosynthesis, and chlorophyll-a in the sea. Deep-Sea Research 37, 951-973.

Chamberlin, S., Marra, J.. 1992. Estimation of photosynthetic rate from measurements of natural fluorescence: analysis of the effects of light and temperature. Deep-Sea Research. 39 (10), 1695-1706.

Chérubin L.M. and P. Richardson, 2007. Caribbean current variability and the influence of the Amazon and Orinoco fresh water plumes. Deep-Sea Res. I 54 1451–1473.

Claustre H., A. Morel, S. B. Hooker, M. Babin, D. Antoine, K. Oubelkheir, Bricaud A., K. Leblanc, B. Que´guiner, and S. Maritorena. 2002. Is desert dust making oligotrophic waters greener? Geophys. Res. Let., VOL. 29, NO. 10, 10.1029.

Corno, G., R. M. Letelier, M. R. Abbott, and D. M. Karl. 2006. Assessing the temporal variability of primary production in the North Pacific Subtropical Gyre: A comparison of fast repetition rate fluorometry and 14C measurements. J. Phycol. 42: 51–60.

Corredor JE, 1979. Phytoplankton response to low-level nutrient enrichment through upwelling in the Colombia Caribbean Basin. Deep-Sea Research 26A: 731–741

Corredor J.E. and Morell J. M. 2001. Seasonal variation of physical and biogeochemical features in eastern Caribbean surface Water. J. of Geophysical Research. 106, 4517-4525.

Cullen, J. J., and R. E. Davis. 2003. The blank can make a big difference in oceanographic measurements. Limnol. Oceanogr. Bull. 12: 29–35.

Dey S. and R.P. Singh, 2003 Comparison of chlorophyll distributions in the northeastern Arabian sea and southern Bay of Bengal using IRS-P4 Ocean Color Monitor Data. Remote Sensing of the environment 85, 424-428.

DuRand, M.D. and R.J. Olson. 1996. Contributions of phytoplankton light scattering and cell concentration changes to diel variations in beam attenuation in the equatorial Pacific from flow cytometric measurements of pico, ultra, and nanoplankton. Deep-Sea Research II, 43:891-906

Eisner, L., M.S. Twardowski, T.J. Cowles, and M.J. Perry. 2003. Resolving phytoplankton photoprotective: photosynthetic carotenoid ratios on fine scales using in situ spectral absorption measurements. Limnol. Oceanogr., 48:632–646.

Falkowski, P.G. 2002. The ocean's invisible forest. Scientific American 287:22, 38-45

Falkowski, P.G., Greene, R.M., Geider, R.J. 1992. Physiological limitations on phytoplankton productivity in the ocean. Oceanography 5, 84}91.

Falkowski PG, LaRoche J. 1991. Acclimation to spectral irradiance in algae. J. Phycol. 27:8-14.

Falkowski, P.G., and Z. Kolber. 1995. Variations in chlorophyll fluorescence yields in the phytoplankton in the world oceans, Aust. J. Plant Physiol., 22, 341-355.
Falkowski, P G. A. Sukenik, and R. Herzig. 1989. Nitrogen limitation in Isochrysis galbana (Haptophyceae). II. Relative abundance of chloroplast proteins. J. Phycol. 25: 471-478.

Falkowski, P.G., D. Ziemann, Z. Kolber, P.K. Bienfang, 1991b Nutrient pumping and phytoplankton response in a subtropical mesoscale eddy. Nature. 352: 544-551.

Ffield, A., 2005. North Brazil current rings viewed by TRMM Microwave Imager SST and the influence of the AmazonPlume. Deep-Sea Research I 52, 137–160.

Frank H. A., Somes Kumar Das, J. A. Bautista, D. Bruce, S. Vasil'ev, M. Crimi, R. Croce and R. Bassi, 2001. The photochemical behavior of xanthophylls in the recombinant photosystem II antenna complex, CP26. Biochemistry 40 1220-1225.

Fuchs E, Zimmerman RC, Jaffe JS, 2002. The effect of elevated levels of phaeophytin in natural waters on variable fluorescence measured from phytoplankton. J Plankton Res. 24:1221–1229.

Fujiki T, Taguchi S., 2002. Variability in chlorophyll a specific absorption coefficient in marine phytoplankton as a function of cell size and irradiance. J Plankton Res 24(9):859–874.

Gao Y., Song-Miao Fan, and J. L. Sarmiento. 2001 Aeolian iron input to the ocean through precipitation scavenging: A modeling perspective and its implication for natural iron fertilization in the ocean. J. Geophys. Res., VOL. 108, NO. D7, 4221.

García-Mendoza E., and H. Maske, 1996. The relationship of solar-stimulated natural fluorescence and primary productivity in Mexicam Pacific waters. Limnology and Oceanography, 41(8):1697-1710

Geider, R. J., T. Plait, and J. A. Raven, 1986. Size dependence of growth and photosynthesis in diatoms: A synthesis. Mar. Ecol. Prog. Ser. 30: 93-109.

Gong and Ohad, 1991. The PQ/PQH2 Ratio and Occupancy of Photosystem-II-QB Site by Plastoquinone Control the Degradation of D1 Protein During Photoinhibition Invivo. Journal of Biological Chemistry 266(31):21293-21299.

Heath, M., K. Richardson, T. Kiørboe. 1990. Optical assessment of phytoplankton nutrient depletion. J. Plank. Res. 12: 381-396.

Hedges, J. I., W. A. Clark, P. D. Quay, J. E. Richey, A. H. Devol, and U. D. M. Santos. 1986. Compositions and fluxes of particulate organic material in the Amazon River. Limnol. Oceanogr., 31: 717-738.

Hernández J. L., D. Erickson III and P. Ginoux, 2001. Atmospheric Iron Flux and Surface Chlorophyll in the North-Western Tropical Atlantic (paper), IX COLACMAR Congress, September/16/2001, San Andres, Colombia

Hernandez-Guerra, A., Joyce, T.M., 2000. Water masses and circulation in the surface layers of the Caribbean at 661W. Geophysical Research Letters 27 (21), 3497–3500.

Hoepffner N, Sathyendranath S. 1992. Bio-optical characteristics of coastal waters: absorption spectra of phytoplankton and pigment distribution in the western North Atlantic. Limnology and Oceanography 37:1660-1679

Johnsen, G., O. Samset, L. Granskog, and E. Sakshaug, 1994. In vivo absorption characteristics in 10 classes of bloom-forming phytoplankton: Taxonomic characteristics and responses to photoadaptation by means of discriminate and HPLC analysis. Mar. Ecol. Prog. Ser. 105: 149–157.

Joint Global Ocean Flux Study, (1991) JGOFS Core Measurements Protocols, JGFOS Report No. 6, Scientific Committee on Oceanic Research, 40pp

Kiefer, D.A., Chamberlin, W.S., 1989. Natural fluorescence of chlorophyll-a: Relationship to photosynthesis and chlorophyll-a concentration in the western South Pacific Gyr e. Limnology and Oceanography. 34 (5), 868-881.

Kirk, J. T. O. 1994. Light & Photosynthesis in Aquatic Ecosystems. Cambridge University Press, New York, New York, 509 pp.

Koblizek, M., D. Kaftan, and L. Nedbal. 2001. On the relationship between the non-photochemical quenching of the chlorophyll fluorescence and the photosystem II light harvesting efficiency. A repetitive flash fluorescence induction study. Photosynth. Res. 68: 141–156.

Kolber, Z. S, and P. G. Falkowski. 1993. Use of active fluorescence to estimate phytoplankton photosynthesis in situ. Limnol. Oceanogr. 38: 1646–1665.

Kolber, Z. S, O. Prasil, and P. G. Falkowski. 1998. Measurements of variable chlorophyll fluorescence using fast repetition rate techniques: defining methodology and experimental protocols. Biochim. Biophys. Acta 1367: 88–106.

Kolber, Z. S, J. Zehr, and P. Falkowski. 1988. Effects of growth irradiance and nitrogen limitation on photosynthetic energy conversion in photosystem II. Plant Physiol. 88: 923-929.

Kolber, Z. S, K. D. Wyman, and P. G. Falkowski. 1990. Natural variability in photosynthetic energy conversion efficiency: a field study in the Gulf of Maine. *Limnol. Oceanogr*. 35, 72-79.

Lee-Borges, Jesús. 2003. Contribution of Picoplankton to Phytoplankton Dynamics and Bio-optics of the Eastern Caribbean Sea. PhD Dissertation. University of Puerto Rico, Mayaguez, P.R.

Lewis, W. M., and J. F. Saunders . 1989. Concentration and transport of dissolved and suspended substances in the Orinoco River, Biogeochemistry, 7 203-240.

Lima, I.D., Olson, D.B. and Dooney, S. 2002. Biological Response to Frontal Dynamics and Mesoscale Variability in Oligotrophic Environments: A numerical modeling study. J. Geophy. Res., 10.1029/2000JC000393,1-21.

Lohrenz, S.E., A.D. Weidemann, and M. Tuel. 2003. Phytoplankton spectral absorption as influenced by community size structure and pigment composition. Journal of Plankton Research. 25:35-61.

Maffione R. A. and D. R. Dana.1997. Instruments and methods for measuring the backward-scattering coefficient of ocean waters. Appl. Opt. **36**, 6057-6067

Maritorena, S., A. Morel, AND B. Gentili. 2000. Determination of the fluorescence quantum yield by oceanic phytoplankton in their natural habitat. Appl. Opt. 39**:** 6725–6737.

Martin, J. H., K. H. Coale, K. S. Johnson, S. E. Fitzwater, R. M. Gordon, S. J. Tanner, C. N. Hunter, V. A. Elrod, J. L. Nowicki, T. L. Coley, R. T. Barber, S. Lindley, A. J. Watson, K. Van Scoy, C. S. Law, M. I. Liddicoat, R. Ling, T. Stanton, J. Stockel, C. Collins, A. Anderson, R. Bidigare, M. Ondrusek, M. Latasa, F. J. Millero, K. Lee, W. Yao, J. Z. Zhang, G. Friederich, C. Sakamoto, F. Chavez, K. Buck, Z. Kolber, R. Greene, P. Falkowski, S. W. Chisholm, F. Hoge, R. Swift, J. Yungel, S. Turner, P. Nightingale, A. Hatton, P. Liss and N. W. Tindale. 1994. Testing the iron hypothesis in ecosystems of the equatorial Pacific Ocean. *Nature* 371: 123-129.

Marra, J., Trees, C.C., Bidigare, R.R., Barber, R.T. 2000. Pigment absorption and quantum yields in the Arabian Sea. Deep-Sea Research II 47, 1279–1299.

Moore, C.M., M.I. Lucas, J.T. Allen, R.J. Davidson, D.A. Smeed, and A.T. Mustard, 2002. Mesoscale controls on phytoplankton community structure, physiology and production within a eutrophic open ocean frontal region (Poster Abstract), in Challenger Centenary Conference: Marine Science 2002, Plymouth.

Moore, C.M., Suggett, D., Holligan, P.M., Sharples, J., Abraham, E.R., Lucas, M.I., Rippeth, T.P., Fisher, N.R., Simpson, J.H. and Hydes, D.J. 2003. Physical controls on phytoplankton physiology and production at a shelf sea front: a fast repetition-rate fluorometer based field study. Marine Ecology - Progress Series, 259, 29-45.

Moore, C. M., and others. 2006. Phytoplankton photoacclimation and photoadaptation in response to environmental gradients in a shelf sea. Limnology and Oceanography. 51: 936–949.

Morel, A. 1991. Light and marine photosynthesis: a spectral model with geochemical and climatological implications. Progress in Oceanography, 26:263-306.

Morrison J. R., 2003. In situ determination of the quantum yield of phytoplankton chlorophyll a fluorescence: A simple algorithm, observations, and a model. Limnology and Oceanography. 48(2) 618-631.

Morrison, J., and Smith, O., January 1990, "Geostrophic Transport Variability along the Aves Ridge in the Eastern Caribbean Sea, 1985-1986", J., Geophys. Res., 95(C1), pp. 699-710.

Murphy S., H. Hulburt and J. O'Brien. 1999. The connectivity of the eddie variability in the Caribbean Sea, the Gulf of Mexico, and the Atlantic Ocean. J Geophysical Res. 104, 1431-1453.

Müller-Karger, F. E., C. R. McClain, T. R. Fisher, W. E. Esaias, and R. Varela, 1989. Pigment distribution in the Caribbean Sea: Observations from Space. Progress in Oceanography. 23. 23-69.

Olaizola, M., J. La Roche, Z. Kolber, and P. G. Falkowski, 1994. Non-photochemical fluorescence quenching and the diadinoxanthin cycle in a marine diatom. Photosynth. Res. 41: 357-370

Olaizola, M., Yamamoto, H.Y., 1993. Short-term response of the diadinoxanthin cycle and fluorescence yield to high irradiance in Chaetocerus muelleri (Bacillariophyceae). Journal of Phycology 30, 606–612.

Olson R.J., H.M. Sosik, A.M. Chekalyuk and A. Shalapyonok. 2000. Effects of Iron enrichment on phytoplankton in the Southern Ocean during late summer: Active fluorescence and Flow Cytometric analyses. Deep-Sea Research I 47, 3181–3200

Parkhill J, Maillet G, Cullen JJ, 2001. Fluorescence based maximal quantum yield for PSII as a diagnostic of nutrient stress. J Phycol 37:517–529

Platt T, C.L. Gallegos and W.G. Harrison,1980. Photoinhibition of photosynthesis in natural assemblages of marine phytoplankton. J Mar Res 38:687–701

Platt, T. and A.D. Jassby. 1976. The relationship between photosynthesis and light for natural assemblages of coastal marine phytoplankton. Journal of Phycology. 12:421-430.

Prasil, O., Adir, N., & Ohad, I. 1992. Dynamics of photosystem II: mechanism of photoinhibition and recovery processes. *In:* The Photosystems: Structure, Function and Molecular Biology. Topics in Photosynthesis, vol. 11 (Barber, J. ed.), pp.295-348, Elsevier publ., Amsterdam, London, New York, Tokyo.

Rabinowitch, E. and Govindjee, 1969. Photosynthesis. John Wiley and sons, New York, 274 pp

Roesler, C. S., M. J. Perry, and K. L. Carder. 1989. Modeling *in situ* phytoplankton absorption from total absorption spectra. Limnol. Oceanogr. 34: 1512-1525.

Sakshaug E, Bricaud A, Dandonneau Y, Falkowski PG and 5 others. 1997. Parameters of photosynthesis: definitions, theory and interpretation of results. J Plankton Res 19: 1637–1670.

Sathyendranath, S., L. Lazzara, and L. Prieur, 1987. Variations in the spectral values of specific absorption of phytoplankton. Limnol. Oceanogr. 32: 403-415.

Sharples J., Moore C.M., Rippeth T.R., Holligan P.M., Hydes D.J., Fisher N.R., and Simpson H. 2001. Phytoplankton distribution and survival in the thermocline. Limnol. Oceanogr., 46(3):486-496.

Sosik H. M. and R. J. Olson. 2002. Phytoplankton and iron limitation of Photosynthetic effiency in the Southern Ocean during late summer. Deep-Sea Research I 49, 1195–1216.

Suggett D., G. Kraay, P. Holligan, M.t Davey, and J. Aiken, 2001.Assessment of photosynthesis in a spring cyanobacterial bloom by use of a fast repetition rate fluorometer Limnol. Oceanogr., 46(4), 802–810.

Stramski, D., and D. Kiefer 1991. Light scattering by microorganisms in the open ocean, Prog. Oceanogr., 28, 343 – 383.

Twardowski, M. S., E. Boss, J. B. Macdonald, W. S. Pegau, A. H. Barnard & J. R. V. Zaneveld. 2001. A model for estimating bulk refractive index from the optical backscattering ratio and the implications for understanding particle composition in Case I and Case II waters. Journal of Geophysical Research 106: 14129–14142

Vaillancourt, R. D., J Marra, M. P. Seki, M. L. Parsons and R. R. Bidigare.2003. Impact of a cyclonic eddy field on phytoplankton community structure and photosynthetic competency in the subtropical North Pacific Ocean. Deep-Sea Res. I 50 829-847.

Vaillancourt, R. D., J. Marra, R. T. Barber and W. O. Smith, Jr. 2003. Primary productivity and in situ quantum yields in the Ross Sea and Pacific Sector of the Antarctic Circumpolar Current, Deep-Sea Research II, vol. 50 , pp. 559-578 .

Vassiliev, I. R., Z. Kolber, K. D. Wyman, D. Mauzerall, V. K. Shukla, AND P. G. Falkowski. 1995. Effects of iron limitation on photosystem-II composition and light utilization in Dunaliella tertiolecta. Plant Physiol. 109: 963–972.

Yentsch, C. S., and D. W. Menzel. 1963. A method for determination of chlorophyll and phaeophytin by fluorescence. Deep-Sea Res. 10: 22 l-23 1

Zhu, X. R., J. M. Prospero, and F. J. Millero. 1997. Diel variability of soluble Fe (II) and soluble total Fe in North African dust in the trade winds at Barbados, J. Geophys. Res., 102:21297-21305.